

Electronic Supplementary Information (ESI) for:

# **Designing Redder and Brighter Fluorophores by Synergistic Tuning of Ground and Excited States**

Cheng Chen,<sup>†</sup> Mikhail S. Baranov,<sup>‡,§</sup> Liangdong Zhu,<sup>†</sup> Nadezhda S. Baleeva,<sup>‡</sup>  
Alexander Yu. Smirnov,<sup>‡</sup> Snizhana O. Zaitseva,<sup>‡</sup> Ilia V. Yampolsky,<sup>‡,§</sup> Kyril M.  
Solntsev,<sup>‡,¶</sup> and Chong Fang<sup>\*,†</sup>

<sup>†</sup>Department of Chemistry, Oregon State University, 153 Gilbert Hall, Corvallis, Oregon 97331,  
United States

<sup>‡</sup>Institute of Bioorganic Chemistry, Russian Academy of Sciences, Miklukho-Maklaya 16/10,  
Moscow117997, Russia

<sup>§</sup>Pirogov Russian National Research Medical University, Ostrovitianov 1, Moscow 117997,  
Russia

<sup>‡</sup>School of Chemistry and Biochemistry, Georgia Institute of Technology, Atlanta, Georgia 30332,  
United States

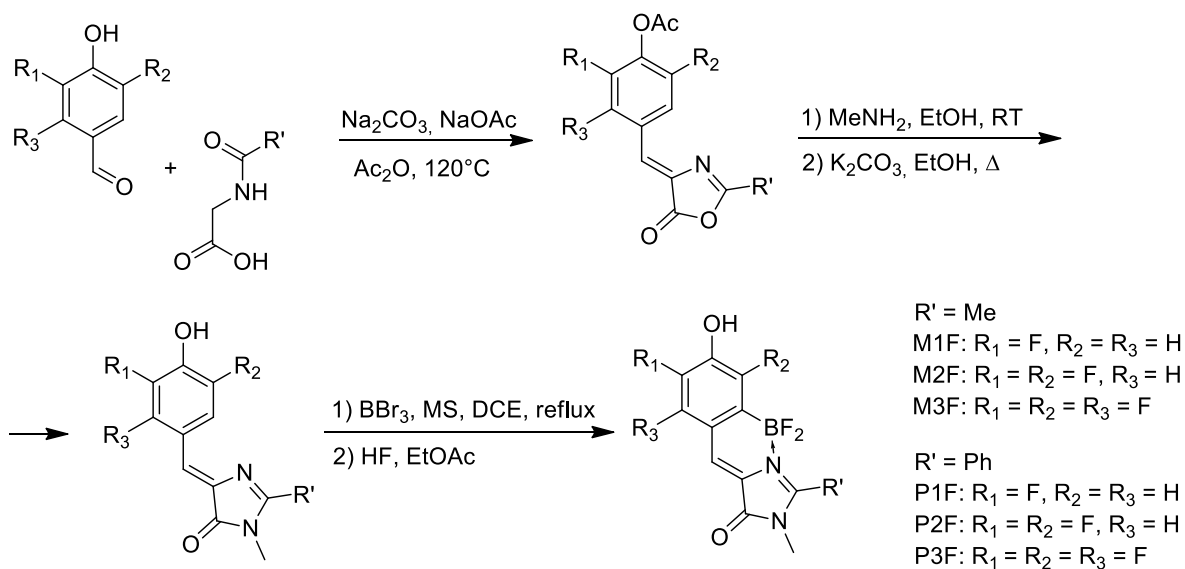
<sup>¶</sup>New York University Abu Dhabi, P.O. Box 129188, Abu Dhabi, UAE

\*To whom correspondence should be addressed. E-mail: Chong.Fang@oregonstate.edu.

<b><u>Table of Contents</u></b>	Page number
<b>ESI Text</b>	<b>S3 – 26</b>
<b>Synthesis Procedures of the Novel Locked MnF and PnF Compounds</b>	S3 – 11
<b>Synthesis Procedures of the Novel Unlocked Compounds with Substitutions</b>	S12 – 26
<b>ESI Figures</b>	<b>S27 – 33</b>
<b>Figure S1.</b> HOMO/LUMO energies and gaps by cumulative substitutions	S27
<b>Figure S2   S3.</b> HOMO   LUMO electron density map of single-site and cumulative substitutions for the methyl series	S28
<b>Figure S4   S5.</b> HOMO   LUMO electron density map of single-site and cumulative substitutions for the phenyl series	S29
Additional <b>discussions</b> for ESI <b>Figures S1–S5</b>	S30 – 31
<b>Figure S6.</b> Comparison of ground and excited state Stokes Raman spectra of anionic M3F and P3F in water by tunable femtosecond stimulated Raman spectroscopy	S32
<b>Figure S7.</b> Fluorescence spectra of the anionic form of the newly synthesized unlocked HBDIs with various substituents in aqueous solution	S33
<b>ESI Tables</b>	<b>S34 – 43</b>
<b>Table S1.</b> Ground-state Raman mode assignments for anionic MnF and PnF	S34
<b>Table S2.</b> Absorption and emission maxima of anionic MnF in various solvents	S35
<b>Table S3.</b> Absorption and emission maxima of anionic PnF in various solvents	S35
<b>Table S4.</b> Kamlet-Taft analysis for anionic MnF and PnF in solution	S36
<b>Table S5.</b> Simulated HOMO/LUMO energies and gaps with different substitutions at the phenolate and imidazolinone rings of the anionic chromophore in water	S37 – 39
<b>Table S6.</b> Ground- and excited-state acidities of MnF and PnF in water	S39
<b>Table S7.</b> Photophysical properties of synthesized unlocked fluorophores in water	S40 – 41
<b>Table S8.</b> Fluorescence quantum yield of the unlocked fluorophores in water	S42 – 43
<b>ESI References</b>	<b>S44 – 46</b>
<b>ESI Appendix:</b>	
<b>Figures S8–S38.</b> <sup>1</sup> H, <sup>13</sup> C, and <sup>19</sup> F NMR spectra of synthesized locked compounds	<b>S47 – 77</b>
<b>Figures S39–S71.</b> <sup>1</sup> H and <sup>13</sup> C NMR spectra of synthesized unlocked compounds	<b>S78 – 110</b>

## ESI Text

**Synthesis Methods and Procedures for the New MnF and PnF Compounds.** Commercially available reagents were used without additional purification. For column chromatography, E. Merck Kieselgel (silica gel) 60 was used. NMR spectra were recorded on a 700 MHz Bruker Avance III spectrometer at room temperature (RT = 293 K, see the Appendix below for results). Chemical shifts were reported relative to residual peaks of DMSO-d<sub>6</sub> (2.51 ppm for <sup>1</sup>H and 39.5 ppm for <sup>13</sup>C). Melting points were measured on an advanced digital apparatus (Stuart SMP30). High-resolution mass spectra (HRMS) were recorded with an LTQ Orbitrap XL (ThermoFisher Scientific, USA) equipped with a dual-nebulizer electrospray ionization (ESI) source. The detailed synthesis steps are summarized in Scheme S1 and presented in the ensuing sections.



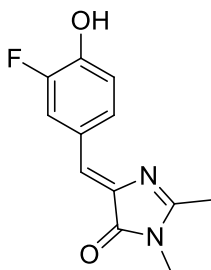
**Scheme S1.** Synthesis of compounds **MnF and PnF (n=1–3)** with functional group substitutions.

**Typical synthetic procedure for imidazolones.**<sup>1</sup> 1 mmol of corresponding fluorinated 4-hydroxybenzaldehyde, 1.1 mmol of hippuric acid or acetylglycine and 1.2 mmol (100 mg) of anhydrous NaOAc were dissolved in 1 ml of warm Ac<sub>2</sub>O, then 1.3 mmol (140 mg) of anhydrous

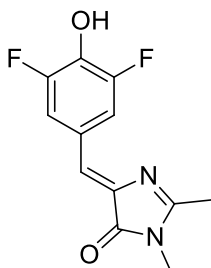
Na<sub>2</sub>CO<sub>3</sub> was added. The mixture was stirred at 165°C in inert atmosphere until no aldehyde was observed by thin-layer chromatography (TLC, typically 2–4 h). Reaction mixture was cooled, all volatiles were removed *in vacuo*. Residue was purified with flash chromatography (eluent – hexane-ethyl acetate 1:1). The crude product was used in the next stage without further purification.

The product of previous stage (1 mmol) was suspended in ethanol (10 mL) and mixed with aqueous methylamine (40%, 1.5 mmol). The mixture was stirred at room temperature for 2 h, potassium carbonate (10 mmol) was added and the mixture was refluxed for 8 h. The mixture was then dried on a rotary evaporator and dissolved in water (20 mL). With aqueous hydrochloric acid (10%), the solution was acidified to pH=6. The precipitate was filtered, washed by cold (–20°C) ethanol and diethyl ether and dried *in vacuo*.

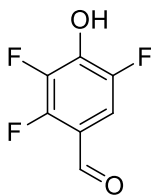
**Typical synthetic procedure for difluoroboryl imidazolones.** The corresponding imidazolone (1.0 mmol) was dissolved in dry C<sub>2</sub>H<sub>4</sub>Cl<sub>2</sub> (50 mL), molecular sieves 4Å (3 g) and 3Å (3 g) added, which was followed by a solution of boron tribromide in C<sub>2</sub>H<sub>4</sub>Cl<sub>2</sub> (1M, 5.0 mmol). The reaction mixture was refluxed for 5 h in inert atmosphere, and then cooled and filtered; molecular sieves were washed twice with ethanol (10 mL) and C<sub>2</sub>H<sub>4</sub>Cl<sub>2</sub> (50 mL). The solution was mixed with aqueous HF (20%, 5 mL) and stirred for 30 minutes. The mixture was dissolved in EtOAc (100 mL), washed with water (3×30 mL) and brine (3×30 mL) and dried over Na<sub>2</sub>SO<sub>4</sub>. The solvent was evaporated and the product was purified by column chromatography (CHCl<sub>3</sub>/EtOH 10:1).



**(Z)-4-(3-fluoro-4-hydroxybenzylidene)-1,2-dimethyl-1H-imidazol-5(4H)-one:**<sup>2</sup> yellow solid (140 mg, 60%); <sup>1</sup>H NMR (700 MHz, DMSO-*d*<sub>6</sub>) δ: 10.52 (s, 1H), 8.19 (m, 1H), 7.76 (m, 1H), 6.99 (t, *J*=8.8 Hz, 1H), 6.89 (s, 1H), 3.09 (s, 3H), 2.34 (s, 3H); <sup>19</sup>F NMR (564 MHz, DMSO-*d*<sub>6</sub>) δ: –135.78 (s) as shown in the experimental NMR spectrum below (Appendix: Figure S8). This compound represents the unlocked version of M1F (see Scheme 1 in main text).

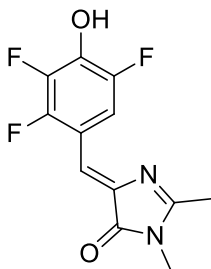


**(Z)-4-(3,5-difluoro-4-hydroxybenzylidene)-1,2-dimethyl-1H-imidazol-5(4H)-one:**<sup>2</sup> yellow solid (146 mg, 58%); <sup>1</sup>H NMR (700 MHz, DMSO-*d*<sub>6</sub>) δ: 10.88 (s, 1H), 7.97 (m, 2H), 6.89 (s, 1H), 3.09 (s, 3H), 2.36 (s, 3H); <sup>19</sup>F NMR (564 MHz, DMSO-*d*<sub>6</sub>) δ: –132.38 (s) as shown in Figure S9. This compound represents the unlocked version of M2F (see Scheme 1 in main text).

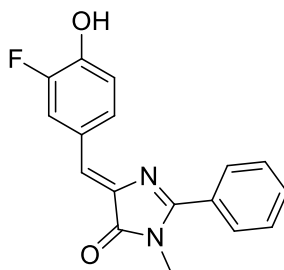


**2,3,5-trifluoro-4-hydroxybenzaldehyde:** 3 g (20.3 mmol) of 2,3,6-trifluorophenol and 3.15 g (22.5 mmol) of hexamethylenetetramine were dissolved in 30 ml of trifluoroacetic acid and then the reaction mixture was gently refluxed for 3 h. All volatiles were removed *in vacuo* and the residue was dissolved in 250 ml of EtOAc. Solution was washed with brine (5×70 ml), dried over Na<sub>2</sub>SO<sub>4</sub> and then evaporated. Product was purified with a column chromatography (eluent – EtOAc-hexane 1:5). Yield 2.3 g (64%) as white solid; m. p. 127–130°C; <sup>1</sup>H NMR (700 MHz,

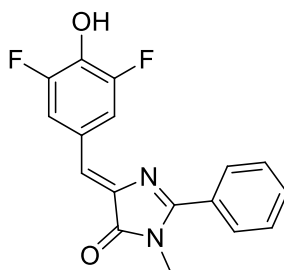
DMSO-*d*<sub>6</sub>)  $\delta$ : 7.4 (ddd,  $J=10.52, 6.08, 2.14$  Hz, 1H), 10.0 (s, 1H) 12.2 (br. s, 1H) (see Figure S10); <sup>13</sup>C NMR (DMSO-*d*<sub>6</sub>)  $\delta$ : 109.7 (d,  $J=21.16$  Hz), 114.5 (t,  $J=6.73$  Hz), 141.9 (ddd,  $J=18.15, 12.86, 3.61$  Hz), 140.5 (ddd,  $J=244.75, 14.43, 6.25$  Hz), 148.3 (ddd,  $J=235.61, 4.33, 1.92$  Hz), 149.4 (ddd,  $J=255.33, 11.06, 2.40$  Hz), 185.2 (see Figure S11); <sup>19</sup>F NMR (564 MHz; DMSO-*d*<sub>6</sub>)  $\delta$ : -155.74 (dd,  $J=20.43, 9.2$  Hz), (-148.92) — (-148.80) (m), (-135.59) — (-135.49) (m) (see Figure S12); HRMS (ESI) calculated for C<sub>7</sub>H<sub>2</sub>F<sub>3</sub>O<sub>2</sub> ([*M*-H]<sup>-</sup>) 175.0012, found 175.0016.



**(Z)-4-(2,3,5-trifluoro-4-hydroxybenzylidene)-1,2-dimethyl-1H-imidazol-5(4H)-one:** yellow solid (130 mg, 48%), m.p. 254–260°C with decomposition; <sup>1</sup>H NMR (700 MHz, DMSO-*d*<sub>6</sub>)  $\delta$ : 2.35 (s, 3 H), 3.08 (s, 3 H), 6.81 (s, 1 H), 8.39 (td,  $J=6.17, 4.77$  Hz, 1 H), 11.55 (br. s., 1 H) (see Figure S13); <sup>13</sup>C NMR (151 MHz, DMSO-*d*<sub>6</sub>)  $\delta$ : 15.4, 26.2, 111.8 (d,  $J=22.78$  Hz), 112.0–112.5 (m), 137.3 (ddd,  $J=18.68, 12.85, 1.85$  Hz), 139.3, 140.7 (ddd,  $J=242.13, 15.37, 7.42$  Hz), 146.8 (ddd,  $J=249.55, 11.13, 2.12$  Hz), 146.9 (ddd,  $J=249.55, 11.13, 2.12$  Hz), 147.9 (dd,  $J=235.24, 3.18$  Hz), 159.5 (p,  $J=21.72$  Hz), 165.6, 169.2 (see Figure S14); <sup>19</sup>F NMR (564 MHz, DMSO-*d*<sub>6</sub>)  $\delta$ : -156.39 (s), -144.07 (s), -135.83 (s) (see Figure S15); HRMS (ESI) calculated for C<sub>12</sub>H<sub>10</sub>F<sub>3</sub>N<sub>2</sub>O<sub>2</sub> ([*M*+H]<sup>+</sup>) 271.0689, found 271.0689. This compound represents the unlocked version of M3F (see Scheme 1 in main text).

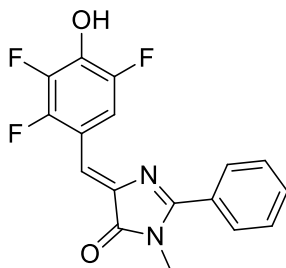


**(Z)-4-(3-fluoro-4-hydroxybenzylidene)-1-methyl-2-phenyl-1H-imidazol-5(4H)-one:** yellow solid (124 mg, 42%), m.p. 206–210°C with decomposition;  $^1\text{H}$  NMR (700 MHz, DMSO- $d_6$ )  $\delta$ : 3.26 (s, 3 H), 7.03 (t,  $J=8.78$  Hz, 1 H), 7.11 (s, 1 H), 7.61 (t,  $J=7.26$  Hz, 2 H), 7.63–7.66 (m, 1 H), 7.87 (d,  $J=8.43$  Hz, 1 H), 7.93 (d,  $J=7.05$  Hz, 2 H), 10.64 (br. s., 1 H) (see Figure S16);  $^{13}\text{C}$  NMR (151 MHz, DMSO- $d_6$ )  $\delta$ : 28.6, 117.8 (d,  $J=2.65$  Hz), 119.1 (d,  $J=19.07$  Hz), 126.0 (d,  $J=7.42$  Hz), 126.3 (d,  $J=2.12$  Hz), 128.6, 128.7, 129.0, 130.0 (d,  $J=2.12$  Hz), 131.4, 137.2, 147.5 (d,  $J=12.18$  Hz), 150.7 (d,  $J=241.06$  Hz), 161.8, 170.4 (see Figure S17);  $^{19}\text{F}$  NMR (564 MHz, DMSO- $d_6$ )  $\delta$ : –135.48 (s) (see Figure S18); HRMS (ESI) calculated for  $\text{C}_{17}\text{H}_{14}\text{FN}_2\text{O}_2$  ( $[M+H]^+$ ) 297.1034, found 297.1035. This compound represents the unlocked version of P1F (see Scheme 1 in main text).



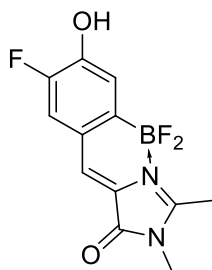
**(Z)-4-(3,5-difluoro-4-hydroxybenzylidene)-1-methyl-2-phenyl-1H-imidazol-5(4H)-one:** yellow solid (160 mg, 51%), m.p. 242–245°C with decomposition;  $^1\text{H}$  NMR (700 MHz, DMSO- $d_6$ )  $\delta$ : 3.26 (s, 3 H), 7.11 (s, 1 H), 7.58–7.64 (m, 2 H), 7.64–7.69 (m, 1 H), 7.90–7.97 (m, 2 H), 8.05 (d,  $J=9.26$  Hz, 2 H), 11.00 (br. s., 1 H) (see Figure S19);  $^{13}\text{C}$  NMR (151 MHz, DMSO- $d_6$ )  $\delta$ : 28.6, 115.5 (dd,  $J=16.95, 5.30$  Hz), 124.7 (t,  $J=9.54$  Hz), 124.9, 128.6, 128.8, 128.9, 131.6,

136.0 (t,  $J=16.42$  Hz), 138.3, 151.8 (dd,  $J=241.60$ , 7.42 Hz), 162.7, 170.3 (see Figure S20);  $^{19}\text{F}$  NMR (564 MHz,  $\text{DMSO-}d_6$ )  $\delta$ : -132.12 (s) (see Figure S21); HRMS (ESI) calculated for  $\text{C}_{17}\text{H}_{13}\text{F}_2\text{N}_2\text{O}_2$  ( $[M+H]^+$ ) 315.0940, found 315.0941. This compound represents the unlocked version of P2F (see Scheme 1 in main text).

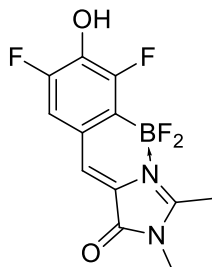


**(Z)-4-(2,3,5-trifluoro-4-hydroxybenzylidene)-1-methyl-2-phenyl-1H-imidazol-5(4H)-one:**

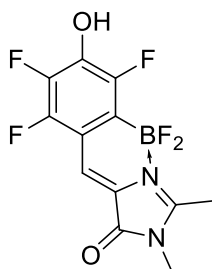
yellow solid (129 mg, 39%), m.p. 250–254°C;  $^1\text{H}$  NMR (700 MHz,  $\text{DMSO-}d_6$ )  $\delta$ : 3.27 (s, 3 H), 7.06 (s, 1 H), 7.62 (t,  $J=7.53$  Hz, 2 H), 7.65–7.69 (m, 1 H), 7.95 (d,  $J=7.19$  Hz, 2 H), 8.53 (dd,  $J=12.09$ , 5.04 Hz, 1 H), 11.72 (br. s., 1 H) (see Figure S22);  $^{13}\text{C}$  NMR (151 MHz,  $\text{DMSO-}d_6$ )  $\delta$ : 28.7, 112.0 (d,  $J=22.25$  Hz), 112.3 (t,  $J=9.80$  Hz), 114.4 (d,  $J=3.18$  Hz), 128.6, 128.7, 128.8, 131.8, 137.8 (dt,  $J=30.73$ , 2.12 Hz), 139.1, 139.8–140.0 (m), 141.5 (dd,  $J=14.84$ , 6.89 Hz), 147.0 (ddd,  $J=238.42$ , 10.07, 1.06 Hz), 148.0 (dd,  $J=239.48$ , 3.18 Hz), 148.8 (d,  $J=3.71$  Hz), 163.7, 170.0 (see Figure S23);  $^{19}\text{F}$  NMR (564 MHz,  $\text{DMSO-}d_6$ )  $\delta$ : -156.31 (dd,  $J=20.44$ , 8.18 Hz), -143.47 (dd,  $J=19.92$ , 11.75 Hz), -135.43 (t,  $J=10.22$  Hz) (see Figure S24); HRMS (ESI) calculated for  $\text{C}_{17}\text{H}_{12}\text{F}_3\text{N}_2\text{O}_2$  ( $[M+H]^+$ ) 333.0845, found 333.0848. This compound represents the unlocked version of P3F (see Scheme 1 in main text).



**(Z)-4-(2-(difluoroboryl)-5-fluoro-4-hydroxybenzylidene)-1,2-dimethyl-1H-imidazol-5(4H)-one (M1F):**<sup>2</sup> yellow solid, <sup>1</sup>H NMR (700 MHz, DMSO-*d*<sub>6</sub>) δ: 10.64 (s, 1H), 7.55 (s, 1H), 7.47 (d, *J*=12.1 Hz, 1H), 7.15 (d, *J*=9.4 Hz, 1H), 3.22 (s, 3H), 2.72 (s, 3H); <sup>19</sup>F NMR (564 MHz, DMSO-*d*<sub>6</sub>) δ: -138.97 (br. s), -138.23 (s) (see Figure S25).

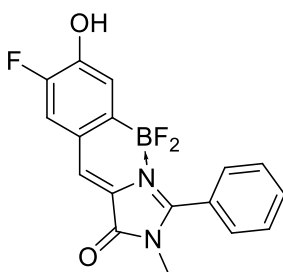


**(Z)-4-(2-(difluoroboryl)-3,5-difluoro-4-hydroxybenzylidene)-1,2-dimethyl-1H-imidazol-5(4H)-one (M2F):**<sup>2</sup> yellow solid, <sup>1</sup>H NMR (DMSO-*d*<sub>6</sub>) δ: 10.91 (s, 1H), 7.55 (s, 1H), 7.39 (d, *J*=10.5 Hz, 1H), 3.22 (s, 3H), 2.73 (s, 3H); <sup>19</sup>F NMR (564 MHz, DMSO-*d*<sub>6</sub>) δ: -138.06 (br. s), -134.30 (d, *J*=14.31 Hz), -125.76 (dd, *J*=12.78, 5.62 Hz) (see Figure S26).

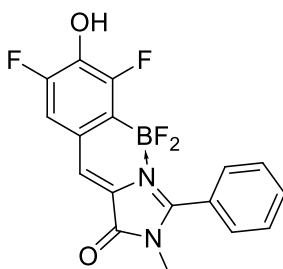


**(Z)-4-(2-(difluoroboryl)-3,5,6-trifluoro-4-hydroxybenzylidene)-1,2-dimethyl-1H-imidazol-5(4H)-one (M3F):** dark yellow solid (98 mg, 31%), m.p. ~310 °C with decomposition; <sup>1</sup>H NMR

(700 MHz, DMSO- $d_6$ )  $\delta$ : 2.75 (s, 3 H), 3.23 (s, 3 H), 7.44 (s, 1 H), 11.56 (br. s., 1 H) (see Figure S27);  $^{13}\text{C}$  NMR (151 MHz, DMSO- $d_6$ )  $\delta$ : 13.2, 26.7, 111.5, 117.2, 126.4, 139.3 (dd,  $J=23.31$ , 12.19 Hz), 139.8 (ddd,  $J=242.66$ , 14.31, 7.42 Hz), 146.2 (dd,  $J=253.78$ , 10.07 Hz), 150.4 (dd,  $J=238.42$ , 2.65 Hz), 162.5, 167.9 (see Figure S28);  $^{19}\text{F}$  NMR (564 MHz, DMSO- $d_6$ )  $\delta$ : -157.55 (dd,  $J=17.36$ , 7.16 Hz), -144.66 (t,  $J=16.86$  Hz), -137.73 (br. s.), -129.90 (s) (see Figure S29); HRMS (ESI) calculated for  $\text{C}_{12}\text{H}_7\text{BF}_5\text{N}_2\text{O}_2$  ( $[M-H]^-$ ) 317.0526, found 317.0530.



**(Z)-4-(2-(difluoroboryl)-5-fluoro-4-hydroxybenzylidene)-1-methyl-2-phenyl-1H-imidazol-5(4H)-one (P1F)**: dark yellow solid (173 mg, 51%), m.p.  $\sim 310$  °C with decomposition;  $^1\text{H}$  NMR (700 MHz, DMSO- $d_6$ )  $\delta$ : 3.09 (s, 3 H), 7.06 (d,  $J=9.21$  Hz, 1 H), 7.53 (d,  $J=11.84$  Hz, 1 H), 7.65 (t,  $J=7.65$  Hz, 2 H), 7.73 (t,  $J=7.56$  Hz, 1 H), 7.75 (s, 1 H), 7.87 (d,  $J=7.40$  Hz, 2 H), 10.76 (br. s., 1 H) (see Figure S30);  $^{13}\text{C}$  NMR (151 MHz, DMSO- $d_6$ )  $\delta$ : 28.0, 118.7 (d,  $J=16.95$  Hz), 120.3, 124.0, 124.6 (br. s), 125.8, 128.0, 129.5, 129.9, 132.1, 149.4 (d,  $J=11.66$  Hz), 150.2 (d,  $J=241.60$  Hz), 162.9, 163.2 (see Figure S31);  $^{19}\text{F}$  NMR (564 MHz, DMSO- $d_6$ )  $\delta$ : -138.29 (t,  $J=10.73$  Hz), -134.81 (br. s) (see Figure S32); HRMS (ESI) calculated for  $\text{C}_{17}\text{H}_{11}\text{BF}_3\text{N}_2\text{O}_2$  ( $[M-H]^-$ ) 343.0871, found 343.0871.

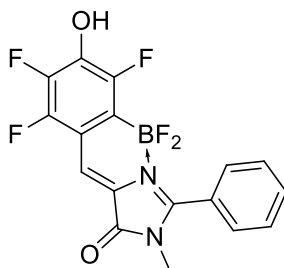


S10

**(Z)-4-(2-(difluoroboryl)-3,5-difluoro-4-hydroxybenzylidene)-1-methyl-2-phenyl-1H-**

**imidazol-5(4H)-one (P2F):** dark yellow solid (89 mg, 25%), m.p. 280–287 °C with decomposition;

$^1\text{H}$  NMR (700 MHz, DMSO- $d_6$ )  $\delta$ : 3.07 (s, 3 H), 7.47 (d,  $J=10.78$  Hz, 1 H), 7.66 (t,  $J=7.74$  Hz, 2 H), 7.71–7.75 (m, 1 H), 7.75 (d,  $J=1.11$  Hz, 1 H), 7.87 (d,  $J=7.19$  Hz, 2 H), 10.92 (s, 1 H) (see Figure S33);  $^{13}\text{C}$  NMR (151 MHz, DMSO- $d_6$ )  $\delta$ : 28.3, 115.4 (d,  $J=18.54$  Hz), 123.6 (br. s), 124.0, 126.6, 128.2, 128.9, 129.6, 132.4, 137.9 (t,  $J=17.22$  Hz), 151.3 (dd,  $J=240.54, 5.83$  Hz), 154.6 (dd,  $J=241.07, 5.83$  Hz), 163.1, 164.2 (see Figure S34);  $^{19}\text{F}$  NMR (564 MHz, DMSO- $d_6$ )  $\delta$ : –134.31 (d,  $J=13.28$  Hz), –133.11 (br. s.), –125.99 (t,  $J=12.27$  Hz) (see Figure S35); HRMS (ESI) calculated for  $\text{C}_{17}\text{H}_{10}\text{BF}_4\text{N}_2\text{O}_2$  ( $[M-H]^-$ ) 361.0777, found 361.0785.

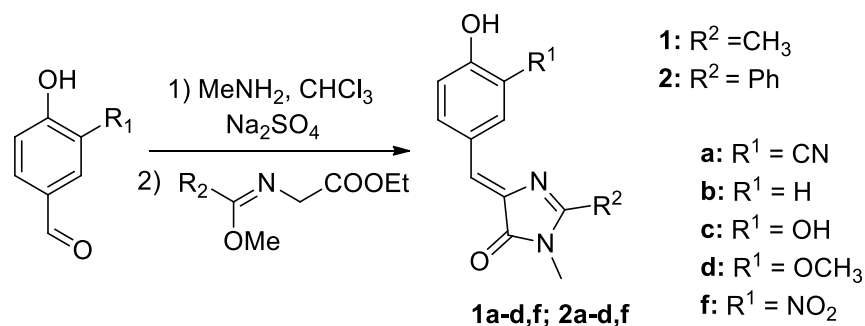


**(Z)-4-(2-(difluoroboryl)-3,5,6-trifluoro-4-hydroxybenzylidene)-1-methyl-2-phenyl-1H-**

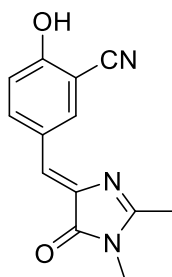
**imidazol-5(4H)-one (P3F):** dark yellow solid (98 mg, 31%), m.p. 277–282°C with decomposition;

$^1\text{H}$  NMR (700 MHz, DMSO- $d_6$ )  $\delta$ : 3.08 (s, 3 H), 7.61 (s, 1 H), 7.66 (t,  $J=7.67$  Hz, 2 H), 7.74 (t,  $J=7.53$  Hz, 1 H), 7.87 (d,  $J=7.46$  Hz, 2 H), 11.60 (br. s, 1 H) (see Figure S36);  $^{13}\text{C}$  NMR (151 MHz, DMSO- $d_6$ )  $\delta$ : 28.2 (s) 119.0 (br. s.) 123.6, 127.1, 128.1, 129.4, 132.4, 139.5 (dd,  $J=19.07, 10.60$  Hz), 146.0 (dd,  $J=320.01, 16.42$  Hz), 146.3 (dd,  $J=271.80, 8.48$  Hz), 150.2 (d,  $J=235.77$  Hz), 162.8, 165.2 (see Figure S37);  $^{19}\text{F}$  NMR (564 MHz, DMSO- $d_6$ )  $\delta$ : –157.56 (dd,  $J=19.92, 9.71$  Hz), –144.20 (t,  $J=16.86$  Hz), –132.84 (br. s.), –130.08 (s) (see Figure S38); HRMS (ESI) calculated for  $\text{C}_{17}\text{H}_9\text{BF}_5\text{N}_2\text{O}_2$  ( $[M-H]^-$ ) 379.0683, found 379.0684.

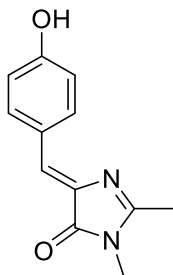
**Synthesis Methods and Procedures for the New Unlocked Compounds with Various Substitutions.** The general method for the preparation of the (*Z*)-3-*R*-4-hydroxybenzylidene-1-methyl-2-*R'*-1*H*-imidazol-5(4*H*)-ones (**1a-d,f**, **2a-d,f**; see Scheme S2) is described in details as follows. The corresponding aromatic aldehyde (10 mmol) was dissolved in 50 mL of CHCl<sub>3</sub> and mixed with 3.3 mL of methylamine solution (40% aqueous, 37 mmol) and anhydrous Na<sub>2</sub>SO<sub>4</sub> (5 g). In case of substantially precipitation, methanol can be used for the complete dissolution. The mixture was stirred for 48 h at room temperature, filtered and dried over the additional Na<sub>2</sub>SO<sub>4</sub>. The solvent was evaporated, the corresponding ethyl 2-((methoxymethylene)amino)acetate (20 mmol) was added and the mixture was stirred for 24 h at room temperature. Then it was dried in vacuum and the product was purified by column chromatography (CH<sub>2</sub>Cl<sub>2</sub>-EtOH 100:1-5).



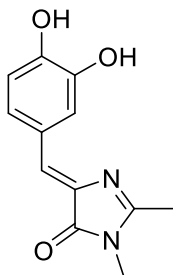
**Scheme S2.** Synthesis of compounds **1a-d, f** and **2a-d, f** with functional group substitutions at the two strategic sites (R<sup>1</sup> = CN, H, OH, OCH<sub>3</sub> or NO<sub>2</sub>; and R<sup>2</sup> = CH<sub>3</sub> or Ph).



**(Z)-4-(3-cyano-4-hydroxybenzylidene)-1,2-dimethyl-1H-imidazol-5(4H)-one (1a):** Pale yellow solid (385 mg, 16%); m.p. ~260 °C with decomposition; <sup>1</sup>H NMR (700 MHz, 303 K, DMSO-*d*<sub>6</sub>) δ ppm: 11.71 (br. s., 1H), 8.48 (d, *J*=1.7 Hz, 1H), 8.35 (dd, *J*=8.9, 1.7 Hz, 1H), 7.08 (d, *J*=8.9 Hz, 1H), 6.92 (s, 1H), 3.09 (s, 3H), 2.35 (s, 3H) (see Figure S39); <sup>13</sup>C NMR (176 MHz, 303 K, DMSO-*d*<sub>6</sub>) δ ppm: 169.6, 164.1, 161.1, 138.0, 137.9, 136.8, 126.0, 122.7, 116.5, 116.5, 99.5, 26.2, 15.3 (see Figure S40); HRMS (ESI) *m/z*: 242.0922 found (calculated for C<sub>13</sub>H<sub>12</sub>N<sub>3</sub>O<sub>2</sub><sup>+</sup>, [M+H]<sup>+</sup> 242.0924).

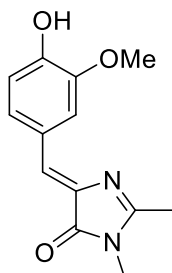


**(Z)-4-(4-hydroxybenzylidene)-1,2-dimethyl-1H-imidazol-5(4H)-one (1b)<sup>3</sup>**

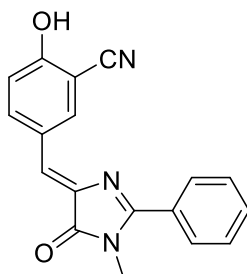


**(Z)-4-(3,4-dihydroxybenzylidene)-1,2-dimethyl-1H-imidazol-5(4H)-one (1c):** Brown solid (1.02 g, 44%); m.p. = 209–211 °C; <sup>1</sup>H NMR (700 MHz, 303 K, DMSO-*d*<sub>6</sub>) δ ppm: 9.57 (br. s., 1H), 9.17 (br. s., 1H), 7.84 (d, *J*=1.6 Hz, 1H), 7.36 (dd, *J*=8.2, 1.6 Hz, 1H), 6.79 (s, 1H), 6.77 (d, *J*=8.2 Hz, 1H), 3.08 (s, 3H), 2.33 (s, 3H) (see Figure S41); <sup>13</sup>C NMR (75 MHz, 293 K, DMSO-*d*<sub>6</sub>)

$\delta$  ppm: 169.9, 162.0, 148.5, 145.3, 136.1, 126.1, 125.7 (2C), 118.5, 115.6, 26.2, 15.3 (see Figure S42); HRMS (ESI)  $m/z$ : 233.0918 found (calculated for  $C_{12}H_{13}N_2O_3^+$ ,  $[M+H]^+$  233.0921).

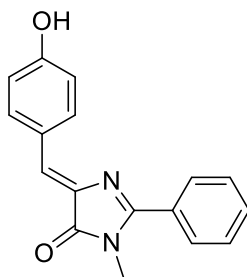


**(Z)-4-(3-methoxy-4-hydroxybenzylidene)-1,2-dimethyl-1H-imidazol-5(4H)-one (1d)<sup>4</sup>**

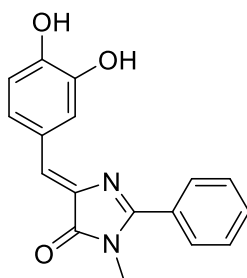


**(Z)-4-(3-cyano-4-hydroxybenzylidene)-1-methyl-2-phenyl-1H-imidazol-5(4H)-one (2a):**

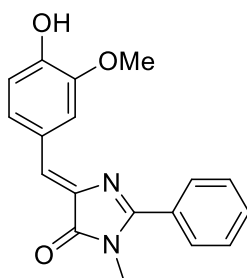
Brown solid (1.03 g, 34%); m.p.  $\sim$ 285  $^{\circ}$ C with decomposition;  $^1H$  NMR (300 MHz, 293 K, DMSO- $d_6$ )  $\delta$  ppm: 8.57–8.45 (m, 2H), 7.94 (d,  $J=7.5$  Hz, 2H), 7.66–7.60 (m, 3H), 7.14 (s, 1H), 7.09 (d,  $J=9.3$  Hz, 1H), 3.26 (s, 3H) (see Figure S45);  $^{13}C$  NMR (176 MHz, 303 K, DMSO- $d_6$ )  $\delta$  ppm: 170.4, 162.3, 161.9, 138.2, 137.6, 137.4, 131.5, 128.9, 128.8, 128.6, 125.8, 125.0, 116.8, 116.5, 99.7, 28.6 (see Figure S46); HRMS (ESI)  $m/z$ : 304.1081 found (calculated for  $C_{18}H_{14}N_3O_2^+$ ,  $[M+H]^+$  304.1081).



**(Z)-4-(4-hydroxybenzylidene)-1-methyl-2-phenyl-1H-imidazol-5(4H)-one (2b)**<sup>5</sup>

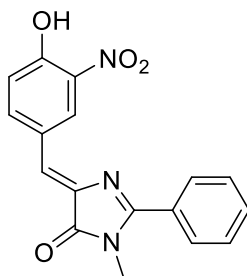


**(Z)-4-(3,4-dihydroxybenzylidene)-1-methyl-2-phenyl-1H-imidazol-5(4H)-one (2c):** Brown solid (650 mg, 22%); m.p. = 214–217 °C; <sup>1</sup>H NMR (700 MHz, 303 K, DMSO-*d*<sub>6</sub>) δ ppm: 9.44 (br. s., 2H), 7.98 (s, 1H), 7.93 (d, *J*=7.2 Hz, 2H), 7.64–7.58 (m, 3H), 7.44 (d, *J*=8.0 Hz, 1H), 7.01 (s, 1H), 6.81 (d, *J*=8.2 Hz, 1H), 3.26 (s, 3H) (see Figure S47); <sup>13</sup>C NMR (176 MHz, 303 K, DMSO-*d*<sub>6</sub>) δ ppm: 170.5, 160.6, 149.0, 145.4, 136.0, 131.2, 129.3, 128.7, 128.6, 128.3, 126.3, 125.8, 118.7, 115.7, 28.5 (see Figure S48); HRMS (ESI) *m/z*: 295.1076 found (calculated for C<sub>17</sub>H<sub>15</sub>N<sub>2</sub>O<sub>3</sub><sup>+</sup>, [M+H]<sup>+</sup> 295.1077).



**(Z)-4-(3-methoxy-4-hydroxybenzylidene)-1-methyl-2-phenyl-1H-imidazol-5(4H)-one (2d):**

Dark red solid (1.69 g, 55%); m.p. = 188–190 °C; <sup>1</sup>H NMR (700 MHz, 303 K, DMSO-*d*<sub>6</sub>) δ ppm: 8.10 (br. s., 1H), 7.94 (d, *J*=6.9 Hz, 2H), 7.71 (d, *J*=7.8 Hz, 1H), 7.64–7.58 (m, 3H), 7.10 (s, 1H), 6.86 (d, *J*=8.2 Hz, 1H), 3.82 (s, 3H), 3.28 (s, 3H) (see Figure S49); <sup>13</sup>C NMR (176 MHz, 303 K, DMSO-*d*<sub>6</sub>) δ ppm: 170.5, 160.7, 149.9, 147.6, 136.2, 131.2, 129.2, 128.8, 128.5, 128.0, 127.3, 125.8, 115.8, 115.7, 55.5, 28.6 (see Figure S50); HRMS (ESI) *m/z*: 309.1235 found (calculated for C<sub>18</sub>H<sub>17</sub>N<sub>2</sub>O<sub>3</sub><sup>+</sup>, [M+H]<sup>+</sup> 309.1234).

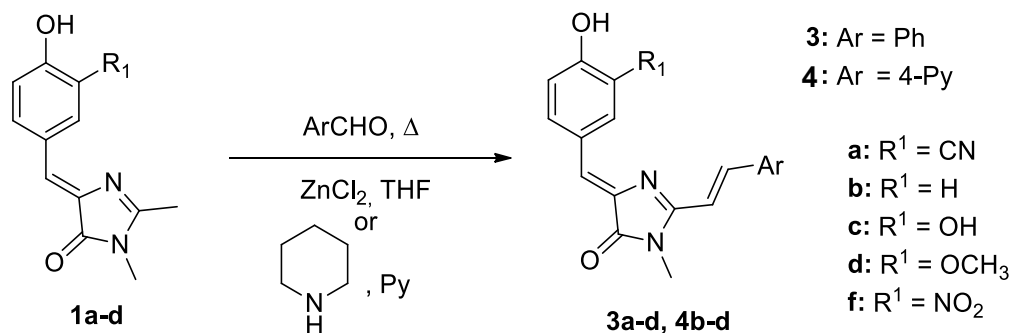


**(Z)-4-(3-nitro-4-hydroxybenzylidene)-1-methyl-2-phenyl-1H-imidazol-5(4H)-one (2f):**

Orange solid (1.58 g, 49%); m.p. = 190–193 °C; <sup>1</sup>H NMR (700 MHz, 303 K, DMSO-*d*<sub>6</sub>) δ ppm: 8.85 (d, *J*=1.3 Hz, 1H), 8.42 (dd, *J*=8.7, 1.3 Hz, 1H), 7.93 (d, *J*=7.2 Hz, 2H), 7.65 (t, *J*=7.3 Hz, 1H), 7.61 (t, *J*=7.3 Hz, 2H), 7.17 (s, 1H), 7.12 (d, *J*=8.8 Hz, 1H), 3.27 (s, 3H) (see Figure S51); <sup>13</sup>C NMR (176 MHz, 303 K, DMSO-*d*<sub>6</sub>) δ ppm: 170.3, 162.0, 138.0, 137.5, 137.4, 131.5, 129.4, 129.0, 128.9, 128.8, 128.6, 128.1, 125.3, 120.4, 28.6 (see Figure S52); HRMS (ESI) *m/z*: 324.0977 found (calculated for C<sub>17</sub>H<sub>14</sub>N<sub>3</sub>O<sub>4</sub><sup>+</sup>, [M+H]<sup>+</sup> 324.0979).

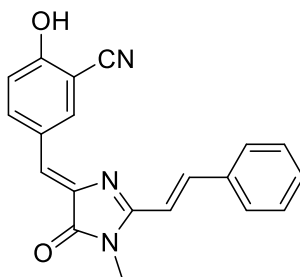
Notably as the synthesis work expanded its scope, the general method for the preparation of **(Z)-4-benzylidene-1-methyl-2-((*E*)-styryl/pyridin-4-yl)vinyl)-1H-imidazol-5(4H)-ones (3b-d, 4b-d)** is described below. A solution of the corresponding (*Z*)-4-benzylidene-1,2-dimethyl-1H-

imidazol-5(4*H*)-one (compound **1**, 1 mmol), aromatic aldehyde (5 mmol), and piperidine (40  $\mu$ L) in pyridine (Py, 10 mL) were stirred for 24–72 h at 115  $^{\circ}$ C (see Scheme S3 below). The mixture was evaporated and the crude solid product was purified by column chromatography ( $\text{CHCl}_3$ -EtOH 50:1).



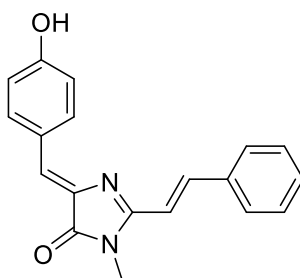
**Scheme S3.** Synthesis of compounds **3a-d, f** and **4a-d, f** with functional group substitutions at the R<sub>1</sub> and Ar sites (R<sup>1</sup> = CN, H, OH, OCH<sub>3</sub> or NO<sub>2</sub>; and Ar = Ph or 4-Py).

Furthermore, the methods for the preparation of **(Z)-4-(3-cyano-4-hydroxybenzylidene)-1-methyl-2-((E)-styryl)-1*H*-imidazol-5(4*H*)-one (3a)** and of **(Z)-4-(3-nitro-4-hydroxybenzylidene)-1-methyl-2-((E)-styryl/pyridin-4-yl)vinyl)-1*H*-imidazol-5(4*H*)-ones (3f and 4f)** are as follows. To the solution of corresponding compound **1** (1 mmol) in THF (5 mL), the anhydrous zinc chloride (30 mg, 0.22 mmol) and corresponding aldehyde (1.2 mmol) were added. The mixture was refluxed for 2–5 h and the solvent was removed in vacuum. The mixture was dissolved in EtOAc (50 mL) and washed by EDTA solution (0.5%, 10 mL), water (3 $\times$ 10 mL) and brine (1 $\times$ 10 mL). The mixture was dried over anhydrous Na<sub>2</sub>SO<sub>4</sub>. The solvent was then evaporated and the product was purified by column chromatography ( $\text{CHCl}_3$ -EtOH 9:1).

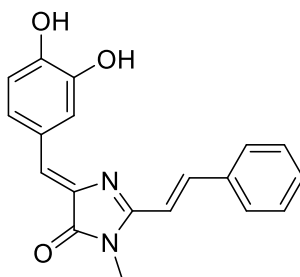


**(Z)-4-(3-cyano-4-hydroxybenzylidene)-1-methyl-2-((E)-styryl)-1H-imidazol-5(4H)-one (3a):**

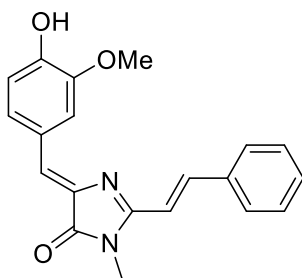
Orange solid (161 mg, 49%); m.p. ~254 °C with decomposition; <sup>1</sup>H NMR (700 MHz, 303 K, DMSO-*d*<sub>6</sub>) δ ppm: 11.77 (br. s., 1H), 8.62 (dd, *J*=8.8, 1.4 Hz, 1H), 8.44 (d, *J*=1.5 Hz, 1H), 8.03 (d, *J*=15.8 Hz, 1H), 7.87 (d, *J*=7.4 Hz, 2H), 7.48 (t, *J*=7.4 Hz, 2H), 7.46–7.43 (m, 1H), 7.25 (d, *J*=15.8 Hz, 1H), 7.14 (d, *J*=8.8 Hz, 1H), 7.00 (s, 1H), 3.29 (s, 3H) (see Figure S55); <sup>13</sup>C NMR (176 MHz, 303 K, DMSO-*d*<sub>6</sub>) δ ppm: 169.8, 161.3, 160.2, 140.4, 138.4, 138.1, 137.2, 135.0, 130.2, 128.9, 128.3, 126.4, 123.1, 116.7, 116.5, 114.0, 99.6, 26.4 (see Figure S56); HRMS (ESI) *m/z*: 330.1237 found (calculated for C<sub>20</sub>H<sub>16</sub>N<sub>3</sub>O<sub>2</sub><sup>+</sup>, [M+H]<sup>+</sup> 330.1237).



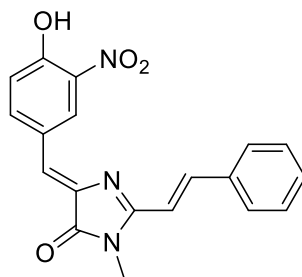
**(Z)-4-(4-hydroxybenzylidene)-1-methyl-2-((E)-styryl)-1H-imidazol-5(4H)-one (3b)<sup>6</sup>**



**(Z)-4-(3,4-dihydroxybenzylidene)-1-methyl-2-((E)-styryl)-1H-imidazol-5(4H)-one (3c):** Dark red solid (109 mg, 34%); m.p. ~224 °C with decomposition; <sup>1</sup>H NMR (700 MHz, 303 K, DMSO-*d*<sub>6</sub>) δ ppm: 8.03 (s, 1H), 7.99 (d, *J*=15.9 Hz, 1H), 7.84 (d, *J*=7.2 Hz, 2H), 7.50–7.43 (m, 4H), 7.23 (d, *J*=15.9 Hz, 1H), 6.88 (s, 1H), 6.81 (d, *J*=8.2 Hz, 1H), 3.27 (s, 3H) (see Figure S57); <sup>13</sup>C NMR (176 MHz, 303 K, DMSO-*d*<sub>6</sub>) δ ppm: 169.9, 158.4, 148.7, 145.3, 139.2, 136.7, 135.2, 129.9, 128.9, 128.1, 126.4, 126.2, 126.1, 118.8, 115.7, 114.2, 26.3 (see Figure S58); HRMS (ESI) *m/z*: 321.1233 found (calculated for C<sub>19</sub>H<sub>17</sub>N<sub>2</sub>O<sub>3</sub><sup>+</sup>, [M+H]<sup>+</sup> 321.1234).

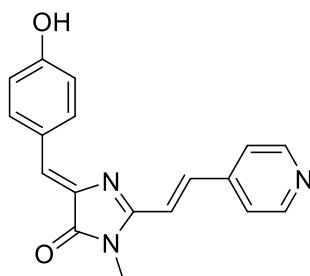


**(Z)-4-(3-methoxy-4-hydroxybenzylidene)-1-methyl-2-((E)-styryl)-1H-imidazol-5(4H)-one (3d):** Orange solid (177 mg, 53%); m.p. = 170–173 °C; <sup>1</sup>H NMR (700 MHz, 303 K, DMSO-*d*<sub>6</sub>) δ ppm: 9.78 (br. s., 1H), 8.15 (s, 1H), 7.97 (d, *J*=15.9 Hz, 1H), 7.83 (d, *J*=7.2 Hz, 2H), 7.70 (d, *J*=8.4 Hz, 1H), 7.53–7.38 (m, 3H), 7.24 (d, *J*=15.9 Hz, 1H), 6.98 (s, 1H), 6.87 (d, *J*=8.2 Hz, 1H), 3.89 (s, 3H), 3.28 (br. s., 3H) (see Figure S59); <sup>13</sup>C NMR (176 MHz, 303 K, DMSO-*d*<sub>6</sub>) δ ppm: 169.9, 158.6, 149.4, 147.6, 139.4, 136.9, 135.1, 130.0, 128.9, 128.2, 127.1, 126.3, 126.1, 115.7, 115.5, 114.1, 55.4, 26.3 (see Figure S60); HRMS (ESI) *m/z*: 335.1390 found (calculated for C<sub>20</sub>H<sub>19</sub>N<sub>2</sub>O<sub>3</sub><sup>+</sup>, [M+H]<sup>+</sup> 335.1391).

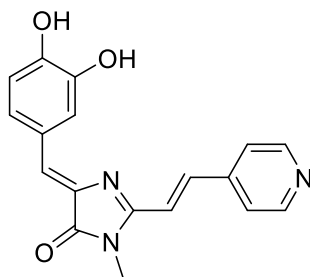


**(Z)-4-(3-nitro-4-hydroxybenzylidene)-1-methyl-2-((E)-styryl)-1H-imidazol-5(4H)-one (3f):**

Red solid (195 mg, 56%); m.p. = 225–228 °C; <sup>1</sup>H NMR (700 MHz, 303 K, DMSO-*d*<sub>6</sub>) δ ppm: 11.61 (br. s., 1H), 8.87 (d, *J*=1.5 Hz, 1H), 8.54 (dd, *J*=8.6, 1.6 Hz, 1H), 8.03 (d, *J*=15.8 Hz, 1H), 7.86 (d, *J*=7.2 Hz, 2H), 7.49 (t, *J*=7.2 Hz, 2H), 7.47–7.44 (m, 1H), 7.26 (d, *J*=15.8 Hz, 1H), 7.23 (d, *J*=8.6 Hz, 1H), 7.06 (s, 1H), 3.29 (s, 3H) (see Figure S61); <sup>13</sup>C NMR (176 MHz, 303 K, DMSO-*d*<sub>6</sub>) δ ppm: 169.8, 160.5, 153.1, 140.5, 138.9, 138.1, 137.2, 135.0, 130.2, 128.9, 128.7, 128.3, 126.0, 122.7, 119.4, 113.9, 26.4 (see Figure S62); HRMS (ESI) *m/z*: 350.1134 found (calculated for C<sub>19</sub>H<sub>16</sub>N<sub>3</sub>O<sub>4</sub><sup>+</sup>, [M+H]<sup>+</sup> 350.1135).

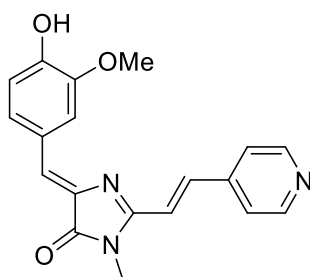


**(Z)-4-(4-hydroxybenzylidene)-1-methyl-2-((E)-2-(pyridin-4-yl)vinyl)-1H-imidazol-5(4H)-one (4b):** The details will be reported in a separate publication.



**(Z)-4-(3,4-dihydroxybenzylidene)-1-methyl-2-((E)-2-(pyridin-4-yl)vinyl)-1H-imidazol-**

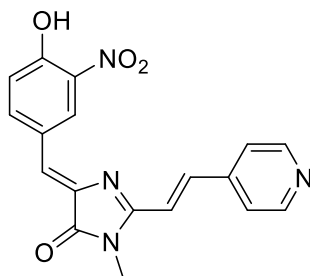
**5(4H)-one (4c):** Brown solid (83 mg, 26%); m.p. ~273 °C with decomposition; <sup>1</sup>H NMR (700 MHz, 303 K, DMSO-*d*<sub>6</sub>) δ ppm: 8.67 (d, *J*=5.9 Hz, 2H), 8.01 (s, 1H), 7.91 (d, *J*=16.0 Hz, 1H), 7.79 (d, *J*=5.9 Hz, 2H), 7.50–7.48 (m, 2H), 6.95 (s, 1H), 6.82 (d, *J*=8.2 Hz, 1H), 3.28 (s, 3H) (see Figure S65); <sup>13</sup>C NMR (176 MHz, 303 K, DMSO-*d*<sub>6</sub>) δ ppm: 169.8, 157.7, 150.3, 149.1, 145.4, 142.2, 136.6, 136.2, 127.8, 126.4, 126.0, 121.9, 119.0, 118.9, 115.8, 26.4 (see Figure S66); HRMS (ESI) *m/z*: 322.1185 found (calculated for C<sub>18</sub>H<sub>16</sub>N<sub>3</sub>O<sub>3</sub><sup>+</sup>, [M+H]<sup>+</sup> 322.1186).



**(Z)-4-(3-methoxy-4-hydroxybenzylidene)-1-methyl-2-((E)-2-(pyridin-4-yl)vinyl)-1H-**

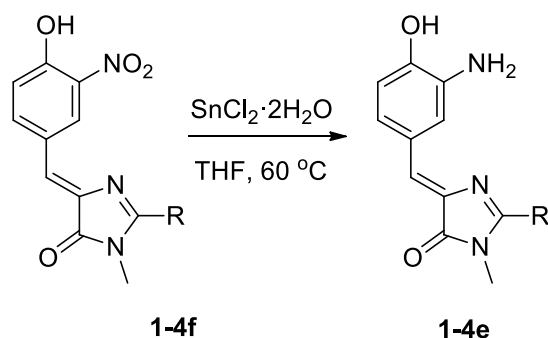
**imidazol-5(4H)-one (4d):** Dark red solid (151 mg, 45%); m.p. = 238–241 °C; <sup>1</sup>H NMR (600 MHz, 303 K, DMSO-*d*<sub>6</sub>) δ ppm: 9.86 (br. s., 1H), 8.66 (d, *J*=5.9 Hz, 2H), 8.12 (d, *J*=1.4 Hz, 1H), 7.90 (d, *J*=15.9 Hz, 1H), 7.79 (d, *J*=5.9 Hz, 2H), 7.74 (dd, *J*=7.9, 1.3 Hz, 1H), 7.50 (d, *J*=15.9 Hz, 1H), 7.05 (s, 1H), 6.88 (d, *J*=8.2 Hz, 1H), 3.88 (s, 3H), 3.29 (s, 3H) (see Figure S67); <sup>13</sup>C NMR (176 MHz, 303 K, DMSO-*d*<sub>6</sub>) δ ppm: 169.7, 157.9, 150.3, 149.7, 147.7, 142.1, 136.8, 136.4, 127.5,

127.4, 126.1, 121.9, 118.8, 115.8, 115.7, 55.5, 26.4 (see Figure S68); HRMS (ESI)  $m/z$ : 336.1343 found (calculated for  $C_{19}H_{18}N_3O_3^+$ ,  $[M+H]^+$  336.1343).

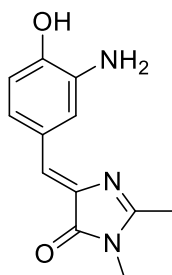


**(Z)-4-(3-nitro-4-hydroxybenzylidene)-1-methyl-2-((E)-2-(pyridin-4-yl)vinyl)-1H-imidazol-5(4H)-one (4f)**: Dark red solid (52 mg, 15%); m.p.  $\sim 243$  °C with decomposition;  $^1H$  NMR (700 MHz, 303 K,  $DMSO-d_6$ )  $\delta$  ppm: 11.68 (br. s., 1H), 8.82 (d,  $J=1.3$  Hz, 1H), 8.68 (br. d.,  $J=4.8$  Hz, 2H), 8.57 (dd,  $J=8.7, 1.3$  Hz, 1H), 7.95 (d,  $J=15.9$  Hz, 1H), 7.80 (d,  $J=5.5$  Hz, 2H), 7.51 (d,  $J=15.9$  Hz, 1H), 7.22 (d,  $J=8.8$  Hz, 1H), 7.13 (s, 1H), 3.30 (br. s., 3H) (see Figure S69);  $^{13}C$  NMR was not recorded due to the extremely low solubility of the compound; HRMS (ESI)  $m/z$ : 351.1088 found (calculated for  $C_{18}H_{15}N_4O_4^+$ ,  $[M+H]^+$  351.1088).

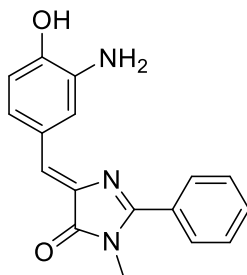
In addition, the general procedure for the reduction of  $NO_2$  group in obtained chromophores (e.g., **2f**, **3f** and **4f**) involves the following steps. The corresponding chromophore (0.55 g, 2 mmol) and tin (II) chloride dihydrate (3.53 g, 17 mmol) were suspended in 10 mL of THF (see Scheme S4). The mixture was refluxed for 3 h. Afterwards it was neutralized with 10%  $Na_2CO_3$  solution, filtered, extracted with dichloromethane (4 $\times$ 75 mL) and dried over  $Na_2SO_4$ . The solvent was evaporated and the crude product was purified by column chromatography ( $CHCl_3$ -EtOH 32:1).



**Scheme S4.** Synthesis of compounds **1-4e** starting from **1-4f** with functional group substitutions at the R site (R = Me, Ph, styryl, or (pyridin-4-yl)vinyl).

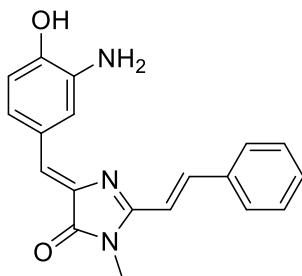


**(Z)-4-(3-amino-4-hydroxybenzylidene)-1,2-dimethyl-1H-imidazol-5(4H)-one (1e):** Orange solid (378 mg, 82%); m.p. ~225 °C with decomposition;  $^1\text{H}$  NMR (700 MHz, 303 K, DMSO- $d_6$ )  $\delta$  ppm: 7.58 (d,  $J=1.9$  Hz, 1H), 7.21 (dd,  $J=8.1, 1.8$  Hz, 1H), 6.73 (s, 1H), 6.70 (d,  $J=8.1$  Hz, 1H), 3.08 (s, 3H) 2.32 (s, 3H) (see Figure S43);  $^{13}\text{C}$  NMR (176 MHz, 303 K, DMSO- $d_6$ )  $\delta$  ppm: 169.8, 161.4, 147.0, 136.7, 135.7, 126.7, 125.7, 123.0, 116.9, 114.2, 26.1, 15.1 (see Figure S44); HRMS (ESI)  $m/z$ : 232.1079 found (calculated for  $\text{C}_{12}\text{H}_{14}\text{N}_3\text{O}_2^+$ ,  $[\text{M}+\text{H}]^+$  232.1081).



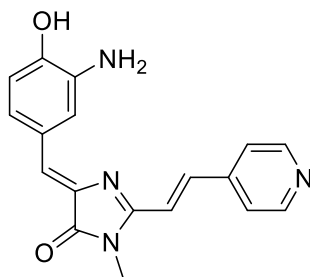
**(Z)-4-(3-amino-4-hydroxybenzylidene)-1-methyl-2-phenyl-1H-imidazol-5(4H)-one (2e):**

Orange solid (193 mg, 33%); m.p. ~223 °C with decomposition; <sup>1</sup>H NMR (700 MHz, 303 K, DMSO-*d*<sub>6</sub>) δ ppm: 7.93 (d, *J*=7.1 Hz, 2H), 7.71 (d, *J*=1.3 Hz, 1H), 7.62 (t, *J*=7.1 Hz, 1H), 7.59 (t, *J*=7.2 Hz, 2H), 7.29 (dd, *J*=8.2, 1.3 Hz, 1H), 6.95 (s, 1H), 6.74 (d, *J*=8.2 Hz, 1H) 3.25 (s, 3H) (see Figure S53); <sup>13</sup>C NMR (176 MHz, 303 K, DMSO-*d*<sub>6</sub>) δ ppm: 170.5, 160.2, 147.6, 136.9, 135.7, 131.1, 129.3, 129.0, 128.7, 128.6, 125.9, 123.8, 117.1, 114.3, 28.5 (see Figure S54); HRMS (ESI) *m/z*: 294.1237 found (calculated for C<sub>17</sub>H<sub>16</sub>N<sub>3</sub>O<sub>2</sub><sup>+</sup>, [M+H]<sup>+</sup> 294.1237).



**(Z)-4-(3-amino-4-hydroxybenzylidene)-1-methyl-2-((E)-styryl)-1H-imidazol-5(4H)-one (3e):**

Red solid (305 mg, 48%); m.p. ~146 °C with decomposition; <sup>1</sup>H NMR (700 MHz, 303 K, DMSO-*d*<sub>6</sub>) δ ppm: 8.04 (d, *J*=15.8 Hz, 1H), 7.90–7.82 (m, 3H), 7.48 (t, *J*=7.4 Hz, 2H), 7.43 (t, *J*=7.4 Hz, 1H), 7.25–7.20 (m, 2H), 6.82 (s, 1H), 6.74 (d, *J*=8.2 Hz, 1H), 3.27 (s, 3H) (see Figure S63); <sup>13</sup>C NMR (176 MHz, 303 K, DMSO-*d*<sub>6</sub>) δ ppm: 170.0, 157.9, 147.4, 139.2, 136.8, 136.4, 135.3, 129.8, 128.9, 128.1, 127.1, 126.3, 123.7, 117.1, 114.3, 114.0, 26.3 (see Figure S64); HRMS (ESI) *m/z*: 320.1393 found (calculated for C<sub>19</sub>H<sub>18</sub>N<sub>3</sub>O<sub>2</sub><sup>+</sup>, [M+H]<sup>+</sup> 320.1394).



**(Z)-4-(3-amino-4-hydroxybenzylidene)-1-methyl-2-((E)-2-(pyridin-4-yl)vinyl)-1H-imidazol-5(4H)-one (4e):** Dark red solid (173 mg, 27%); m.p. ~214 °C with decomposition; <sup>1</sup>H NMR (700 MHz, 303 K, DMSO-*d*<sub>6</sub>) δ ppm: 8.67 (br. s., 2H), 7.97 (d, *J*=15.8 Hz, 1H), 7.87 (s, 1H), 7.79 (d, *J*=4.8 Hz, 2H), 7.48 (d, *J*=15.8 Hz, 1H), 7.27 (d, *J*=7.8 Hz, 1H), 6.89 (s, 1H), 6.75 (d, *J*=8.2 Hz, 1H), 3.28 (s, 3H) (see Figure S70); <sup>13</sup>C NMR (176 MHz, 303 K, DMSO-*d*<sub>6</sub>) δ ppm: 169.8, 157.3, 150.3, 147.7, 142.3, 136.9, 136.2, 136.2, 128.4, 126.2, 124.1, 121.9, 118.8, 117.2, 114.3, 26.3 (see Figure S71); HRMS (ESI) *m/z*: 321.1345 found (calculated for C<sub>18</sub>H<sub>17</sub>N<sub>4</sub>O<sub>2</sub><sup>+</sup>, [M+H]<sup>+</sup> 321.1346).

Notably, the steady-state electronic spectral data (absorption and emission) of these newly synthesized, unlocked GFP chromophore derivatives in aqueous solution (see Figure 3 in main text) are listed in Table S7 with fluorescence quantum yield (FQY) values in Table S8 (vide infra). Particularly regarding the emission of the anionic form to substantiate our proposed color tuning strategy uncovered in this work (Scheme 2), the corresponding fluorescence spectra of the unlocked HBDIs with various EDG and EWG substituents at opposite ends of the conjugated chromophore ring system are shown in Figure S7 (vide infra). We expect that the conjugated EWGs would better stabilize the LUMO than EDGs because the EWGs promote ICT. This effort represents a broader phase space for the bioinspired design and synthesis to effectively engineer and tune these functional chromophore motifs for controllable fluorescence emission in solution.

We also stress that our current borylation methodology for GFP chromophore derivatives as shown above includes the action of boron tribromide, which is incompatible with a number of functional groups proposed here (see Scheme S3 above or Table S5 below for example).<sup>7</sup> That is why we highlight the red-shifted emission in Scheme 2 while explicitly stating that locking of the GFP chromophore derivatives could achieve high brightness, which overcomes one practical obstacle of using the synthesized unlocked GFP chromophore derivatives with low FQY (see Figure 3 in main text, and Tables S7 and S8 below) for bioimaging. Fortunately, there are plenty of other aryl borylation approaches that can be perspectivevely used for creating the locked derivatives.<sup>8</sup> For instance, the palladium-catalyzed reactions of the corresponding ortho-halogenated derivatives can be used.<sup>9</sup> Moreover, amino group can be introduced by the sequential nitration and reduction of the corresponding borylated phenols. Since our current work conveys and validates a new concept of synergistic tuning of the electronic ground and excited states with an additive effect and a generalizable “double-donor-one-acceptor” design concept to achieve redder and brighter fluorescence emission, we hope to inspire future chemical synthesis methods and bioimaging applications to realize the full potential of mechanism-driven biomimetics (Scheme 2) so more results can be presented as demonstrated facts in the near future for a broader science and engineering community.

## ESI Figures

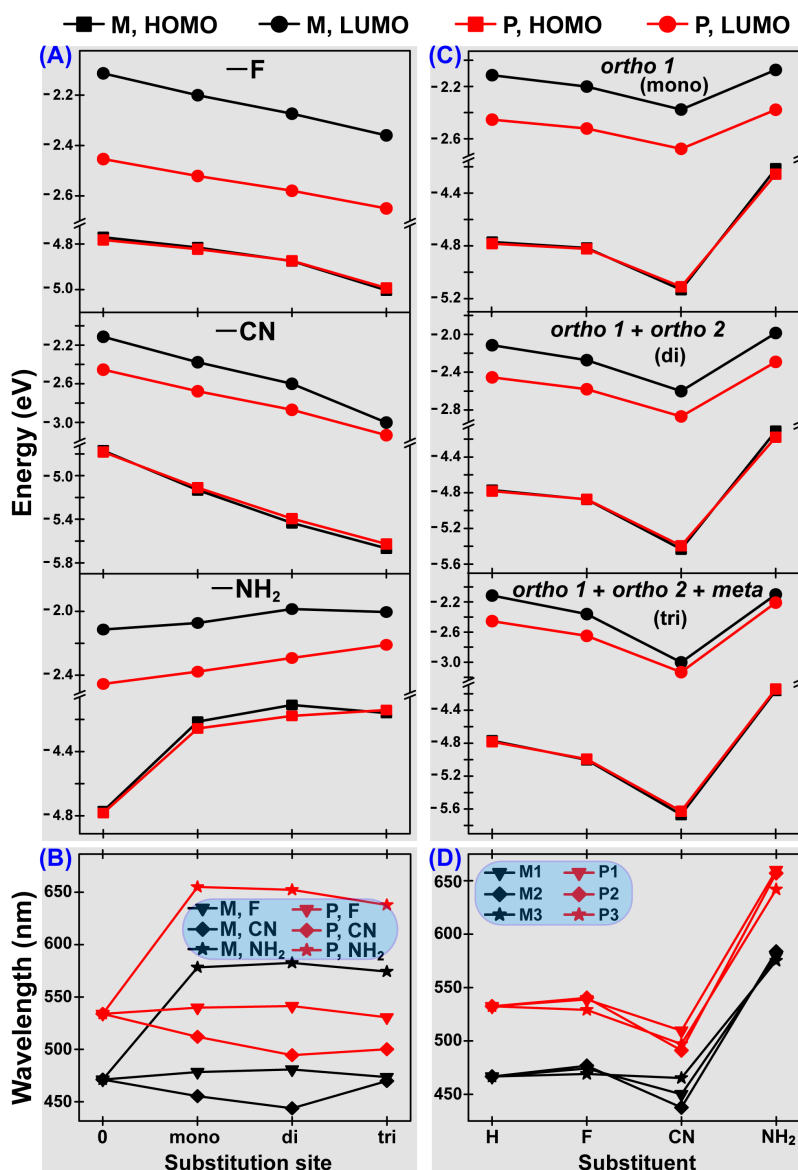


**Figure S1.** (A, B) Calculated HOMO and LUMO energies (A) and gaps (B) of cumulative substitutions at different sites at the phenolate ring. (C, D) Calculated HOMO and LUMO energies (C) and gaps (D) of cumulative substitutions by different substituents. The information in the right panels is identical to the left panels, highlighting the parametric dependence of energy trends.

Notably, data analyses in predicting trends of energy gap change and solvatochromism are more reliable for the structurally similar molecules studied here (e.g., the MnF and PnF series).

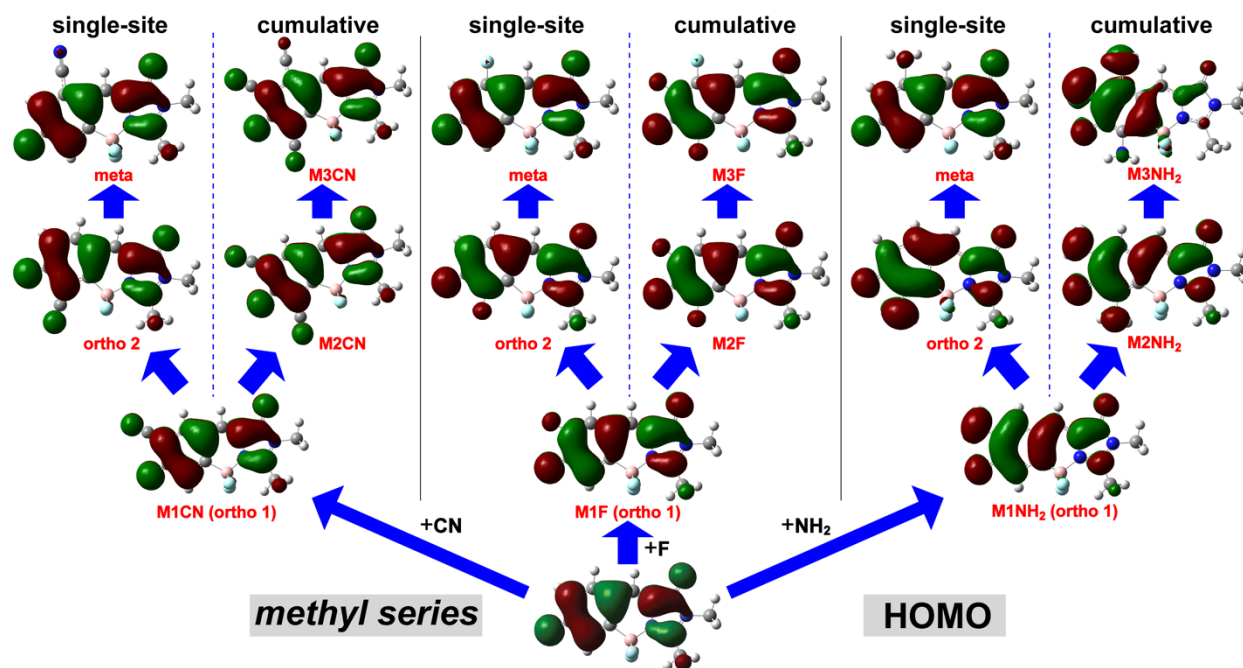


**Figure S2.** HOMO electron density distribution of the single-site and cumulative substitutions at phenolate by  $-\text{CN}$ ,  $-\text{F}$ ,  $-\text{NH}_2$  with methyl incorporated at the 2-position of imidazolinone ring.

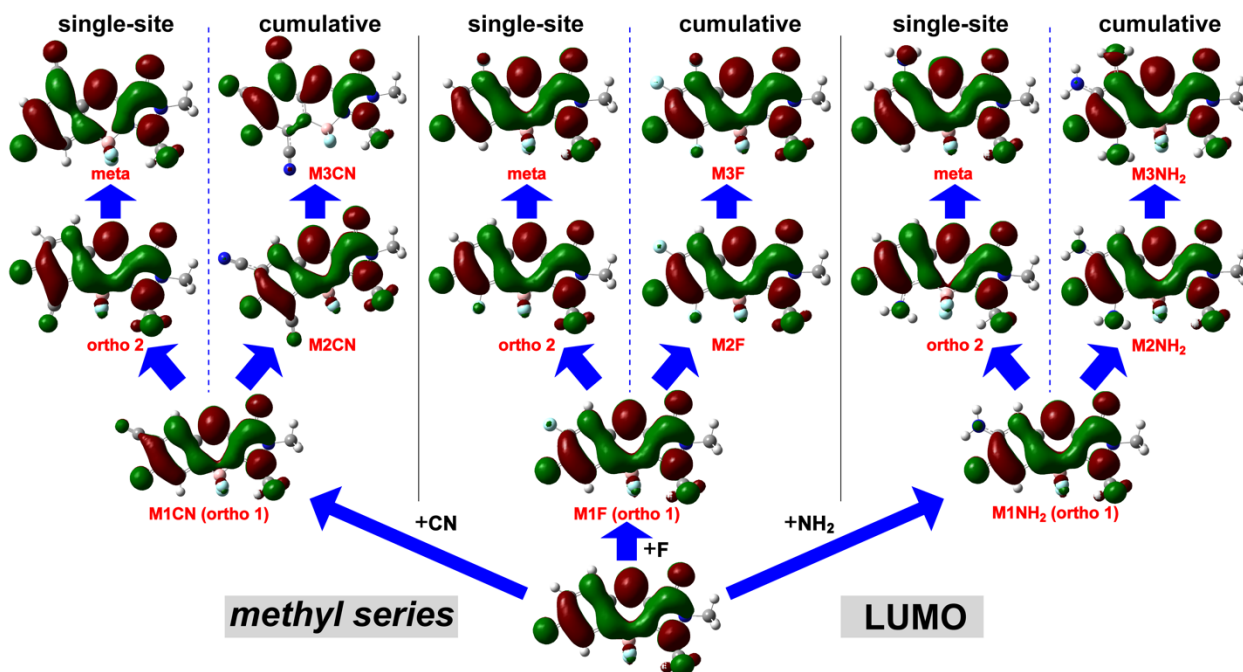


**Figure S3.** LUMO electron density distribution of the single-site and cumulative substitutions at phenolate by  $-\text{CN}$ ,  $-\text{F}$ ,  $-\text{NH}_2$  with methyl incorporated at the 2-position of imidazolinone ring.

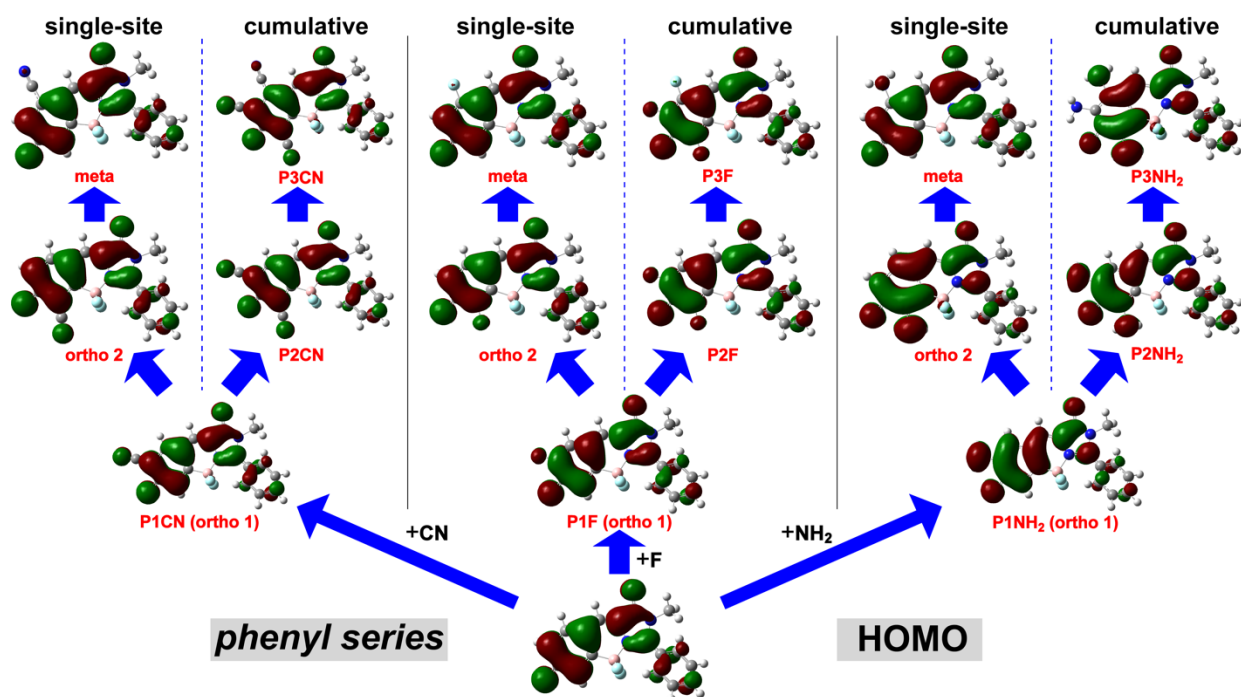


**Figure S4.** HOMO electron density distribution of the single-site and cumulative substitutions at phenolate by  $-\text{CN}$ ,  $-\text{F}$ ,  $-\text{NH}_2$  with phenyl incorporated at the 2-position of imidazolinone ring.

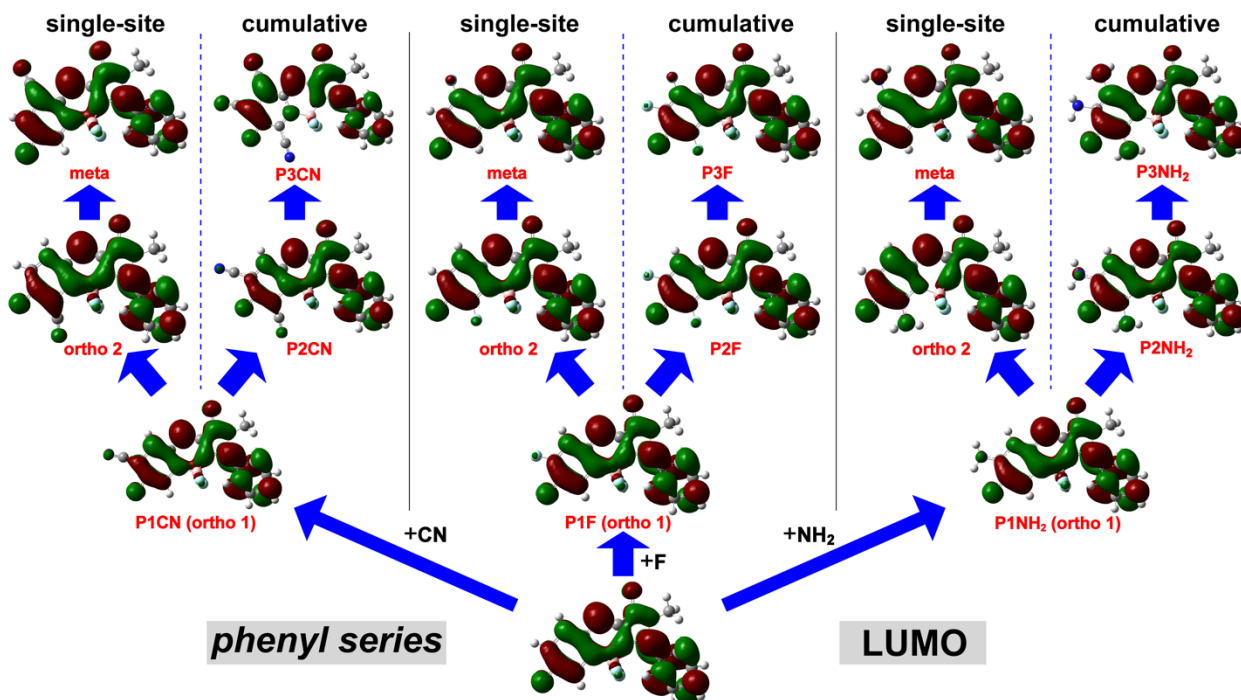


**Figure S5.** LUMO electron density distribution of the single-site and cumulative substitutions at phenolate by  $-\text{CN}$ ,  $-\text{F}$ ,  $-\text{NH}_2$  with phenyl incorporated at the 2-position of imidazolinone ring.

## NOTES for Figure S1–S5:

1. EWGs (e.g., –F, –CN) exhibit a clear additive effect from mono- to tri-substitution while EDGs (e.g., –NH<sub>2</sub>) do not (see Figure S1A). This is probably because EDGs restructure the electron density distribution due to the adjacent electron-donating –O<sup>(-)</sup> (see Scheme 1 and 2 for the chemical structure of the chromophore). In contrast, EWGs do not exert a notable effect on the  $\pi$ -electron structure due to the push-pull mechanism (Figure S2–S5).
2. At the electron-rich sites, stronger EWGs lower the orbital energy more than weak EWGs (e.g., –CN > –F on the phenolate ring, see Figure 2 and S1); stronger EDGs increase the orbital energy more than weak EDGs (e.g., –NH<sub>2</sub> > –OCH<sub>3</sub> > –CH<sub>3</sub>, see Table S5).
3. Interestingly, at the electron-poor sites, e.g., *meta* site in HOMO, both –CN and –F stabilize the HOMO as well (see Figure 2). It is probably because EWGs induce electron migration from nearby sites and hence achieve better electron delocalization (Figure S2 and S4). In contrast, –NH<sub>2</sub> only slightly destabilizes HOMO due to a small orbital overlap between the nitrogen atom and the phenolate ring.
4. The BF<sub>2</sub> group (i.e., for conformational locking) may change the electron density at the conjugated chromophore ring system but to a lesser extent than the donor and acceptor groups on the phenolate and imidazolinone rings on opposite ends (see Scheme 1).<sup>7a</sup>
5. Our DFT and TD-DFT calculations of the locked chromophore PnF series (see Scheme 1) show that the dihedral angles between the sidechain phenyl and backbone imidazolinone rings differ by >20° from the electronic ground to excited state, indicative of the ring twisting in S<sub>1</sub>. Since the optimized excited state geometry is not fully planar, steric hindrance may reduce the overall chromophore twisting and improve fluorescence to some extent.<sup>10</sup> On the other hand, such twisting motions in the excited state could lead to internal

conversion from the higher-lying emissive state ( $>S_1$ ) to a lower-lying dark  $S_1$  state<sup>11</sup> or the electronic ground state  $S_0$  via an  $S_1/S_0$  conical intersection,<sup>12</sup> in accord with the lower FQY (by an approximately two-fold decrease) observed for the phenyl series in comparison to its methyl counterparts (Table 1). In general, the deviation from molecular planarity and the increase of flexibility or rotatability of the sidechain (e.g., phenyl ring) could work collectively to enhance nonradiative relaxation pathways and quench radiative emission (i.e., fluorescence).<sup>2,7a,11,13</sup> The quantitative effect on the FQY cannot be predicted due to the complex solution environment and an intricate interplay between the chromophore backbone flexibility and sidechain flexibility, hence an experimental characterization is necessary as the data shown in Table 1 (main text) and Table S8 (see below).

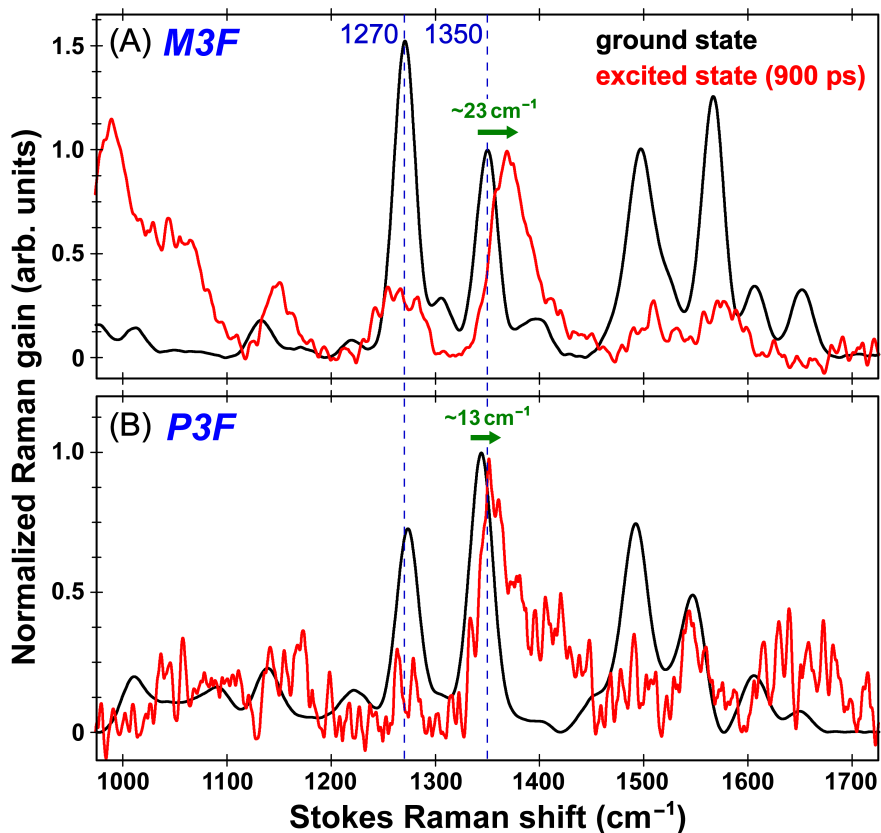


**Figure S6.** Comparison of the excited and ground state vibrational modes in Stokes FSRS spectra for the anionic (A) M3F and (B) P3F in water. The excited state spectrum was taken at 900 ps after 400 nm photoexcitation of the neutral chromophore (i.e., it is then dominated by the anionic modes due to ultrafast ESPT on the sub-picosecond time scale). For ground state FSRS, the Raman pump is at 560 nm. For excited state FSRS, the Raman pump is at 520 nm for M3F and 560 nm for P3F (to account for their different electronic profiles and achieve pre-resonance Raman enhancement). The clear blue shift of the marker band at  $\sim 1350\text{ cm}^{-1}$  is denoted by the green arrow, which represents a key spectroscopic evidence for the occurrence of intramolecular charge transfer (ICT) in the excited state of the anionic chromophore from the phenolate (donor) to the imidazolinone (acceptor) ring. As a result, the imidazolinone ring C–N stretching mode at  $\sim 1350\text{ cm}^{-1}$  (see Table S1) exhibits a frequency blue shift, while the shifted peak is broader due to its  $S_1$  nature.

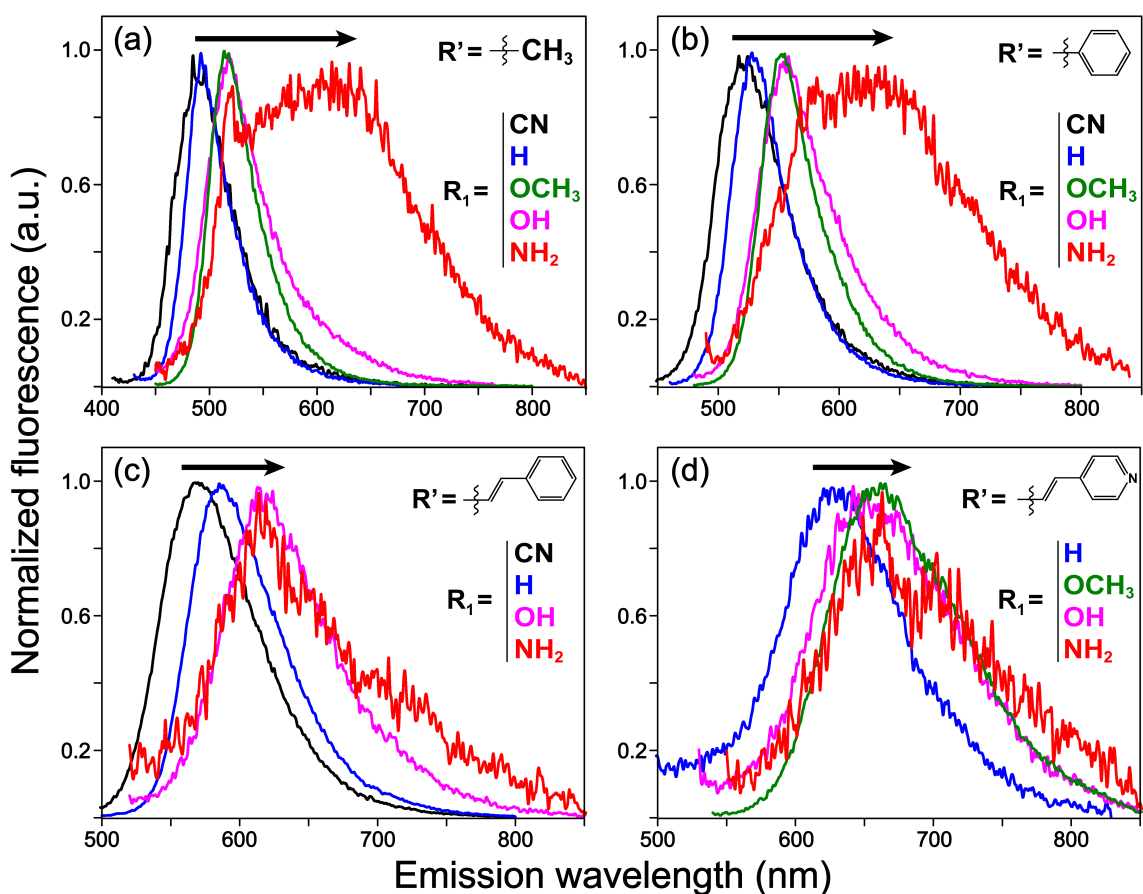


**Figure S7.** Steady-state emission spectra of the anionic form of the newly synthesized unlocked HBDI derivatives with various substitutions at the  $R_1$  and  $R'$  sites (see Figure 3 inset and Table S7 below for the chemical structure of the GFP model chromophore). The signal-to-noise ratio is low mainly due to the weak emission of these unlocked compounds in aqueous solution, exhibiting the effect of significant nonradiative decay pathways (see main text, and Table S8 below for the measured FQYs).<sup>2,7a</sup> The color-coded spectra display a notable fluorescence peak frequency redshift as the electron-donating capability increases at the  $R_1$  site (black arrow in each panel) and as the electron-withdrawing/conjugation capability increases at the  $R'$  site (panel a→d).

Such a detailed and informative comparison becomes feasible for the precisely substituted chromophores in solution, enabling deeper mechanistic insights into the dependence of emission properties on the electronic structure and charge distribution over the chromophore ring system.

## ESI Tables

**Table S1.** Ground state Raman mode assignments for MnF and PnF in basic aqueous solution

	freq. <sup>a</sup>	M1F	M2F	M3F	P1F	P2F	P3F	vibrational motions (major)
Mode 1	exp.	1268	1265	1271	1270	1267	1274	Imidazolinone ring deformation, bridge-H rocking, phenolate ring deformation and ring-H rocking <sup>c</sup>
	calc. <sup>b</sup>	1270	1263	1264	1273	1267	1268	
Mode 2	exp.	1335	1341	1350	1336	1338	1344	Imidazolinone C–N stretching, bridge-H rocking, phenolate ring-H rocking <sup>c</sup>
	calc. <sup>b</sup>	1346	1346	1336	1346	1344	1330	

<sup>a</sup>The Raman mode frequency in cm<sup>-1</sup> unit.

<sup>b</sup>The ground state vibrational normal mode frequencies are calculated by density functional theory (DFT) at the RB3LYP level with 6-311G(d,p) basis sets of the geometrically optimized anionic chromophore structure using the Gaussian 09 software.<sup>14</sup> Water is used as solvent in the integral equation formalism variant polarizable continuum model (IEFPCM). The frequency scaling factor is 0.99.

<sup>c</sup>Phenolate ring-H rocking motions are suppressed as the ring becomes fluorinated. The M3F and P3F have no phenolate ring-H motions due to complete substitution at those sites (i.e., H→F). The higher sensitivity of mode 2 to the photoinduced ICT is likely due to its main composition of the C–N stretching motion that is more localized on the imidazolinone ring (see Figure S6 above).

**Table S2.** Absorption and emission maxima (in nm)<sup>a</sup> of anionic MnF in various solvents

Solvent	solvent parameters <sup>b</sup>			M0F		M1F		M2F		M3F	
	$\pi^*$	$\beta$	$\alpha$	$\lambda_{abs}$	$\lambda_{em}$	$\lambda_{abs}$	$\lambda_{em}$	$\lambda_{abs}$	$\lambda_{em}$	$\lambda_{abs}$	$\lambda_{em}$
Water	1.09	0.4	1.17	485	520	485	528	479	532	474	520
MeOH	0.6	0.62	0.93	498	531	498	535	493	536	490	530
EtOH	0.54	0.77	0.83	512	532	514.5	536	511	537	500	529
Dioxane	0.49	0.37	0	529	541	506	530	504	531	504	529
EtOAc	0.45	0.45	0	533	543	507	530.5	505	533	498	529
CH <sub>2</sub> Cl <sub>2</sub>	0.73	0	0.3	536	551	514	540	510	540	509	540
Et <sub>2</sub> O	0.24	0.47	0	539	543	502	531	507	530	455	533
ACN	0.66	0.31	0.19	533	540	537	545	533	545	501	535
THF	0.55	0.55	0	536	544	512	543.5	509	534.5	509	535
Toluene	0.49	0.11	0	535	543	511	530.5	511	531.5	509	530
DMSO	1.0	0.76	0	538	545	542	549.5	539	548	528	540
Acetone	0.62	0.48	0.08	531	552	543	547.5	540	548	505	537
DMF	0.88	0.69	0	543	550	548	552	545	546	531	539
Pyridine	0.87	0.64	0	543	551	548	553	547	554	536	544

<sup>a</sup> The UV-Visible and emission spectra were recorded with a Varian Cary 100 and Agilent Cary Eclipse fluorescence spectrophotometer, respectively.

<sup>b</sup> The solvent parameters from literature.<sup>15</sup>

**Table S3.** Absorption and emission maxima (in nm) of anionic PnF in various solvents

Solvent	solvent parameters			P0F		P1F		P2F		P3F	
	$\pi^*$	$\beta$	$\alpha$	$\lambda_{abs}$	$\lambda_{em}$	$\lambda_{abs}$	$\lambda_{em}$	$\lambda_{abs}$	$\lambda_{em}$	$\lambda_{abs}$	$\lambda_{em}$
Water	1.09	0.4	1.17	512	545	511	555	508	558	499	545
MeOH	0.6	0.62	0.93	526	565	527	572	521	568	516	563
EtOH	0.54	0.77	0.83	534	570	537	572	537	576	530	566
Dioxane	0.49	0.37	0	497	–	535	591	535	591	526	580
EtOAc	0.45	0.45	0	537	590	528	594	537	590	528	580
CH <sub>2</sub> Cl <sub>2</sub>	0.73	0	0.3	543	591	548	594	543	593	530	585
Et <sub>2</sub> O	0.24	0.47	0	540	593	543	598	540	594	532	583
ACN	0.66	0.31	0.19	545	584	551	600	535	591	535	583
THF	0.55	0.55	0	–	588	545	600	541	597	532	584
Toluene	0.49	0.11	0	541	594	545	600	543	592	533	585
DMSO	1.0	0.76	0	551	604	557	604	554	602	545	587
Acetone	0.62	0.48	0.08	547	600	554	604	553	601	533	586
DMF	0.88	0.69	0	549	599	555	606	553	603	546	587
Pyridine	0.87	0.64	0	553	605	547	608	543	604	538	594

**Table S4.** Kamlet-Taft analysis<sup>a</sup> for the anionic form of MnF and PnF in solution

Compound		<i>a</i>	<i>b</i>	<i>p</i>	$\nu_0$	<i>R</i> <sup>b</sup>
M0F	Abs.	1.5	0	-0.1	18.7	0.95
	Em.	0.7	0	-0.2	18.4	0.86
M1F	Abs.	1.3	-1.0	-1.5	20.4	0.80
	Em.	0.4	-0.5	-0.7	19.1	0.79
M2F	Abs.	1.5	-1.0	-1.3	20.3	0.81
	Em.	0.3	-0.3	-0.7	19.1	0.75
M3F	Abs.	1.3	-0.5	-2.3	21.3	0.74
	Em.	0.5	-0.1	-0.5	19.0	0.82
P0F	Abs.	0.7	-0.4	-0.5	19.0	0.52
	Em.	1.2	-0.2	-0.2	16.9	0.94
P1F	Abs.	0.9	-0.2	-0.4	18.6	0.75
	Em.	1.1	-0.1	-0.2	16.8	0.95
P2F	Abs.	0.9	-0.4	-0.2	18.6	0.83
	Em.	1.0	-0.2	-0.3	17.0	0.96
P3F	Abs.	0.9	-0.6	-0.2	19.0	0.85
	Em.	0.9	0	-0.1	17.1	0.93

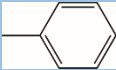
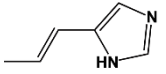
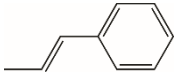
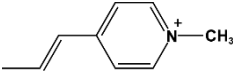
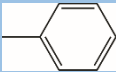
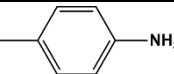
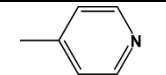
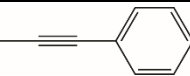
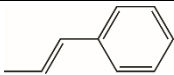
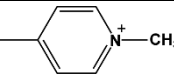
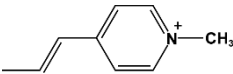
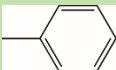
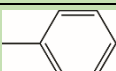
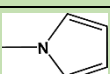
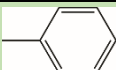
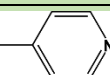
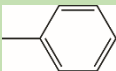
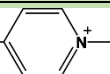
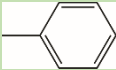
<sup>a</sup> Kamlet-Taft analysis characterizes solvatochromism by correlating the spectral shift ( $\nu$ , in  $10^3$   $\text{cm}^{-1}$  unit that is also the unit for  $\nu_0$ ) of solute with solvent parameters that measure the hydrogen bond donating ( $\alpha$ , or acidity, see Tables S2 and S3), hydrogen bond accepting ( $\beta$ , or basicity), and dipolarity/polarizability ( $\pi^*$ , polar solvating) properties.

$$\nu = \nu_0 + a\alpha + b\beta + p\pi^*$$

Such a linear regression analysis was shown to work well with the locked HBDI anion absorption and emission data.<sup>7a</sup> In the same context, the positive coefficient *a* and mostly negative coefficient *b* values can also be rationalized as the decreased solvent acidity and increased solvent basicity (see Tables S2 and S3) correlates with the redshift of anionic chromophore emission, indicating that the anionic chromophore is a weaker base in the excited state than that in the ground state, in accord with excited state ICT (i.e., from the phenolate to the imidazolinone ring). The negative coefficient *p* value, indicating a smaller dipole in  $S_1$ , also supports the excited-state ICT.

<sup>b</sup> The linear correlation coefficient from the multivariable regression fits (a statistics measure).

**Table S5.** Simulated HOMO and LUMO energies and gaps with different functional groups at the phenolate and imidazolinone ring sites of the anionic chromophore in water<sup>a</sup>

R <sub>1</sub>	R'	HOMO (eV)	LUMO (eV)	Gap (nm)
-H		- 4.782670	- 2.454190	532.5 <sup>b</sup>
-H	-COCH <sub>3</sub>	- 5.114924	- 2.956244	574.4
-H		- 4.894783	- 2.796786	591.0
-H		- 4.664575	- 2.600319	600.6 <sup>c</sup>
-H		- 4.745665	- 2.759506	624.2
-H		- 5.135876	- 3.492853	754.6 <sup>d</sup>
-NH <sub>2</sub>		- 4.256132	- 2.377458	660.0
-NH <sub>2</sub>		- 4.159260	- 2.200040	632.8
-NH <sub>2</sub>		- 4.365522	- 2.612292	707.2
-NH <sub>2</sub>		- 4.364978	- 2.711886	750.0
-NH <sub>2</sub>		- 4.342664	- 2.689029	750.0
-NH <sub>2</sub>		- 4.280622	- 2.672430	771.0
-NH <sub>2</sub>		- 4.677364	- 3.268903	880.3
-NH <sub>2</sub>		- 4.689065	- 3.383463	949.6 <sup>d</sup>
-CH <sub>3</sub>		- 4.714916	- 2.425078	541.5
-OCH <sub>3</sub>		- 4.568247	- 2.408207	574.0
		- 4.760087	- 2.533652	556.9
		- 4.877640	- 2.552155	533.2
		- 5.132883	- 2.730390	516.1

<sup>a</sup> See Scheme 1 in main text for substitution sites of the locked HBDI chromophore. The ortho 1 site is selected as the single substitution site to evaluate the emission wavelength trend (as shown in Figure 2a). The HOMO and LUMO energies are calculated by TD-DFT at the RB3LYP level with 6-311G(d,p) basis sets from the geometrically optimized chromophore in Gaussian 09 (IEFPCM = water).<sup>14</sup>

<sup>b</sup> This configuration serves as a reference point because it represents P0F (see main text) that we have collected experimental data on its optical properties (Table 1). In comparison to the anionic P0F emission at 545 nm, the calculated HOMO-LUMO energy gap of 532.5 nm is slightly bluer (see Figure 1c lower panel). This could be due to the transient ICT character of the fluorescent state in water which differs from the TD-DFT calculated electronic excited state, and the complex solute-solvent interaction that cannot be fully described by the IEFPCM solvation model. However, the calculated energy gap for structurally similar molecules with specific substitutions provides systematic, useful information about the effect of EWGs and EDGs with different strengths and sizes on HOMO, LUMO energies and the resultant fluorophore emission wavelength.

<sup>c</sup> This R' group is reminiscent of the Kaede-like red fluorescent protein (RFP) chromophore<sup>10,16</sup> wherein a bridge ethylene double bond exists between the His-ring and the imidazolinone ring of the core HBDI-like conjugated  $\pi$ -ring system.

<sup>d</sup> This combination achieves the reddest emission with the -H (or -NH<sub>2</sub>) group at R<sub>1</sub> due to an effective Donor- $\pi$ -Acceptor configuration<sup>17</sup> across the locked HBDI molecular scaffold with the specific substituents. This clear trend suggests the effective strategy of incorporating a strong EDG (e.g., -NH<sub>2</sub>) near the phenolate end (i.e., adjacent to the phenolate O<sup>(-)</sup> group) to destabilize the HOMO energy, simultaneously incorporating a conjugated moiety with EWG character (e.g., picolinium moiety, increasing the quantum box size)<sup>17a</sup> at the imidazolinone end to stabilize the

LUMO energy (see Scheme 2 in main text), therefore leading to much redder emission (e.g., ~950 nm in the near-IR region, highlighted by the semi-transparent red cell). Note that the fluorescence quantum yield for such designed compounds may be low (e.g., <1%) which can be mitigated by further locking the ethylene fragment.<sup>10</sup> Moreover, it may be beneficial to turn some of these compounds into fluorogenic dyes that do not fluoresce in free state, but become highly emissive upon binding targets like RNA or proteins<sup>18</sup> as powerful and versatile biosensors.

**Table S6.** Ground and excited state acidities of the MnF and PnF compounds in water<sup>a</sup>

	<b>M0F</b>	<b>M1F</b>	<b>M2F</b>	<b>M3F</b>
$pK_a$	6.4	5.8	4.7	4.2
$pK_a^*$	- 2.3	- 3.3	- 4.7	- 5.0
	<b>P0F</b>	<b>P1F</b>	<b>P2F</b>	<b>P3F</b>
$pK_a$	7.5	6.1	4.9	4.2
$pK_a^*$	- 1.3	- 3.4	- 5.2	- 5.5

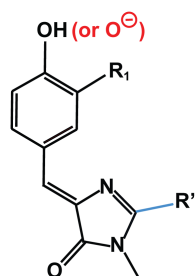
<sup>a</sup>The  $pK_a$  values of the anionic forms of MnF and PnF compounds were measured by titration of 10–20  $\mu$ M chromophore in water.

The excited-state  $pK_a$  (i.e.,  $pK_a^*$ ) of the synthetic fluorophores can be calculated by the Förster equation:<sup>2,7a</sup>

$$pK_a^* = pK_a - \frac{hc}{2.303k_B T} \left( \frac{1}{\lambda_{HA}} - \frac{1}{\lambda_{A^-}} \right)$$

We used the electronic absorption peak wavelengths (see Table 1 in main text, because some emission peak wavelengths of the chromophore cannot be accurately measured due to extremely fast ESPT reaction in water)<sup>7a</sup> to approximate the electronic transition gaps for both the acid and base forms of the synthesized series of fluorophores at room temperature (~295 K).

**Table S7.** Photophysical properties of the synthesized unlocked fluorophores (general chemical structure depicted below) with different R<sub>1</sub> and R' substituents



R <sub>1</sub>	R'	CH <sub>3</sub>							
		HA	A <sup>-</sup>	HA	A <sup>-</sup>	HA	A <sup>-</sup>	HA	A <sup>-</sup>
CN	Abs.	371	408	382	434	426	465	–	–
	Em. <sup>a</sup>	481	485	475	520	535	570	–	– <sup>b</sup>
H	Abs.	367	425	390	454	424	490	430	511
	Em. <sup>a</sup>	453	491	479	526	528	585	545	626
OH <sup>c</sup>	Abs.	379	442	401	474	437	511	446	529
	Em. <sup>a</sup>	475	518	500	555	542	617	575	657
OCH <sub>3</sub>	Abs.	378	448	402	480	370	408	442	536
	Em. <sup>a</sup>	471	515	495	552	465	488 <sup>d</sup>	581	660
NH <sub>2</sub>	Abs.	388	454	412	486	448	523	450	543
	Em. <sup>a</sup>	474	~600	–	~620	–	~620	~582	~650

<sup>a</sup> The emission peak wavelengths of the anionic chromophores in aqueous solution are highlighted in red and the experimental spectral data are shown above (Figure S7, and Figure 3 in main text).

<sup>b</sup> The synthesis of HBDI-derived compounds with the CN substitutions became generally more challenging and they underwent various degrees of decomposition especially upon heating. This particular CN | C=C-pyridine substitution only yielded traces of the target compound in the product mixture which could not be purified for further spectroscopic characterization.

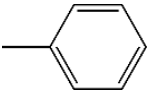
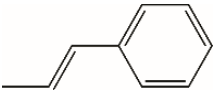
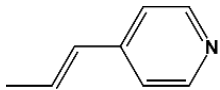
<sup>c</sup> In basic aqueous solution that the anionic form dominates, this hydroxyl group becomes –O<sup>(-)</sup>.

<sup>d</sup> The anomaly of observed spectral data of this compound could be due to the methoxy group being electron-donating by resonance but also electron withdrawing by the inductive effect of the O atom,

which can be specifically affected by the substituted (*E*)-styryl group at the R' site of the imidazolinone ring.

Notably, such a comprehensive comparison and mechanistic elucidation (see main text, Schemes 1 and 2) are enabled by the systematic investigation of precisely modified chromophores that arise from the functionalization of the GFP core in solution (i.e., outside a complex protein matrix wherein the nearby residues exert various effects on the embedded chromophore). Though this series of newly synthesized unlocked “double-donor-one-acceptor” chromophores following the design strategy proposed in Scheme 2 exhibit small FQYs (see Table S8 below), the clear trend of emission wavelength redshift upon adding EDGs at the phenolate “donor” site (going down the column) and adding EWGs at the imidazolinone “acceptor” site (going rightward in each row) substantiates the fundamental principle and opens the door to future engineering efforts to synthesize the locked version of the fluorophores that can provide further advantages for a broad range of imaging applications. In particular, we reported that the locked M0F (520 nm) and M2F (530 nm) anionic chromophore has redder emission than the unlocked M0F (~500 nm) and M2F (500 nm) in water, respectively.<sup>2</sup> In an earlier report, the synthesized chromophores 4b and 4d are the BF<sub>2</sub>-locked versions of two chromophores in this work (Fig. 3) with R<sub>1</sub>=H, R'=styryl and R<sub>1</sub>=H, R'=vinylpyridine, respectively, and the former two “locked” chromophores in their anionic forms (representative values: 639 nm and 681 nm in EtOH) indeed exhibit redder emission than the latter two compounds (representative values: 585 nm and 626 nm in water, see Table S7 above). Given the smaller magnitude of peak wavelength change expected from water to EtOH as <20 nm (Table S3), the aforementioned redshift of >50 nm provides convincing evidence that BF<sub>2</sub> locking is effective to achieve emission redshift. Moreover, the FQYs have been demonstrated to increase significantly in a conformationally locked chromophore versus an unlocked version.<sup>2,7,10,19</sup>

**Table S8.** Fluorescence quantum yield (FQY)<sup>a</sup> of the synthesized unlocked fluorophores (general chemical structure depicted above Table S7) with different R<sub>1</sub> and R' substituents

R <sub>1</sub> \ R'		CH <sub>3</sub>							
		HA	A <sup>-</sup>	HA	A <sup>-</sup>	HA	A <sup>-</sup>	HA	A <sup>-</sup>
CN	FQY, %	0.2	0.2	0.2	0.08	0.1	0.1	- <sup>b</sup>	- <sup>b</sup>
H	FQY, %	0.03	0.06	0.04	0.08	0.2	0.2	0.03	0.03
OH	FQY, %	0.06	0.06	0.04	0.06	0.1	0.05	0.06	0.03
OCH <sub>3</sub>	FQY, %	0.06	0.1	0.08	0.1	0.05	0.09	0.2	0.1
NH <sub>2</sub>	FQY, %	0.04	0.05	- <sup>c</sup>	0.02	- <sup>c</sup>	0.03	0.07	0.02

<sup>a</sup> The FQYs for the synthesized compounds were measured according to the procedure described in literature<sup>20</sup> with use of quinine sulfate dihydrate (green), coumarin 153 (blue), fluorescein (magenta), rhodamine 6G (red), and rhodamine 101 (cyan) as standards. The FQYs were calculated by the formula:

$$\Phi_x = \Phi_{st} \times \frac{F_x}{F_{st}} \times \frac{f_{st}}{f_x} \times \frac{n_x^2}{n_{st}^2}$$

where  $F$  is the integrated area under the emission peak,  $f$  is the absorption factor (see below),  $n$  is the refractive index of the solvent at the emission peak wavelength (ideally at the mean or average emission wavelength),  $\Phi$  is the quantum yield, the subscript  $x$  corresponds to the novel compounds, and the subscript  $st$  represents the standards. And to obtain the electronic absorption factor:

$$f = 1 - 10^{-A}$$

where  $A$  is the absorbance (unit in optical density) at the excitation wavelength.

<sup>b</sup> Not synthesized (see Table S7 above).

<sup>c</sup> Unavailable due to the extremely fast ESPT and low quantum yield. Note that all the measured FQYs in this table are the percentage values, equivalent to ( $\times 10^{-2}$ ).

Notably, the FQYs of these synthesized unlocked compounds are very small ( $\leq 2 \times 10^{-3}$ ), which pose challenges to measure them accurately due to significant difference from the highly emissive standards (see those color-coded dyes above) being used. One significant digit of the FQY is used to summarize the experimental data with an upper limit in Table S8 for comparison. A general observation is that the R<sub>1</sub> substituents on the phenolate “donor” ring with more electron-donating (ED) capabilities (e.g., going down the column) do not exert a clear trend in FQY, the same holds true for the R’ substituents on the imidazolinone “acceptor” ring with more electron-withdrawing (EW) capabilities (e.g., going rightward along each row). For the anionic fluorophore with the vinylpyridine substituent, the associated FQYs are the smallest (the rightmost column) among all the synthesized compounds tabulated, indicating that a large flexible sidechain like the vinylpyridine could effectively facilitate nonradiative relaxation pathways of S<sub>1</sub> species hence reduce fluorescence intensity.<sup>7a,10-11,21</sup>

In essence, the locked or unlocked scaffolds are not the hurdle to apply this red-shifting rational design principle firmly supported by Fig. 3. Since conformational locking of the chromophore rings to reach coplanarity has been demonstrated to result in redder fluorescence emission,<sup>2,7a,10</sup> we envision that our current work can inspire further chemical synthesis methods to efficiently achieve the locked “double-donor-one-acceptor” compound (see Scheme 2), thereby realizing the full potential of synergistic tuning of the electronic ground and excited states in one conjugated/compact molecular framework as well as an NIR fluorophore with a much improved FQY that can directly benefit the bioimaging community.

## ESI References

- 1 P. Štěpánek, T. Y. Cowie, M. Šafařík, J. Šebestík, R. Pohl and P. Bouř, *ChemPhysChem*, 2016, **17**, 2348-2354.
- 2 C. Chen, W. Liu, M. S. Baranov, N. S. Baleeva, I. V. Yampolsky, L. Zhu, Y. Wang, A. Shamir, K. M. Solntsev and C. Fang, *J. Phys. Chem. Lett.*, 2017, **8**, 5921-5928.
- 3 S. Kojima, H. Ohkawa, T. Hirano, S. Maki, H. Niwa, M. Ohashi, S. Inouye and F. I. Tsuji, *Tetra. Lett.*, 1998, **39**, 5239-5242.
- 4 C.-Y. Lee, Y.-C. Chen, H.-C. Lin, Y. Jhong, C.-W. Chang, C.-H. Tsai, C.-L. Kao and T.-C. Chien, *Tetrahedron*, 2012, **68**, 5898-5907.
- 5 S. Chatterjee and P. Karuso, *Tetra. Lett.*, 2016, **57**, 5197-5200.
- 6 I. V. Yampolsky, A. A. Kislukhin, T. T. Amatov, D. Shcherbo, V. K. Potapov, S. Lukyanov and K. A. Lukyanov, *Bioorg. Chem.*, 2008, **36**, 96-104.
- 7 (a) M. S. Baranov, K. A. Lukyanov, A. O. Borissova, J. Shamir, D. Kosenkov, L. V. Slipchenko, L. M. Tolbert, I. V. Yampolsky and K. M. Solntsev, *J. Am. Chem. Soc.*, 2012, **134**, 6025-6032; (b) M. S. Baranov, K. M. Solntsev, N. S. Baleeva, A. S. Mishin, S. A. Lukyanov, K. A. Lukyanov and I. V. Yampolsky, *Chem. Eur. J.*, 2014, **20**, 13234-13241.
- 8 J. W. B. Fyfe and A. J. B. Watson, *Chem*, 2017, **3**, 31-55.
- 9 W. K. Chow, O. Y. Yuen, P. Y. Choy, C. M. So, C. P. Lau, W. T. Wong and F. Y. Kwong, *RSC Adv.*, 2013, **3**, 12518-12539.
- 10 N. S. Baleeva, K. A. Myannik, I. V. Yampolsky and M. S. Baranov, *Eur. J. Org. Chem.*, 2015, **2015**, 5716-5721.
- 11 H. Qian, M. E. Cousins, E. H. Horak, A. Wakefield, M. D. Liptak and I. Aprahamian, *Nat. Chem.*, 2017, **9**, 83-87.

- 12 (a) B. G. Levine and T. J. Martínez, *Annu. Rev. Phys. Chem.*, 2007, **58**, 613-634; (b) T. Kumpulainen, B. Lang, A. Rosspeintner and E. Vauthey, *Chem. Rev.*, 2017, **117**, 10826-10939.
- 13 Y. Hong, J. W. Y. Lam and B. Z. Tang, *Chem. Soc. Rev.*, 2011, **40**, 5361-5388.
- 14 M. J. Frisch, G. W. Trucks, H. B. Schlegel, G. E. Scuseria, M. A. Robb, J. R. Cheeseman, G. Scalmani, V. Barone, B. Mennucci, G. A. Petersson, et al., *Gaussian 09*, Revision B.1, Gaussian, Inc., Wallington, CT, 2009.
- 15 M. J. Kamlet, J.-L. M. Abboud, M. H. Abraham and R. W. Taft, *J. Org. Chem.*, 1983, **48**, 2877-2887.
- 16 F. V. Subach and V. V. Verkhusha, *Chem. Rev.*, 2012, **112**, 4308-4327.
- 17 (a) N. Karton-Lifshin, L. Albertazzi, M. Bendikov, P. S. Baran and D. Shabat, *J. Am. Chem. Soc.*, 2012, **134**, 20412-20420; (b) B. Dereka, M. Koch and E. Vauthey, *Acc. Chem. Res.*, 2017, **50**, 426-434.
- 18 (a) H. Huang, N. B. Suslov, N.-S. Li, S. A. Shelke, M. E. Evans, Y. Koldobskaya, P. A. Rice and J. A. Piccirilli, *Nat. Chem. Biol.*, 2014, **10**, 686-691; (b) C. L. Walker, K. A. Lukyanov, I. V. Yampolsky, A. S. Mishin, A. S. Bommarius, A. M. Duraj-Thatte, B. Azizi, L. M. Tolbert and K. M. Solntsev, *Curr. Opin. Chem. Biol.*, 2015, **27**, 64-74; (c) N. V. Povarova, N. G. Bozhanova, K. S. Sarkisyan, R. Gritcenko, M. S. Baranov, I. V. Yampolsky, K. A. Lukyanov and A. S. Mishin, *J. Mater. Chem. C*, 2016, **4**, 3036-3040.
- 19 Y.-H. Hsu, Y.-A. Chen, H.-W. Tseng, Z. Zhang, J.-Y. Shen, W.-T. Chuang, T.-C. Lin, C.-S. Lee, W.-Y. Hung, B.-C. Hong, et al., *J. Am. Chem. Soc.*, 2014, **136**, 11805-11812.
- 20 C. Würth, M. Grabolle, J. Pauli, M. Spieles and U. Resch-Genger, *Nat. Protoc.*, 2013, **8**, 1535-1550.

- 21 (a) N. Amdursky, Y. Erez and D. Huppert, *Acc. Chem. Res.*, 2012, **45**, 1548-1557; (b) C. Fang, L. Tang, B. G. Oscar and C. Chen, *J. Phys. Chem. Lett.*, 2018, **9**, 3253–3263.

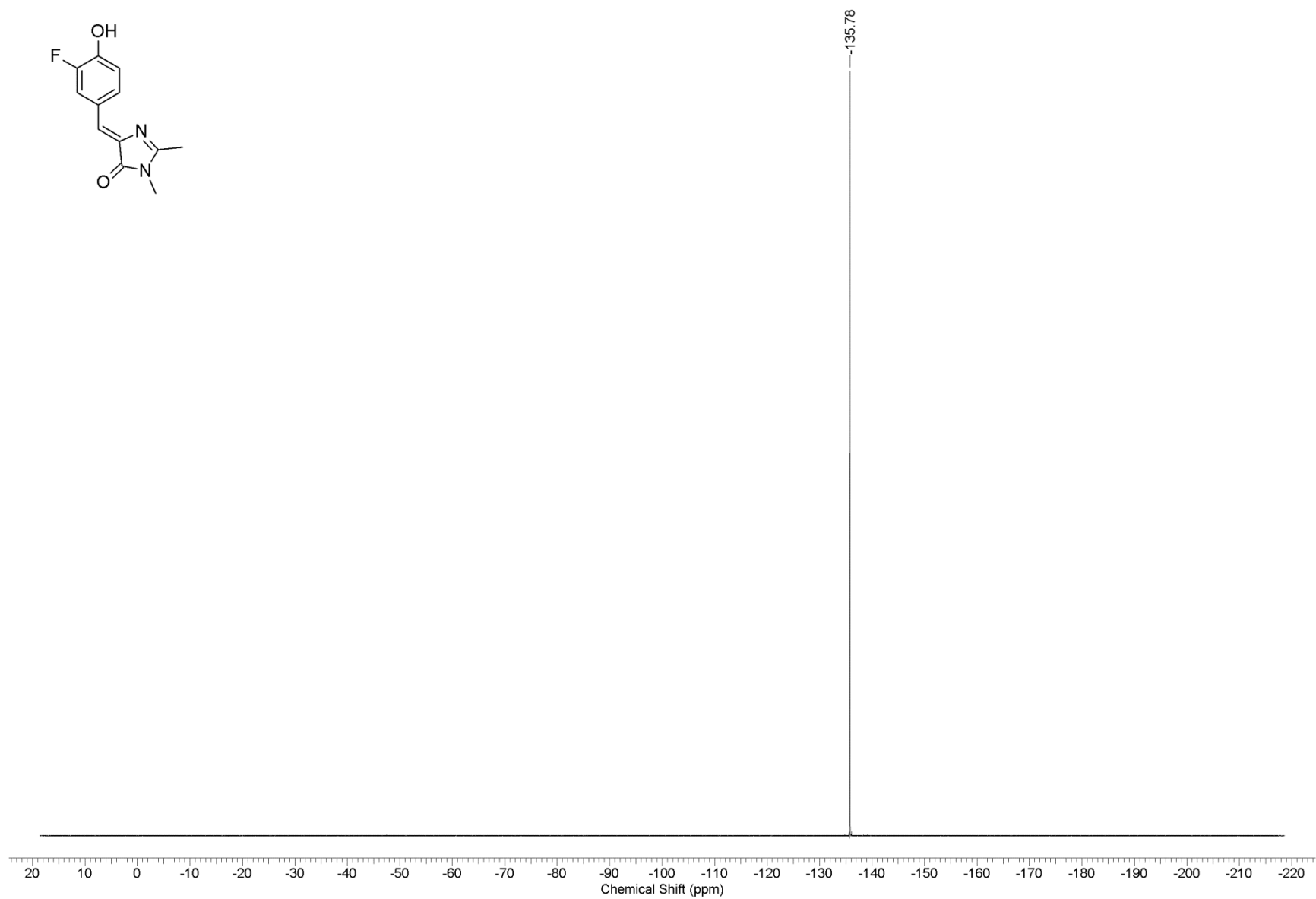


**Figure S8.** <sup>19</sup>F NMR spectrum of (Z)-4-(3-fluoro-4-hydroxybenzylidene)-1,2-dimethyl-1*H*-imidazol-5(4*H*)-one

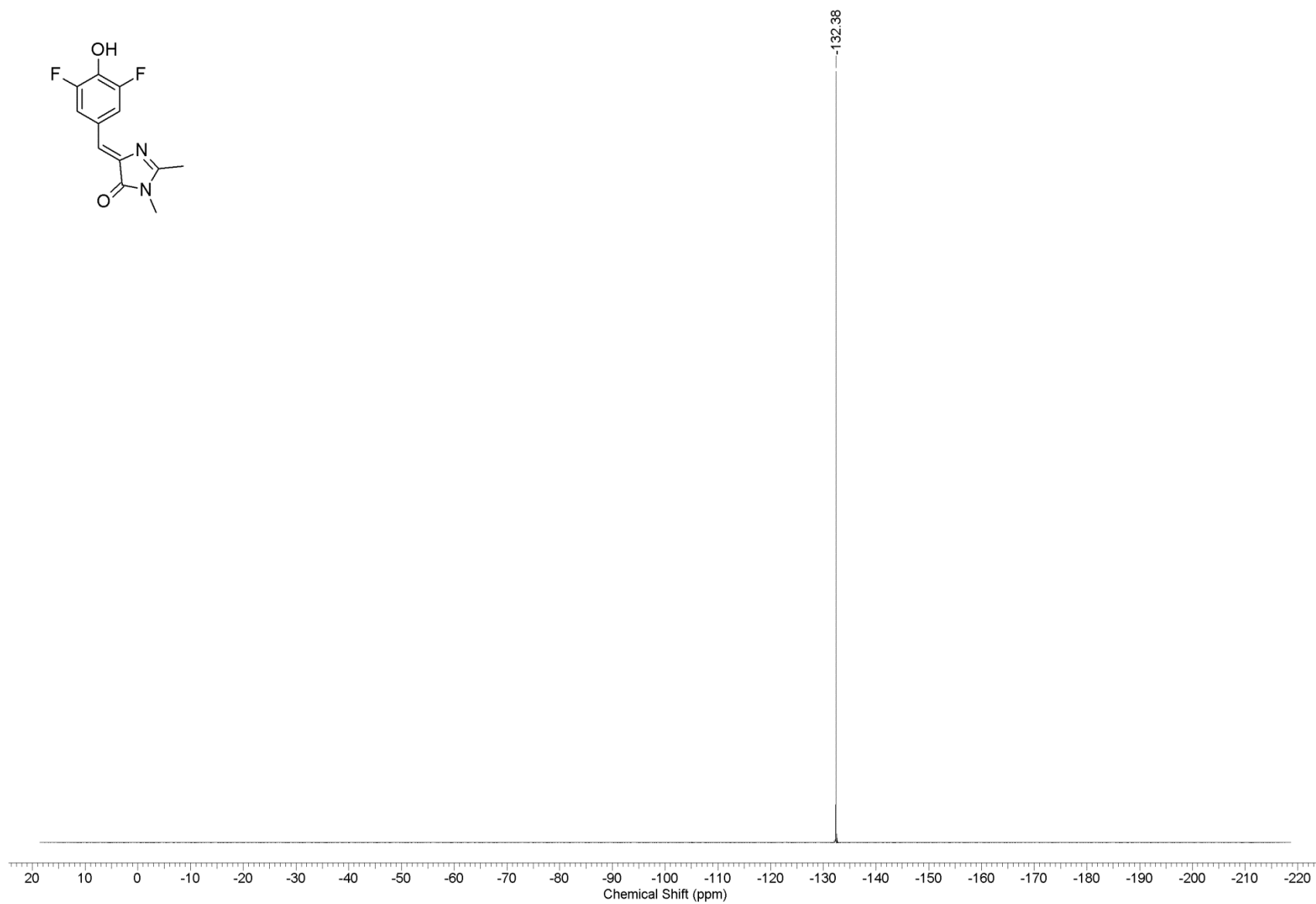


**Figure S9.** <sup>19</sup>F NMR spectrum of (Z)-4-(3,5-difluoro-4-hydroxybenzylidene)-1,2-dimethyl-1H-imidazol-5(4H)-one

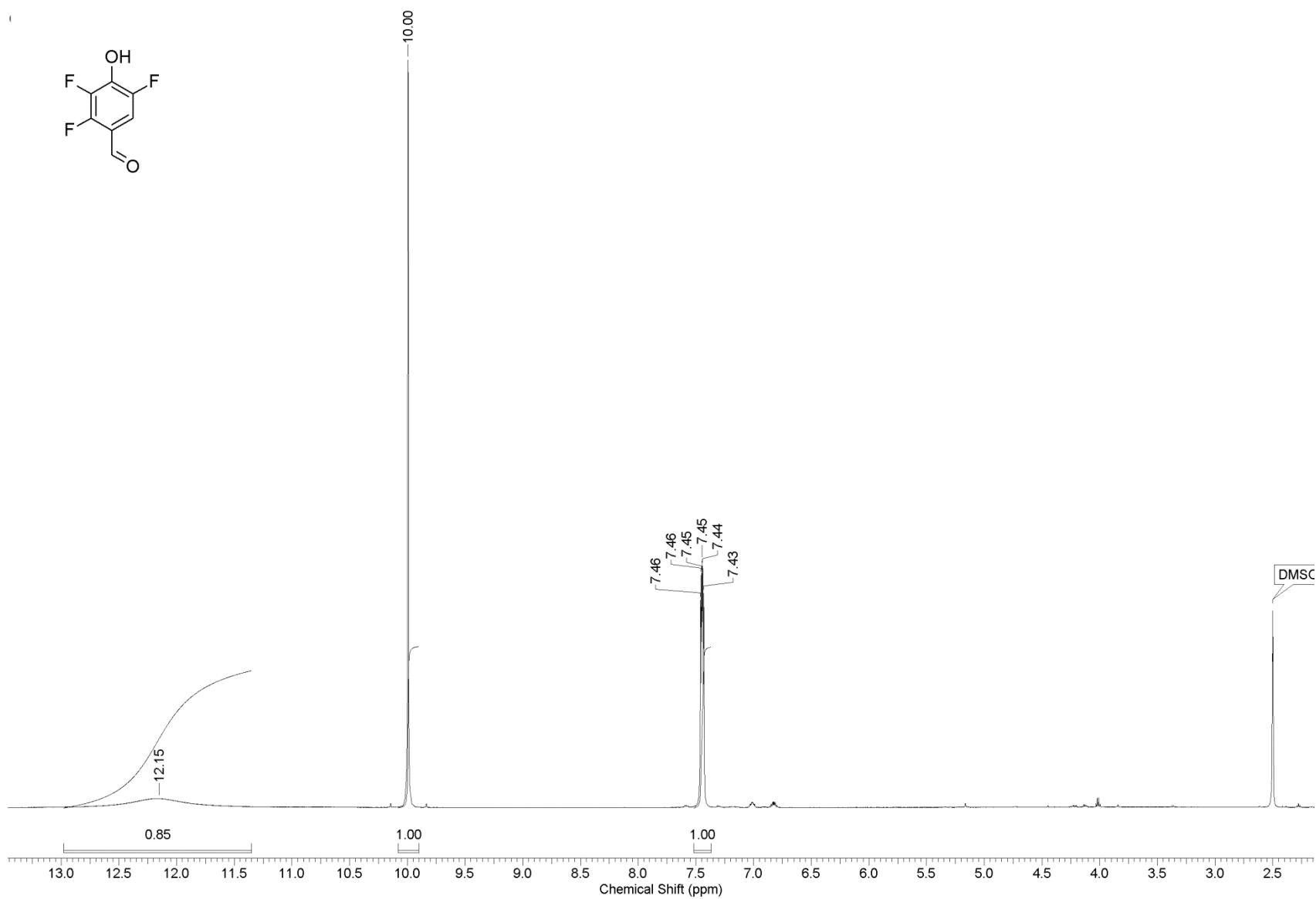


**Figure S10.**  $^1\text{H}$  NMR spectrum of 2,3,5-trifluoro-4-hydroxybenzaldehyde

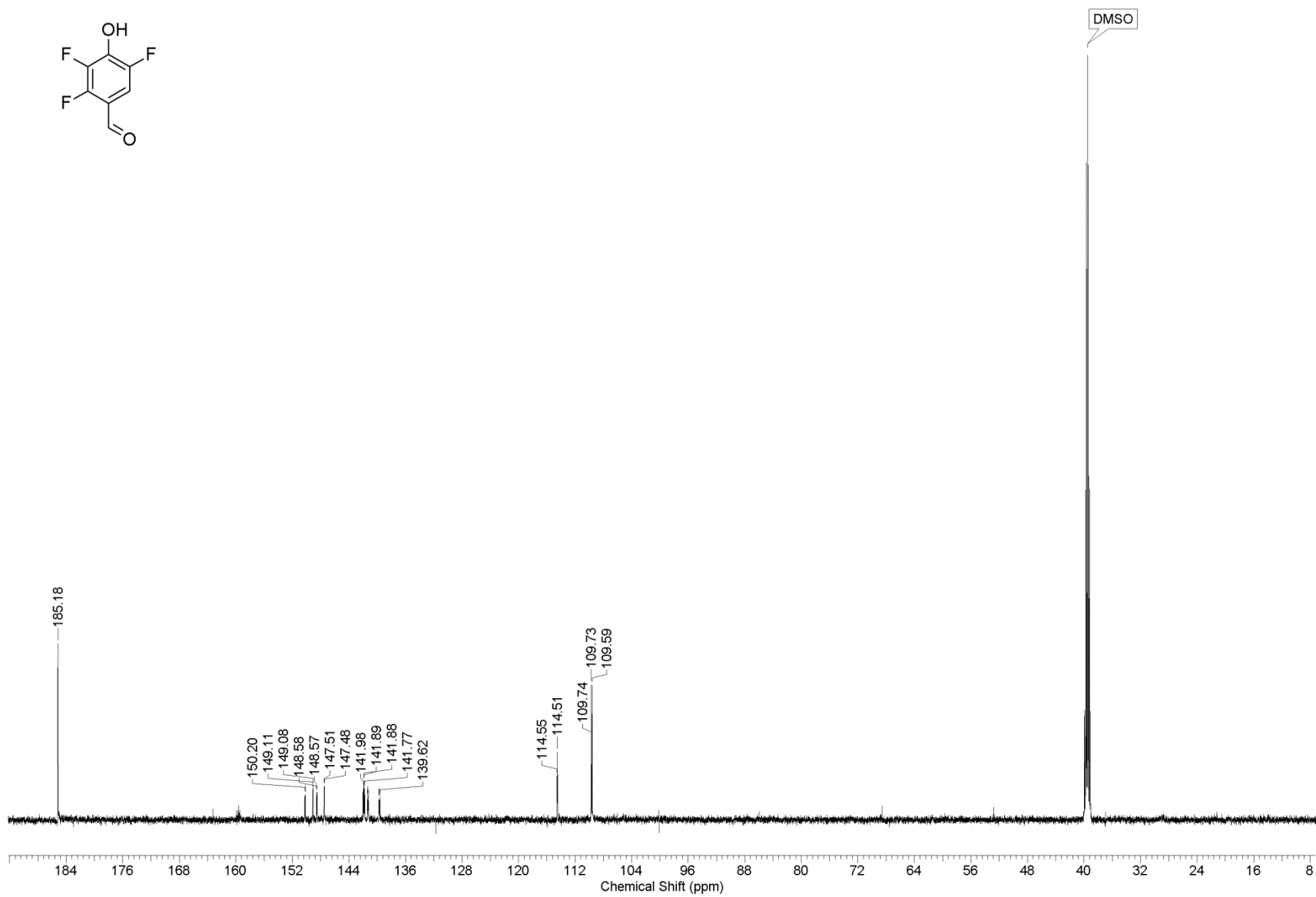
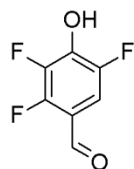
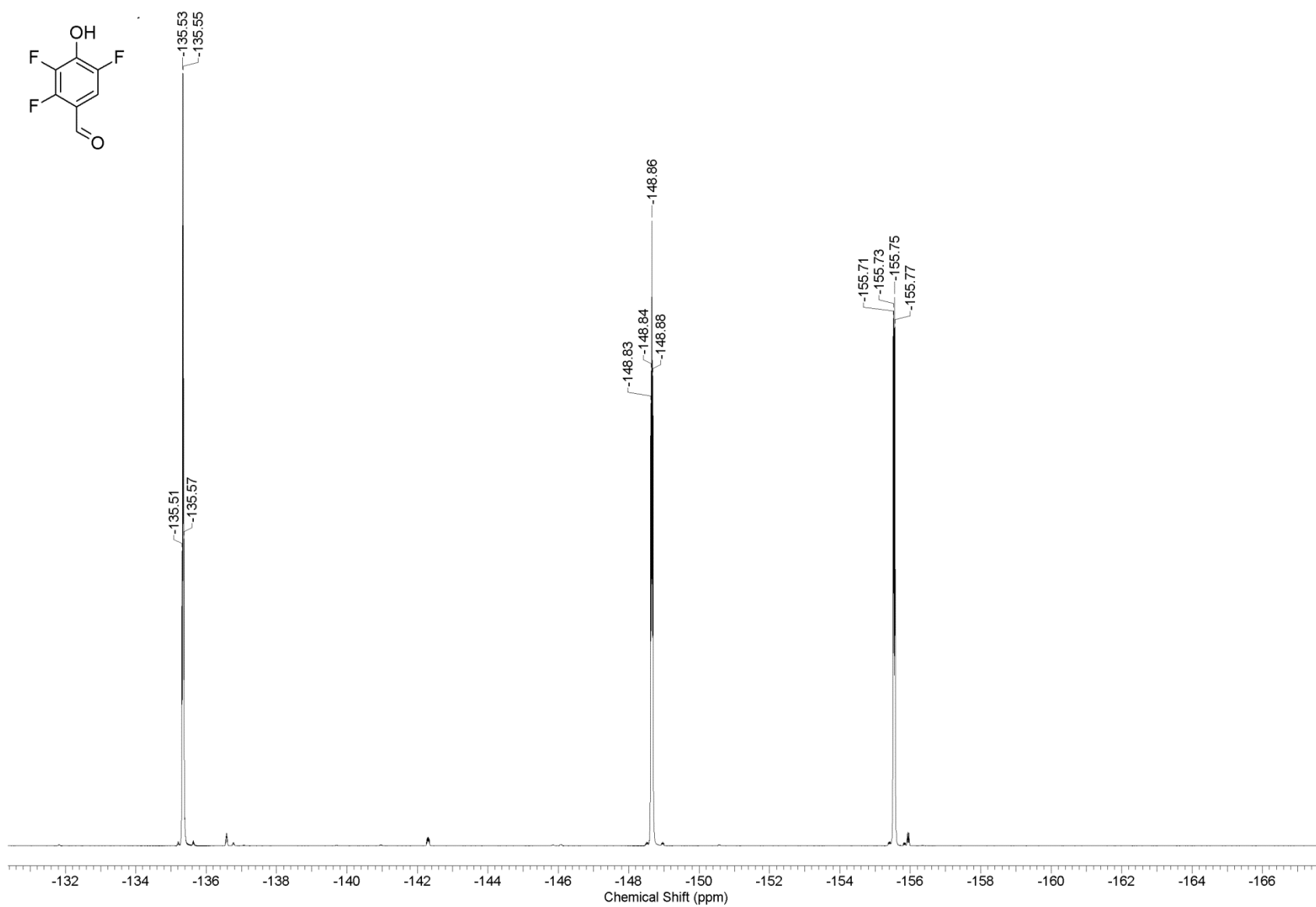
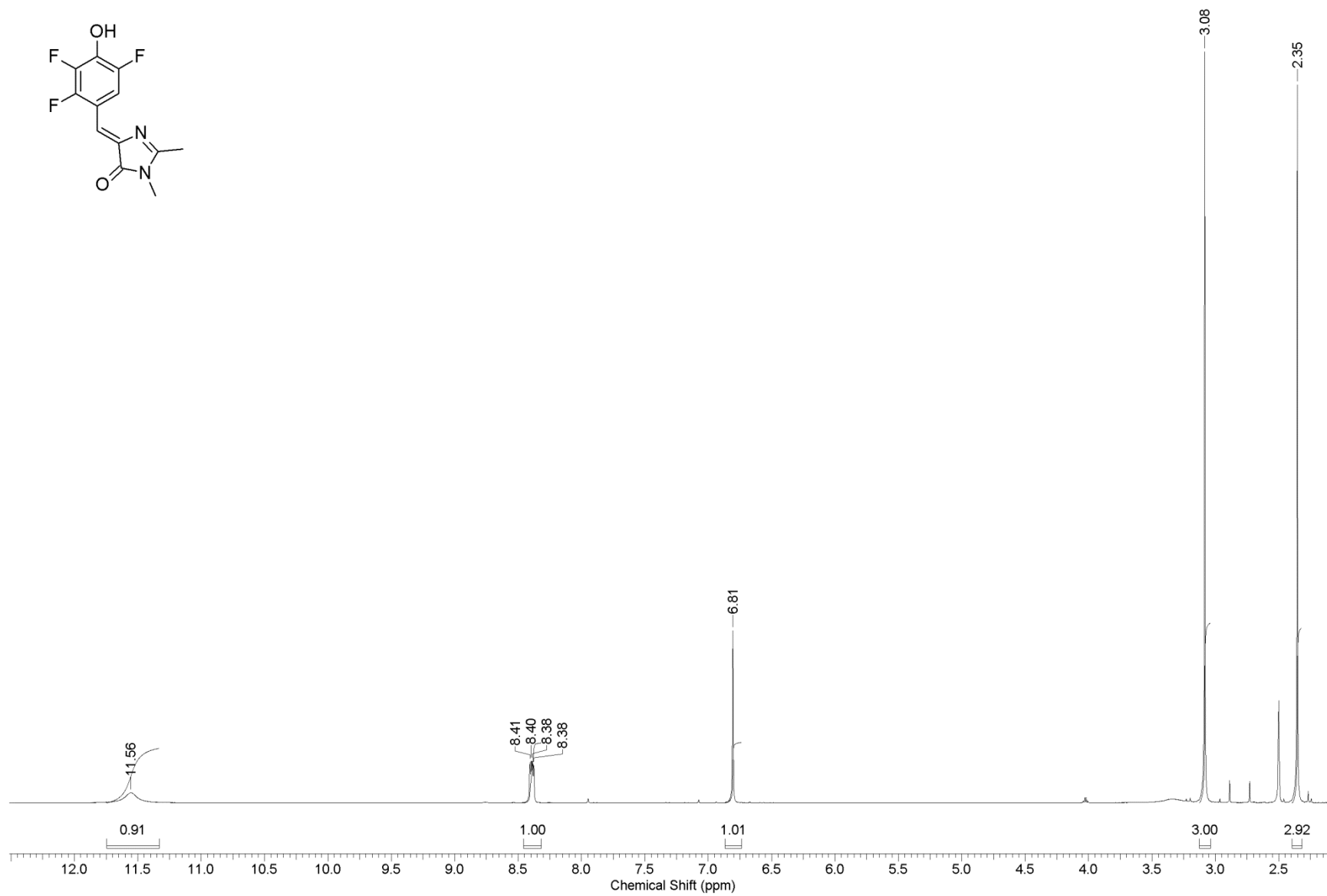


Figure S11.  $^{13}\text{C}$  NMR spectrum of 2,3,5-trifluoro-4-hydroxybenzaldehyde



**Figure S12.** <sup>19</sup>F NMR spectrum of 2,3,5-trifluoro-4-hydroxybenzaldehyde



**Figure S13.** <sup>1</sup>H NMR spectrum of (Z)-4-(2,3,5-trifluoro-4-hydroxybenzylidene)-1,2-dimethyl-1H-imidazol-5(4H)-one

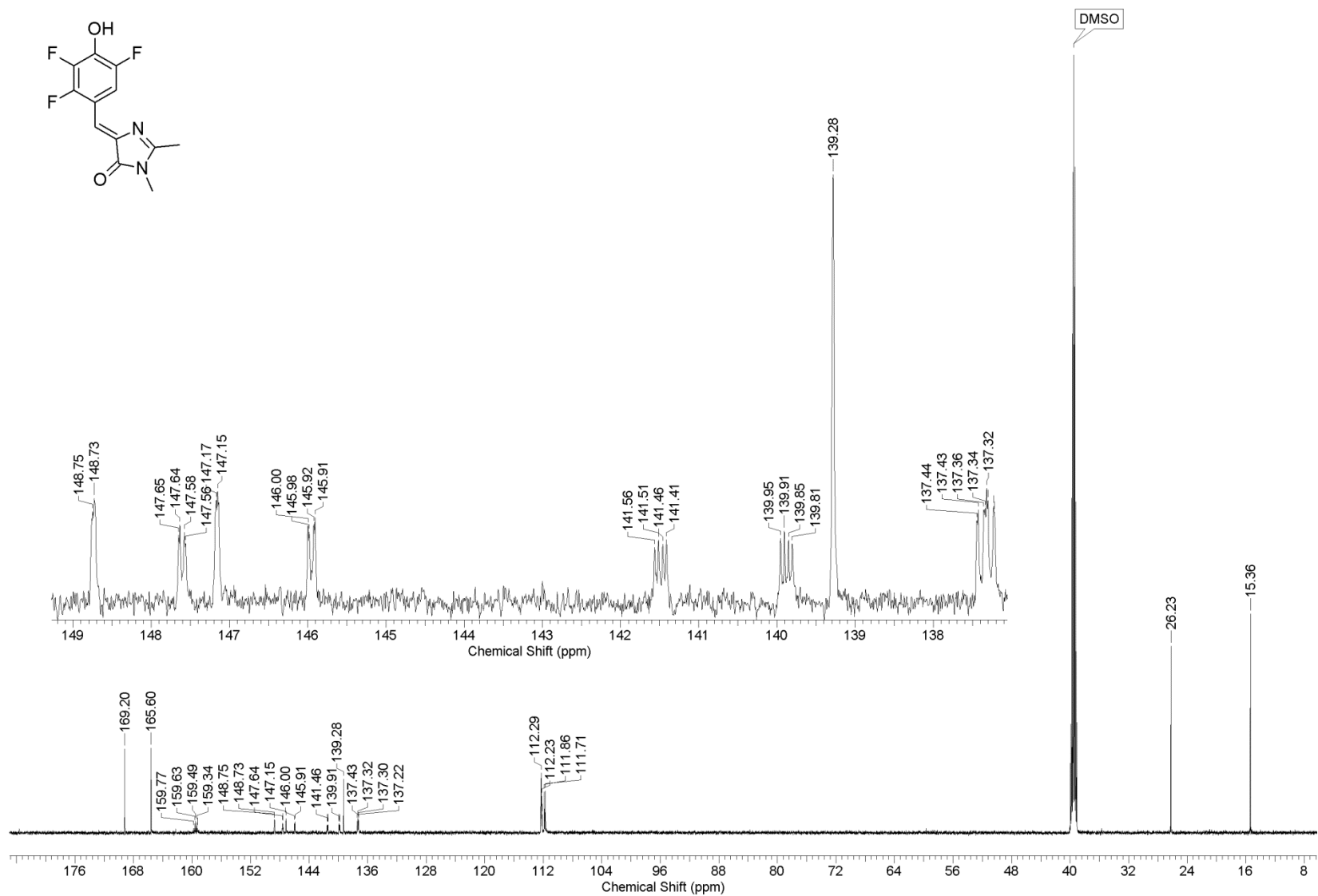


**Figure S14.** <sup>13</sup>C NMR spectrum of (Z)-4-(2,3,5-trifluoro-4-hydroxybenzylidene)-1,2-dimethyl-1H-imidazol-5(4H)-one

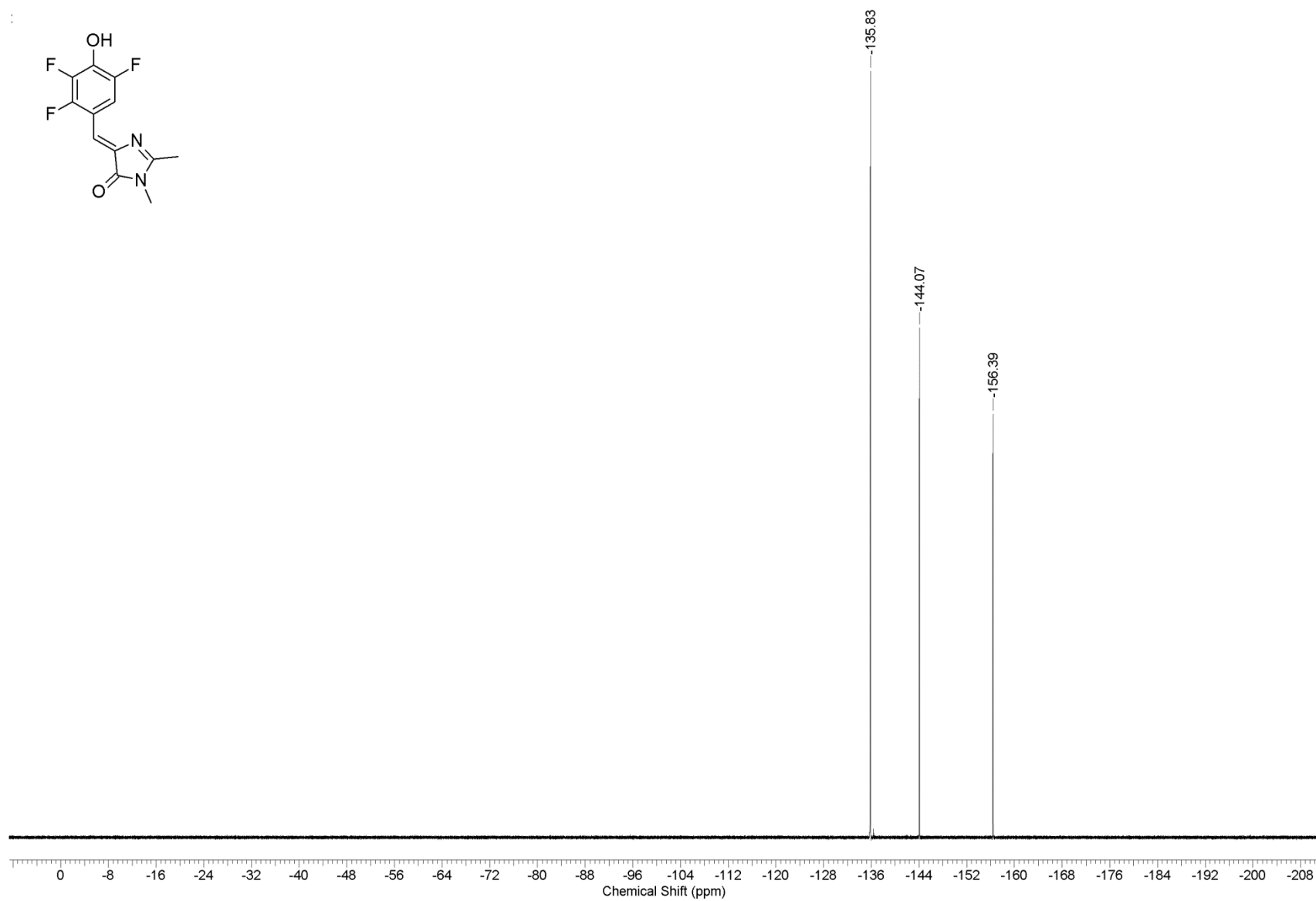


**Figure S15.** <sup>19</sup>F NMR spectrum of (Z)-4-(2,3,5-trifluoro-4-hydroxybenzylidene)-1,2-dimethyl-1H-imidazol-5(4H)-one

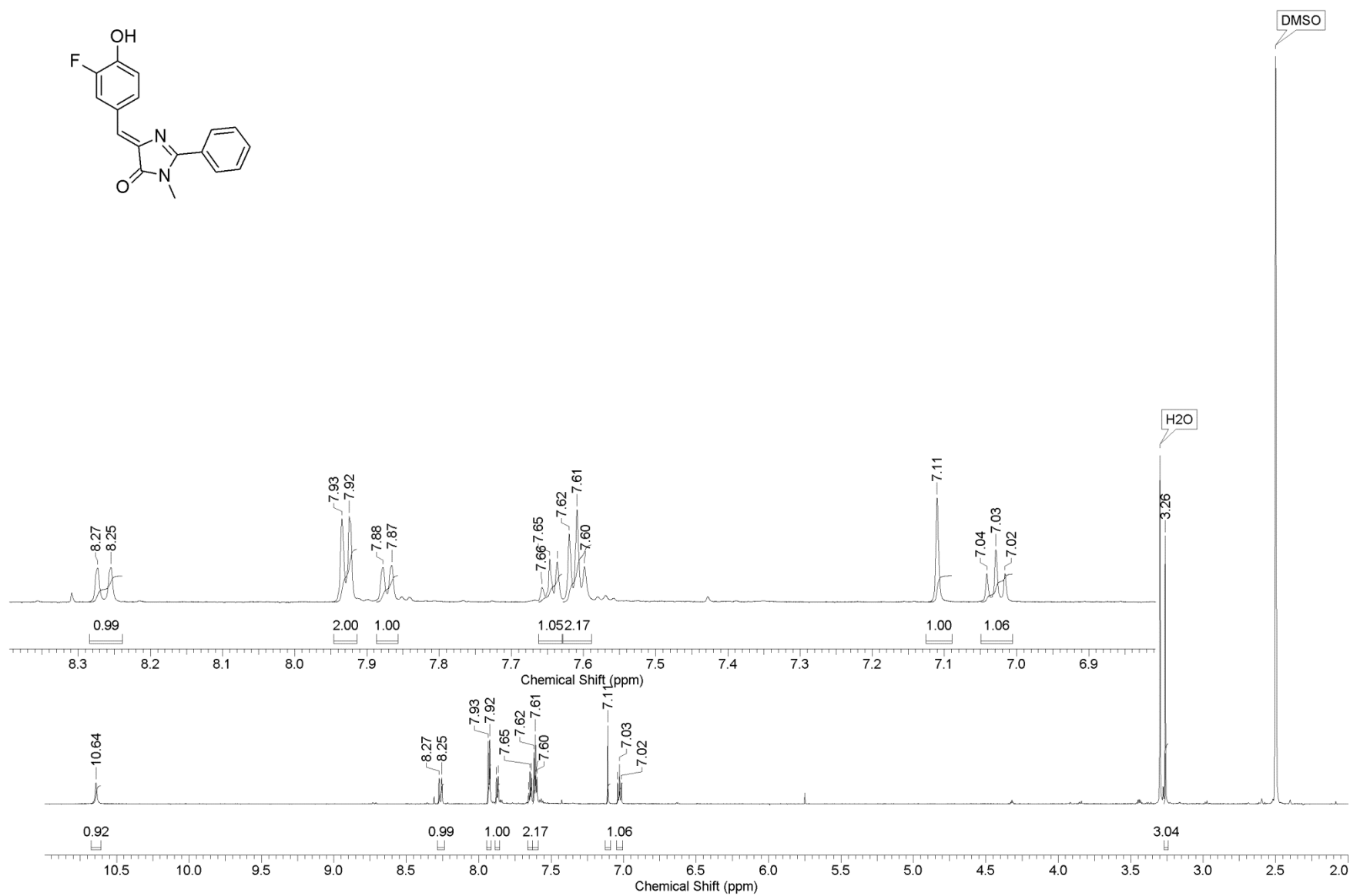


**Figure S16.** <sup>1</sup>H NMR spectrum of (Z)-4-(3-fluoro-4-hydroxybenzylidene)-1-methyl-2-phenyl-1H-imidazol-5(4H)-one

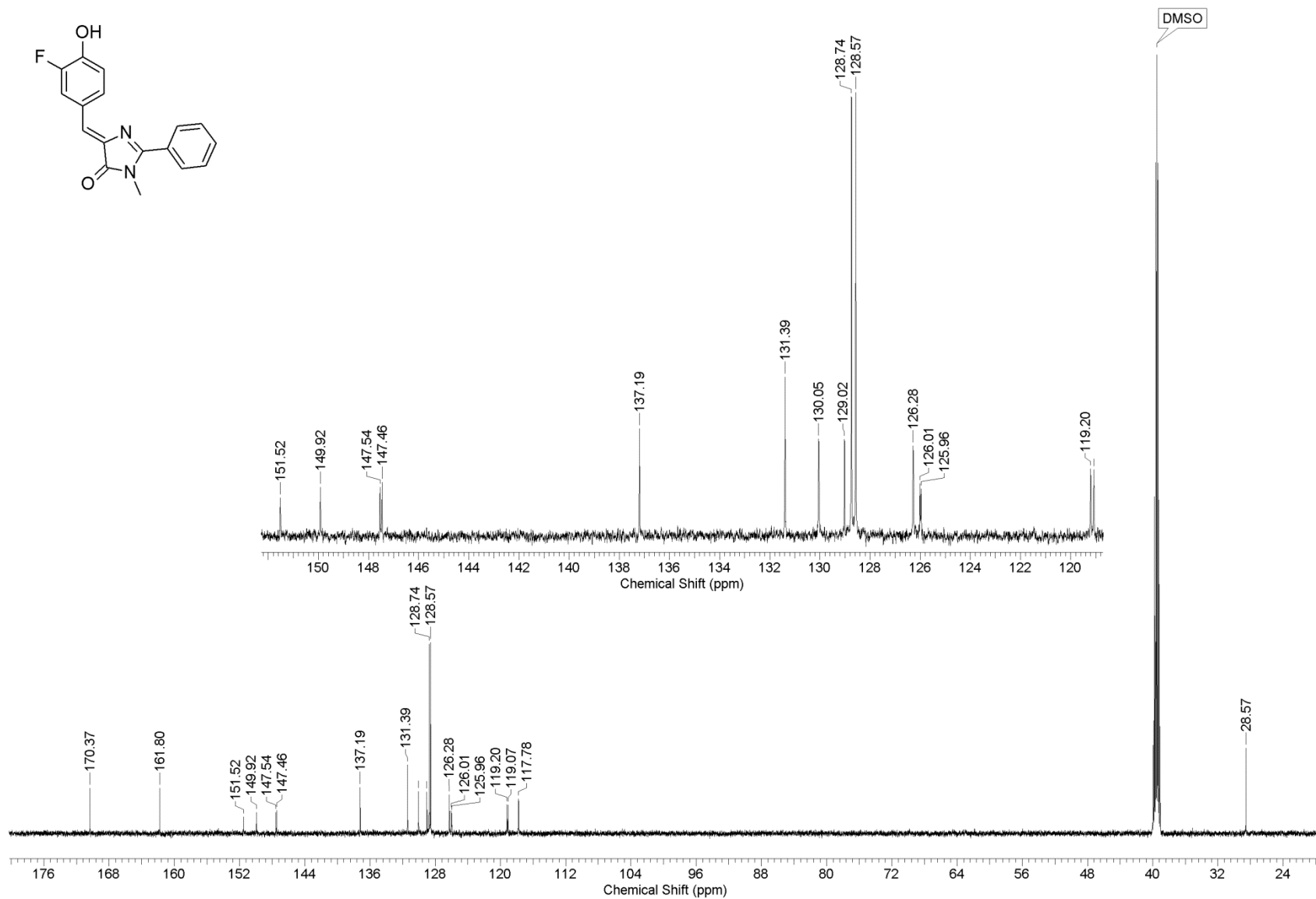
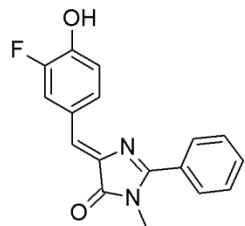
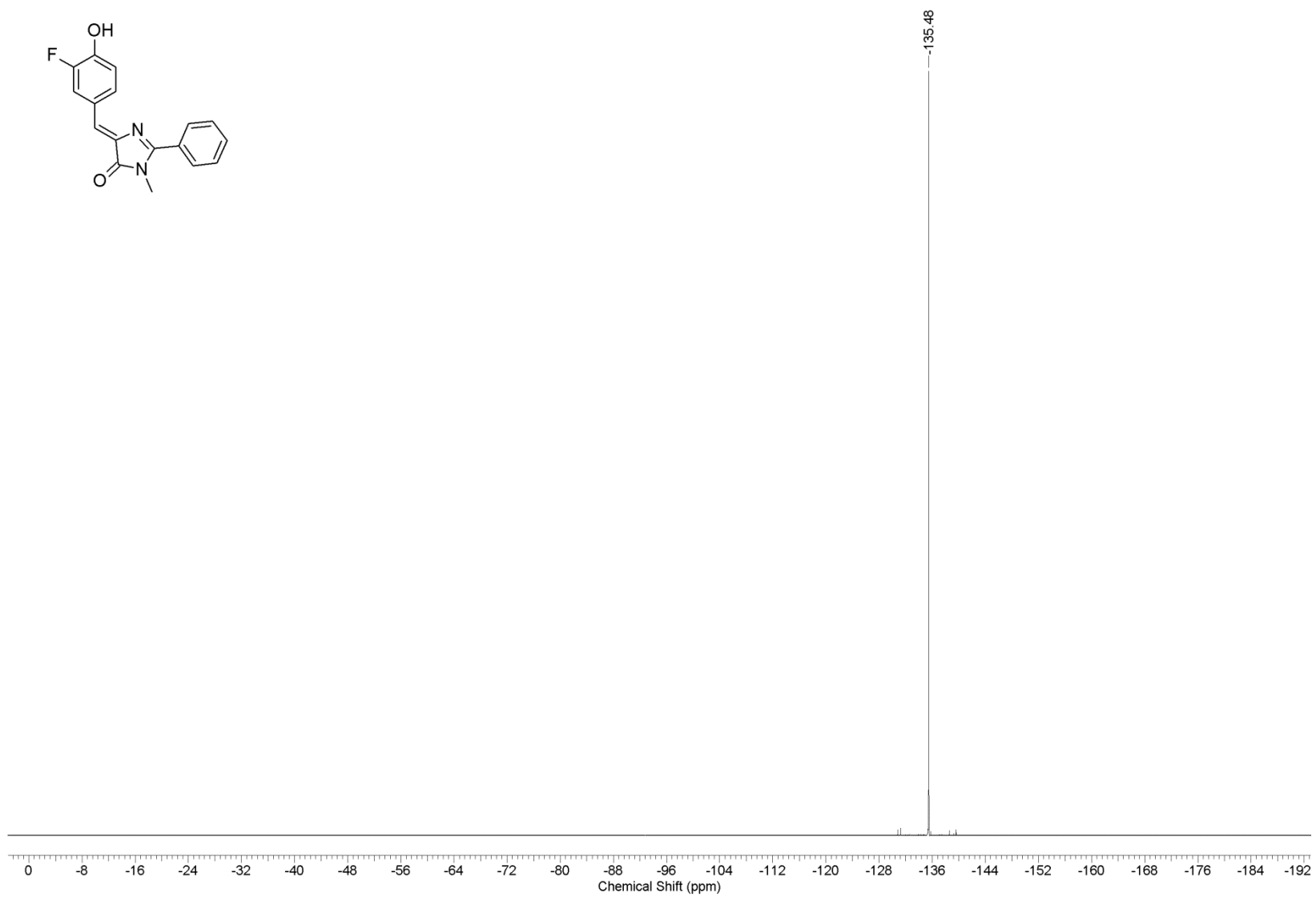
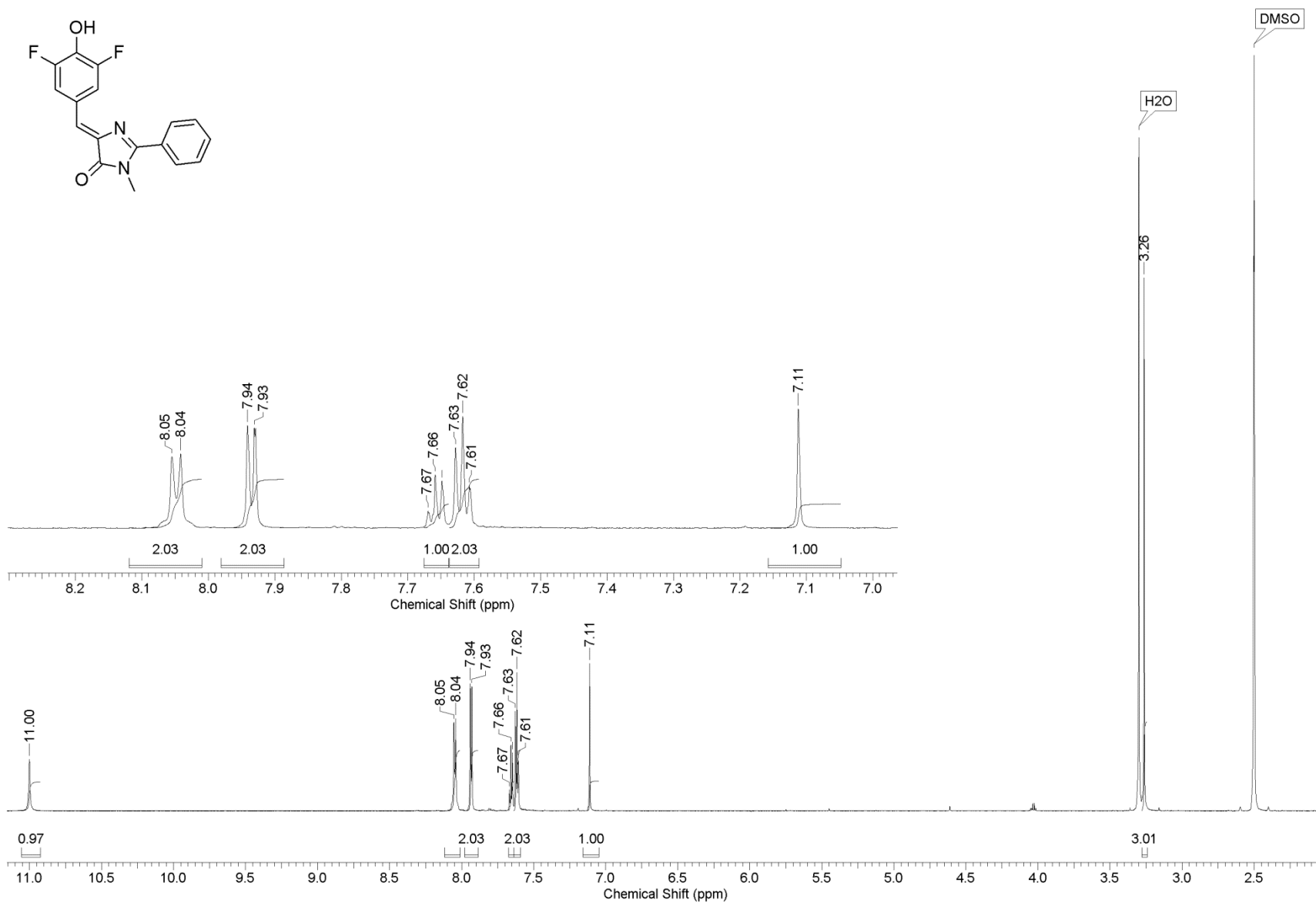


Figure S17.  $^{13}\text{C}$  NMR spectrum of (Z)-4-(3-fluoro-4-hydroxybenzylidene)-1-methyl-2-phenyl-1H-imidazol-5(4H)-one



**Figure S18.** <sup>19</sup>F NMR spectrum of (Z)-4-(3-fluoro-4-hydroxybenzylidene)-1-methyl-2-phenyl-1H-imidazol-5(4H)-one



**Figure S19.**  $^1\text{H}$  NMR spectrum of (Z)-4-(3,5-difluoro-4-hydroxybenzylidene)-1-methyl-2-phenyl-1H-imidazol-5(4H)-one

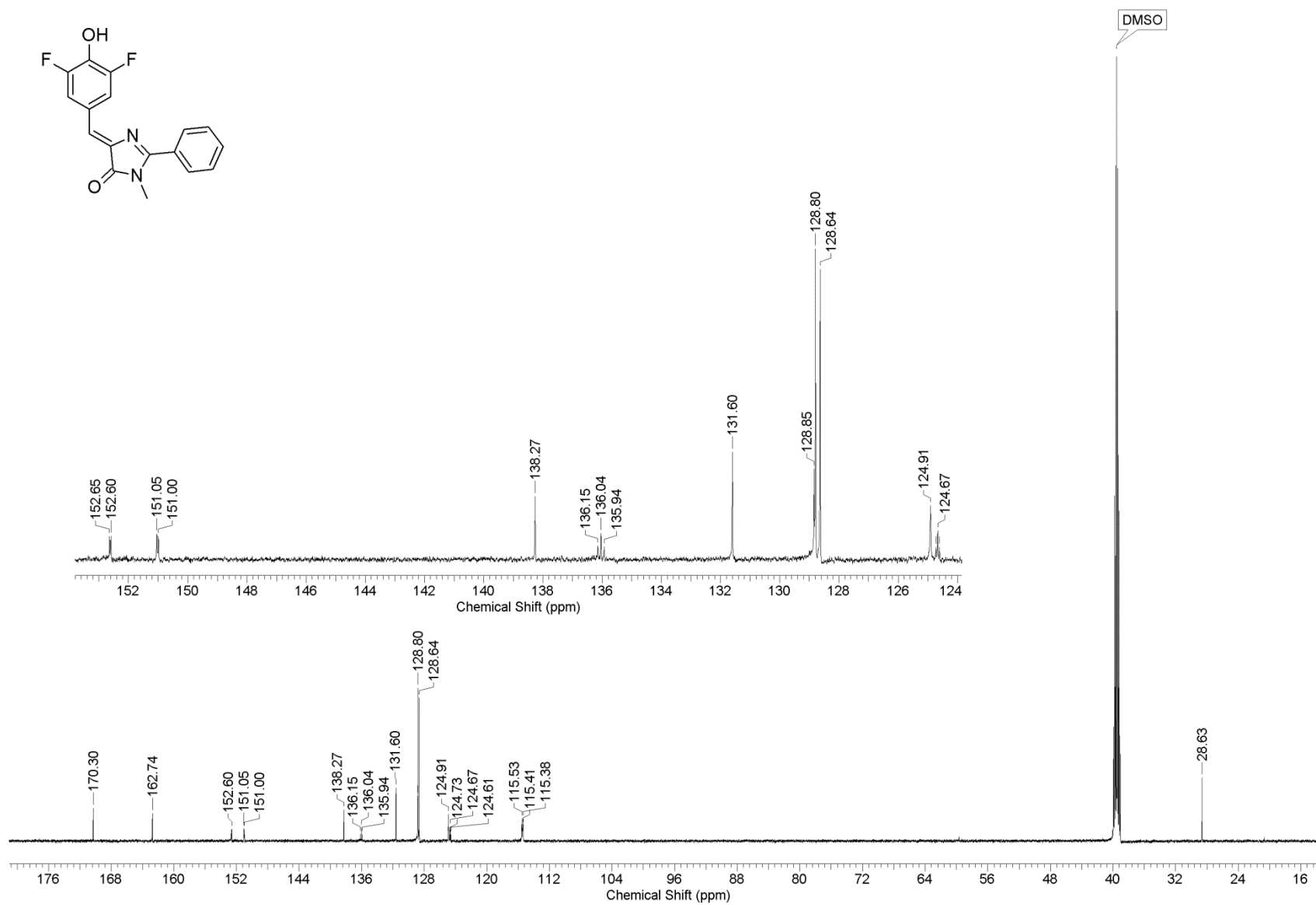


**Figure S20.** <sup>13</sup>C NMR spectrum of (Z)-4-(3,5-difluoro-4-hydroxybenzylidene)-1-methyl-2-phenyl-1H-imidazol-5(4H)-one

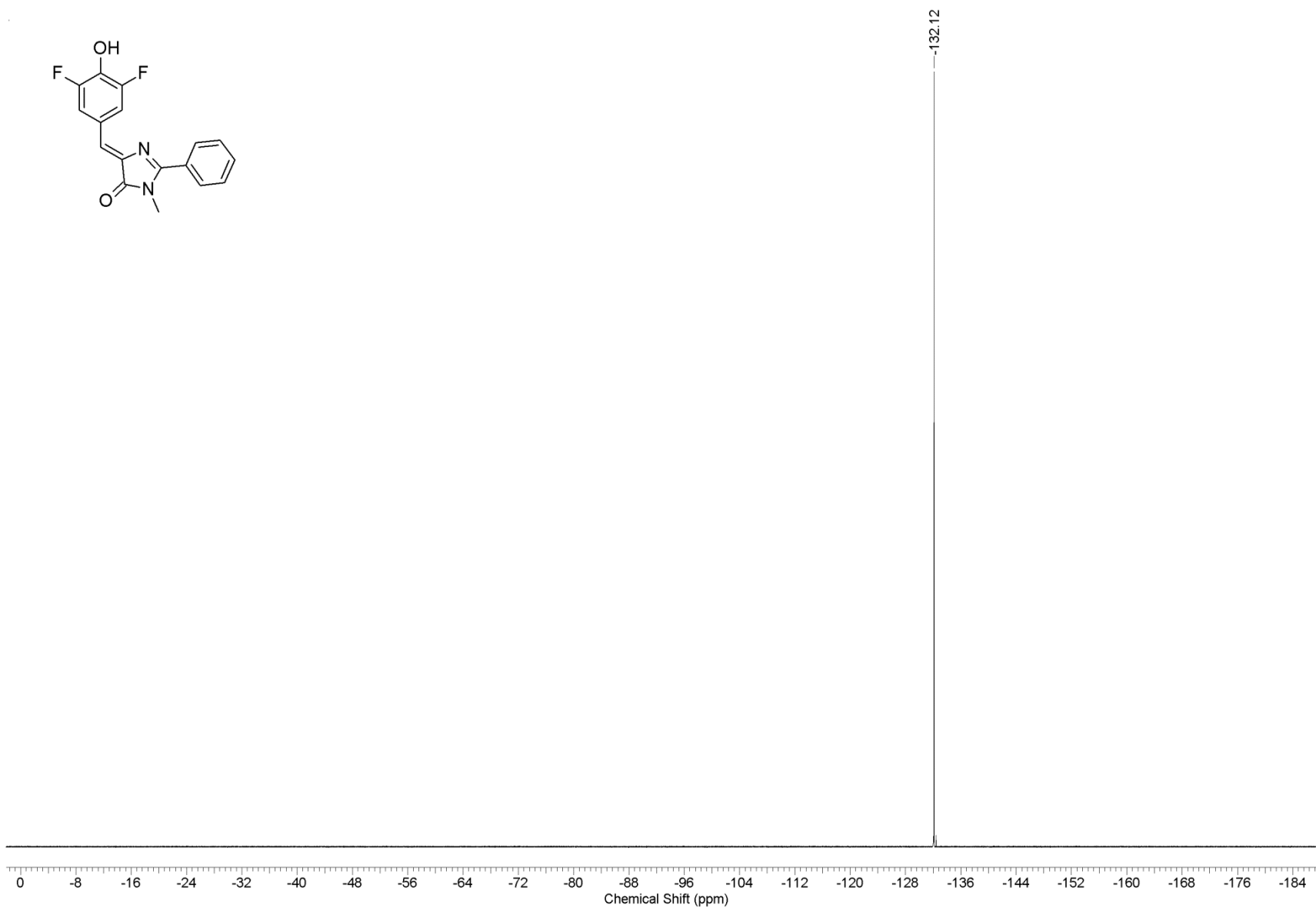
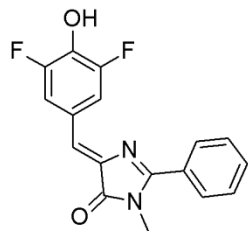


**Figure S21.**  $^{19}\text{F}$  NMR spectrum of (Z)-4-(3,5-difluoro-4-hydroxybenzylidene)-1-methyl-2-phenyl-1*H*-imidazol-5(4*H*)-one

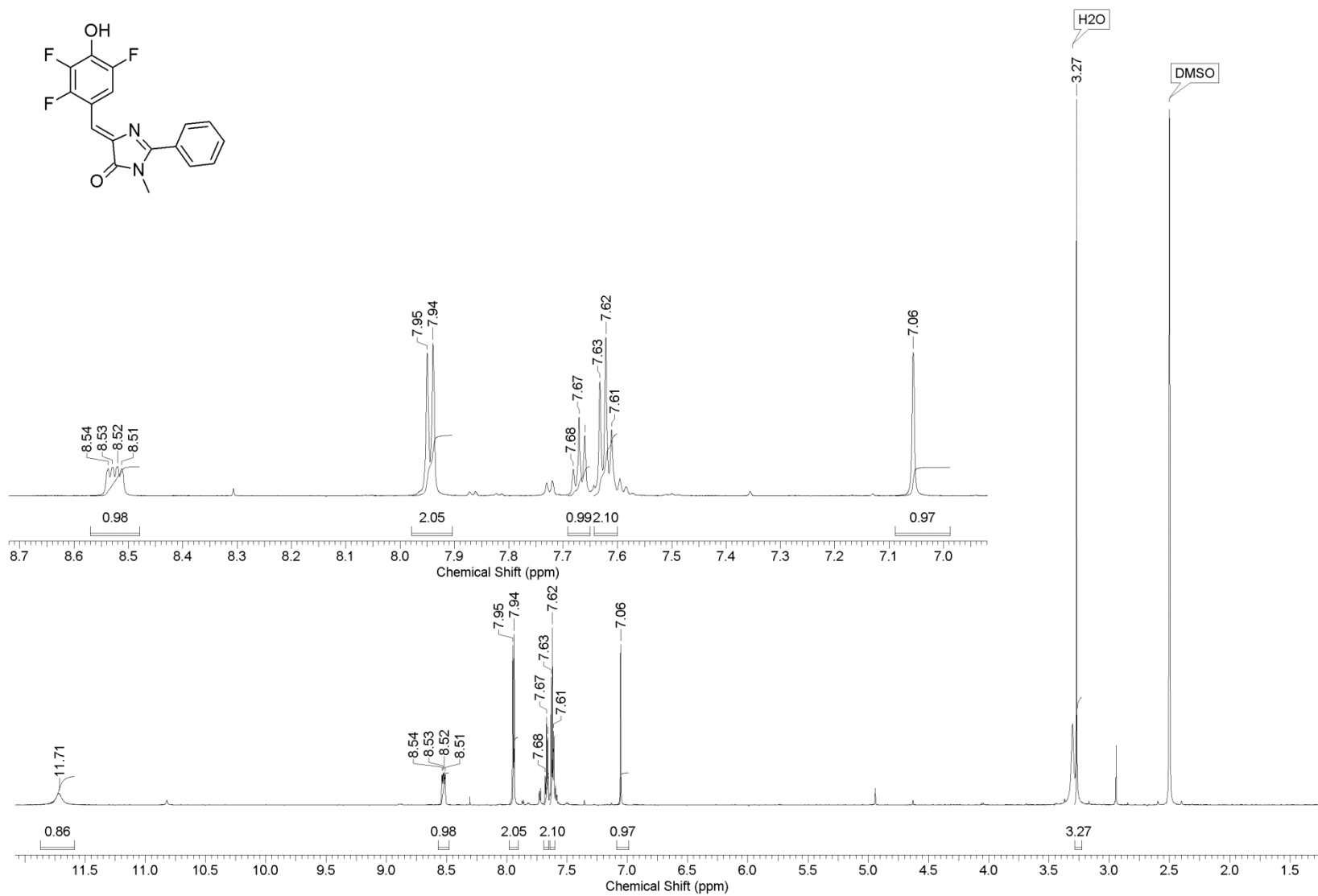


**Figure S22.**  $^1\text{H}$  NMR spectrum of (Z)-4-(2,3,5-trifluoro-4-hydroxybenzylidene)-1-methyl-2-phenyl-1H-imidazol-5(4H)-one

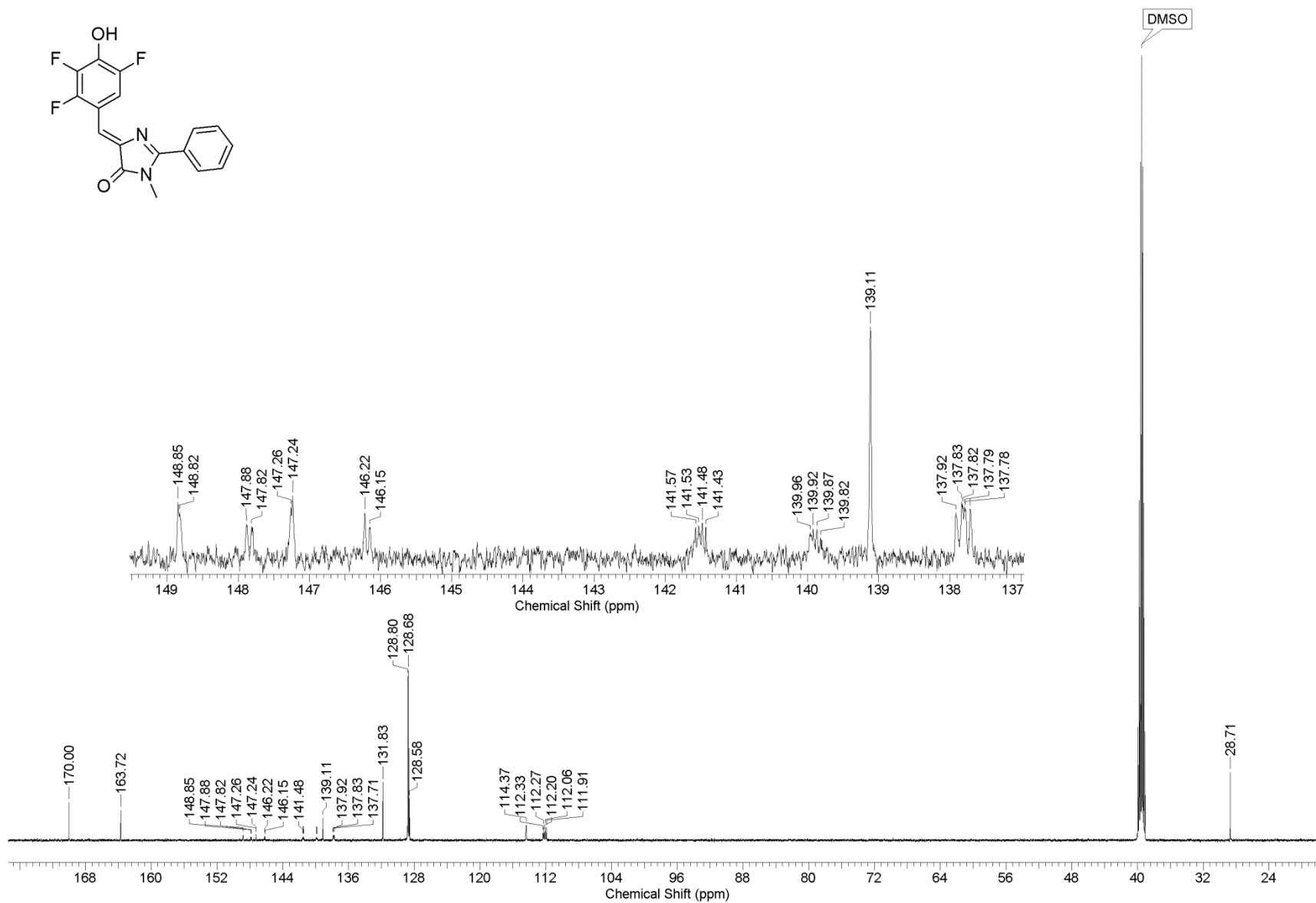


**Figure S23.** <sup>13</sup>C NMR spectrum of (Z)-4-(2,3,5-trifluoro-4-hydroxybenzylidene)-1-methyl-2-phenyl-1H-imidazol-5(4H)-one

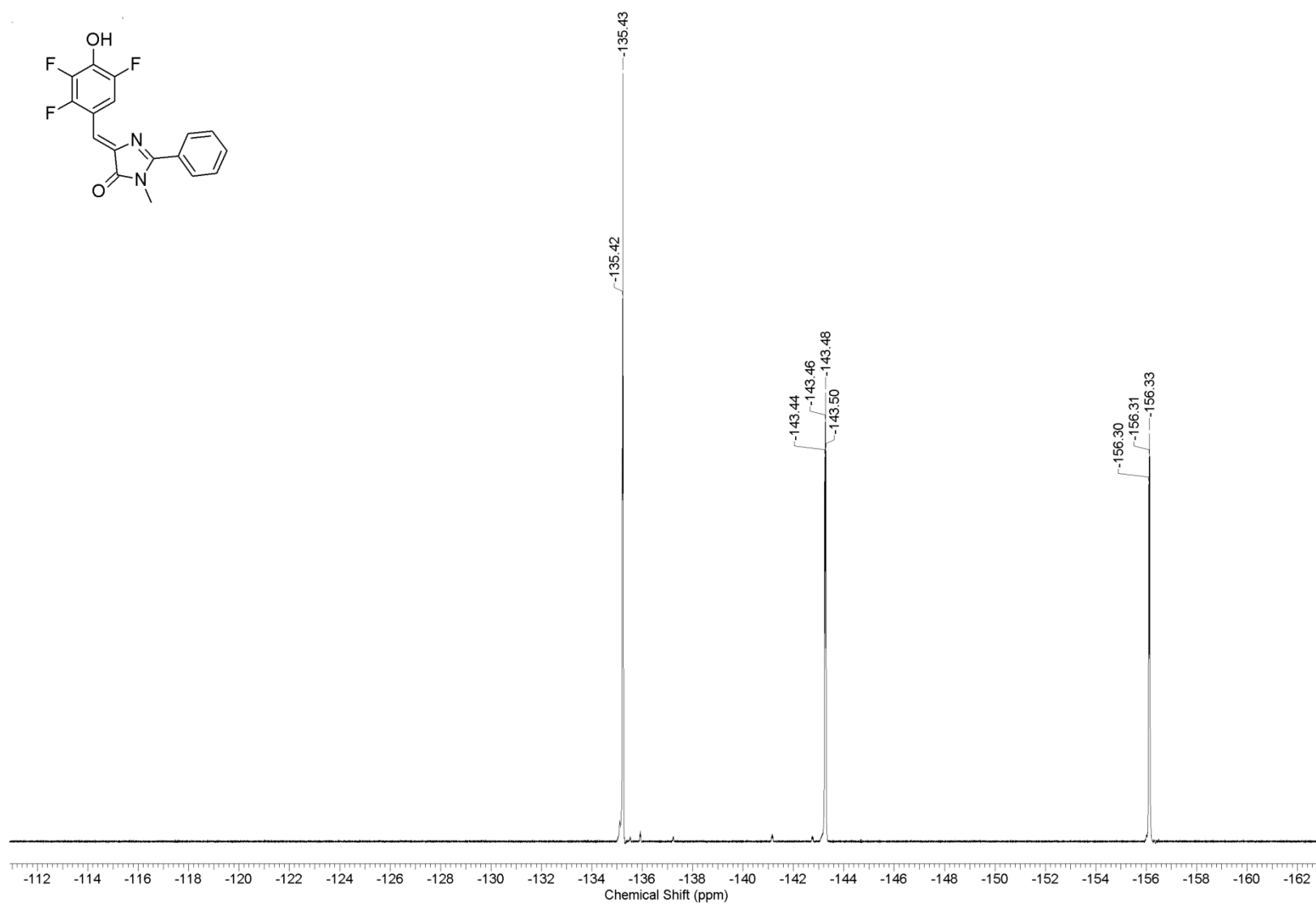


**Figure S24.** <sup>19</sup>F NMR spectrum of (Z)-4-(2,3,5-trifluoro-4-hydroxybenzylidene)-1-methyl-2-phenyl-1H-imidazol-5(4H)-one

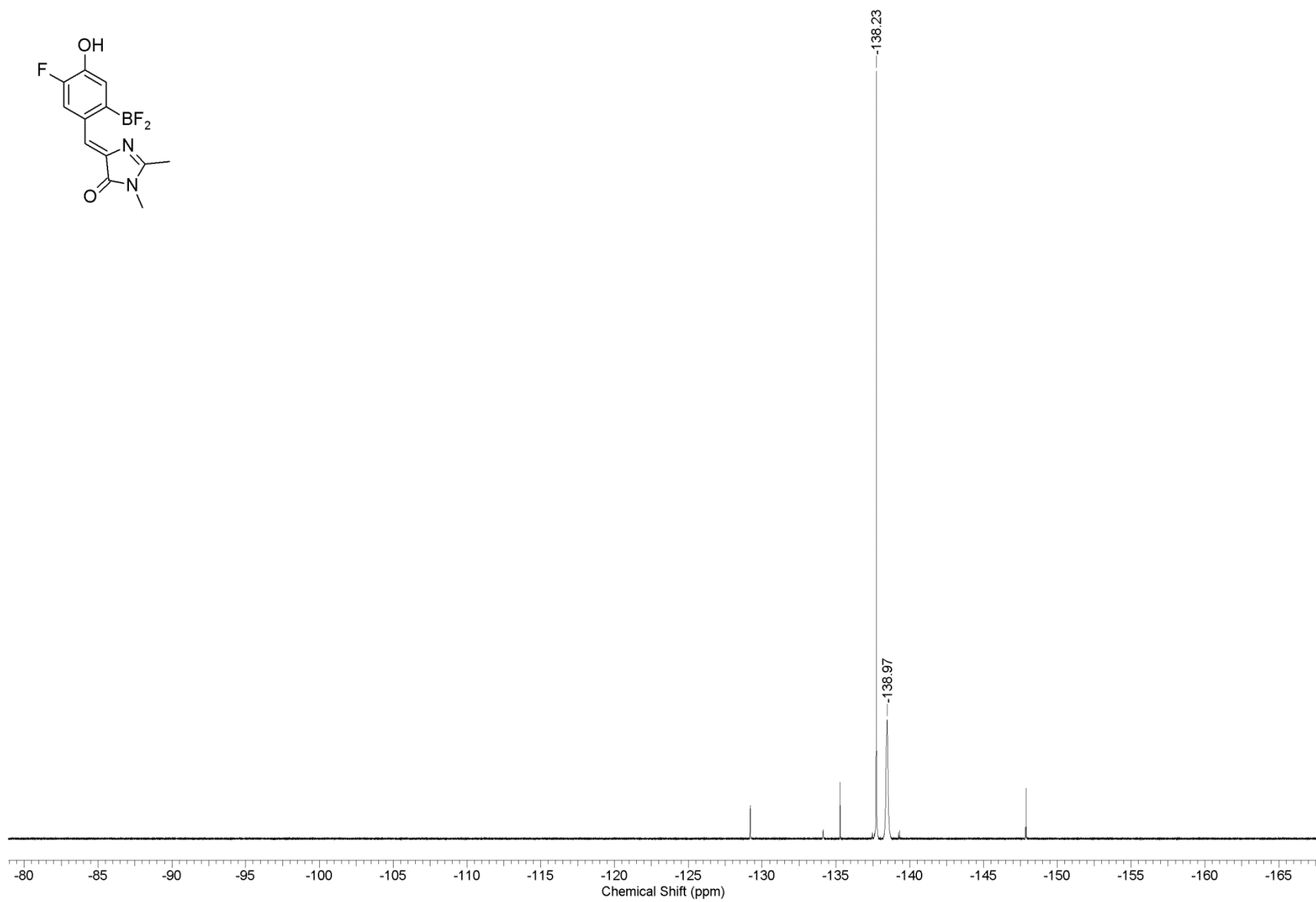


**Figure S25.**  $^{19}\text{F}$  NMR spectrum of **M1F**

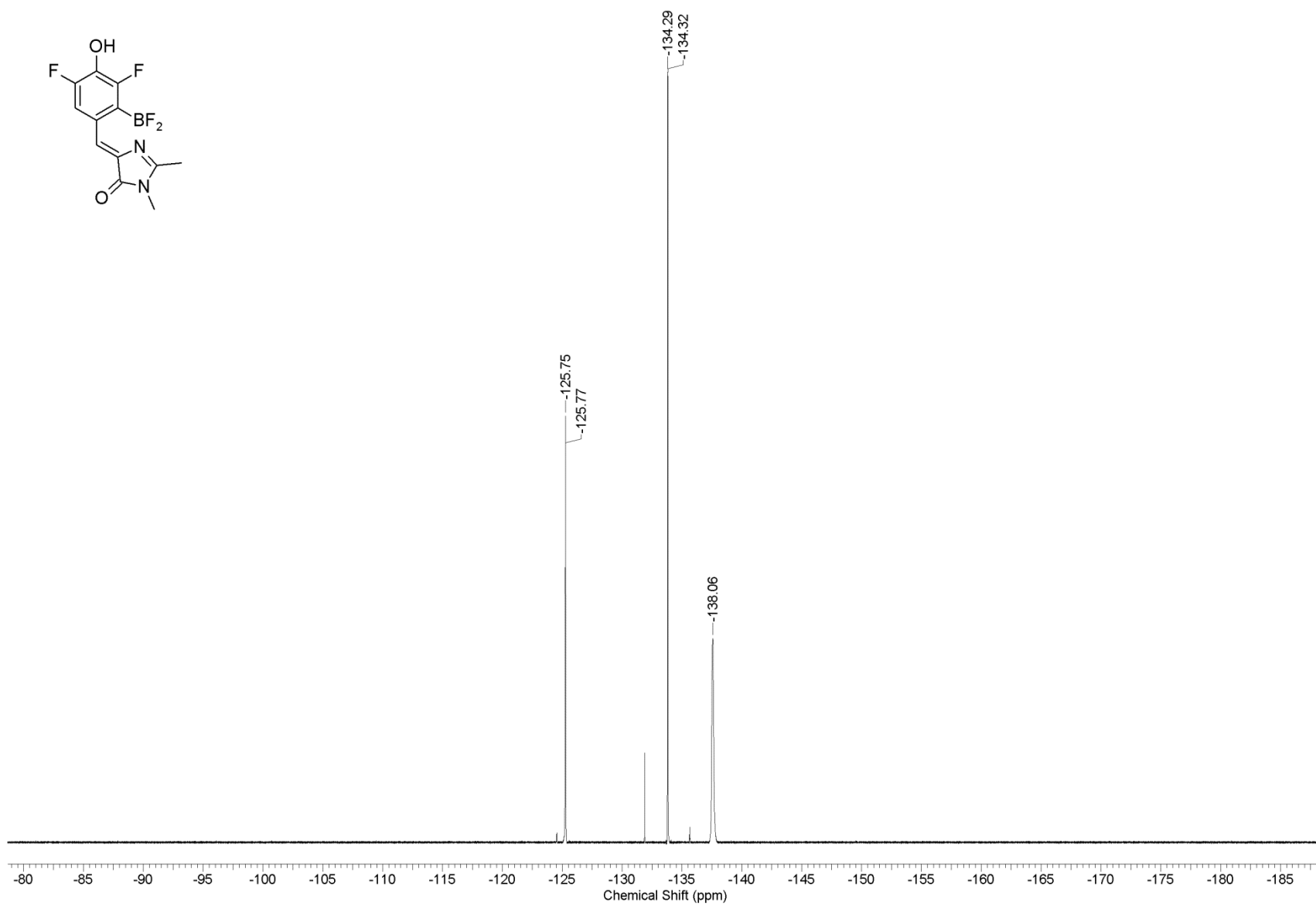


**Figure S26.** <sup>19</sup>F NMR spectrum of **M2F**

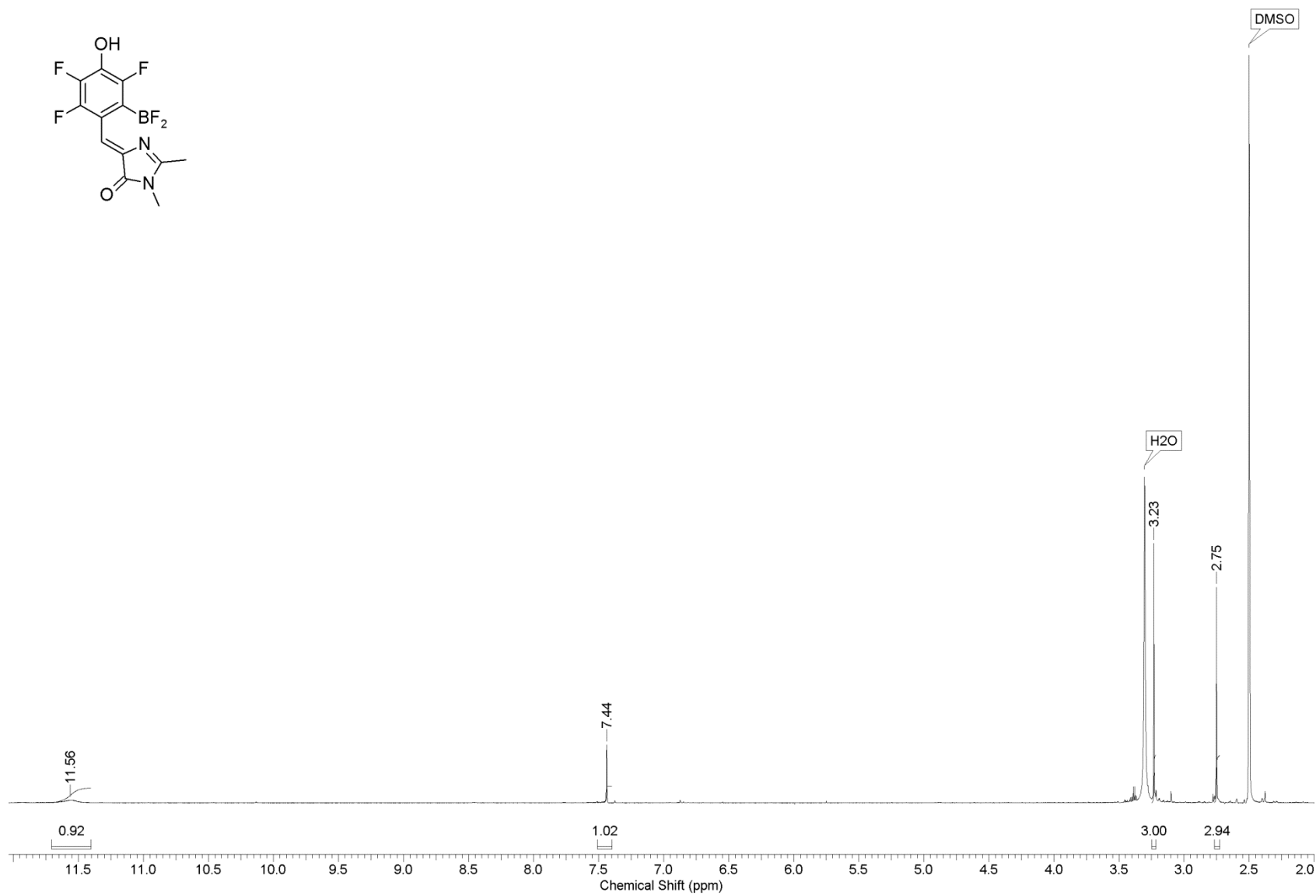


**Figure S27.** <sup>1</sup>H NMR spectrum of M3F

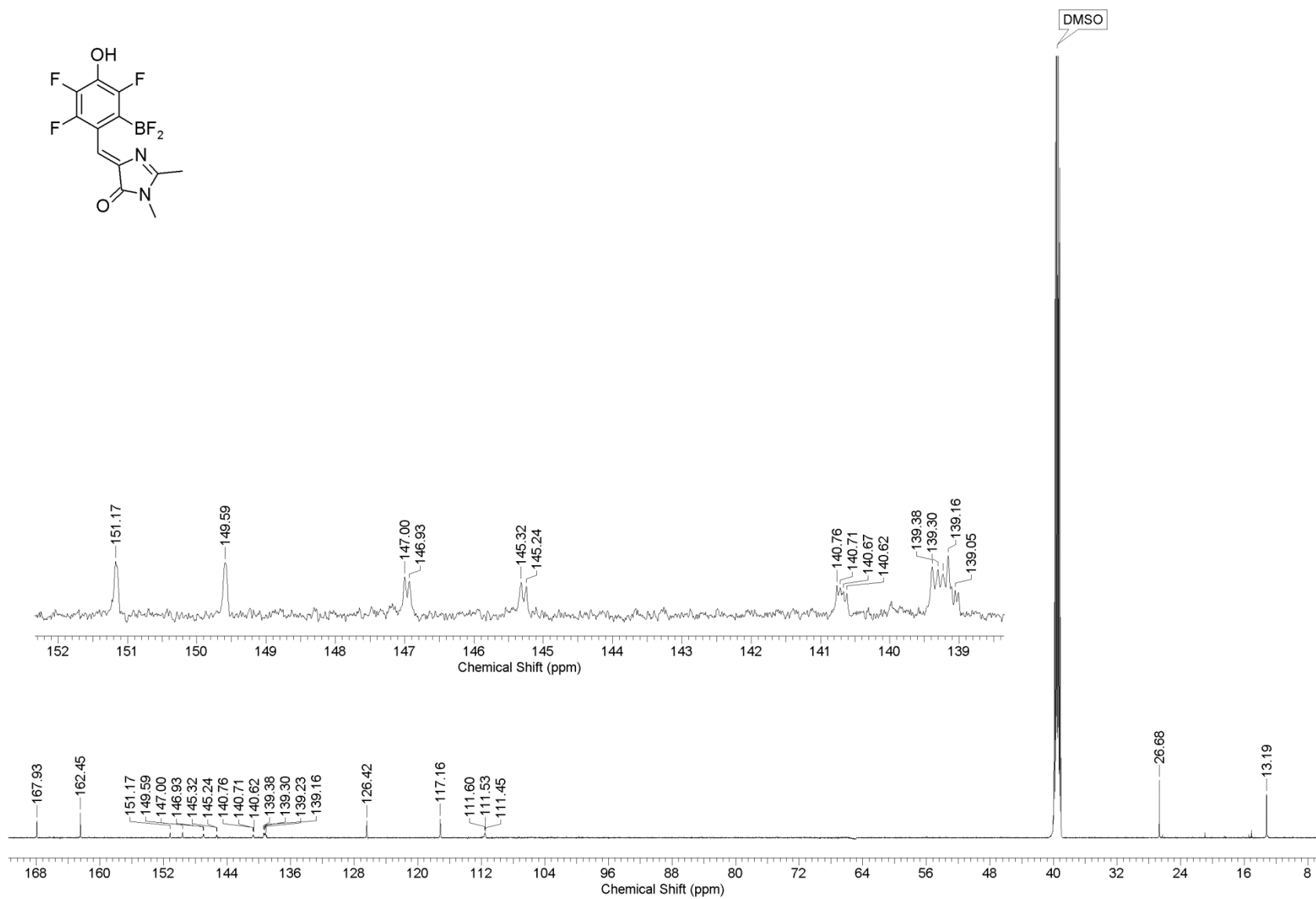


Figure S28. <sup>13</sup>C NMR spectrum of M3F

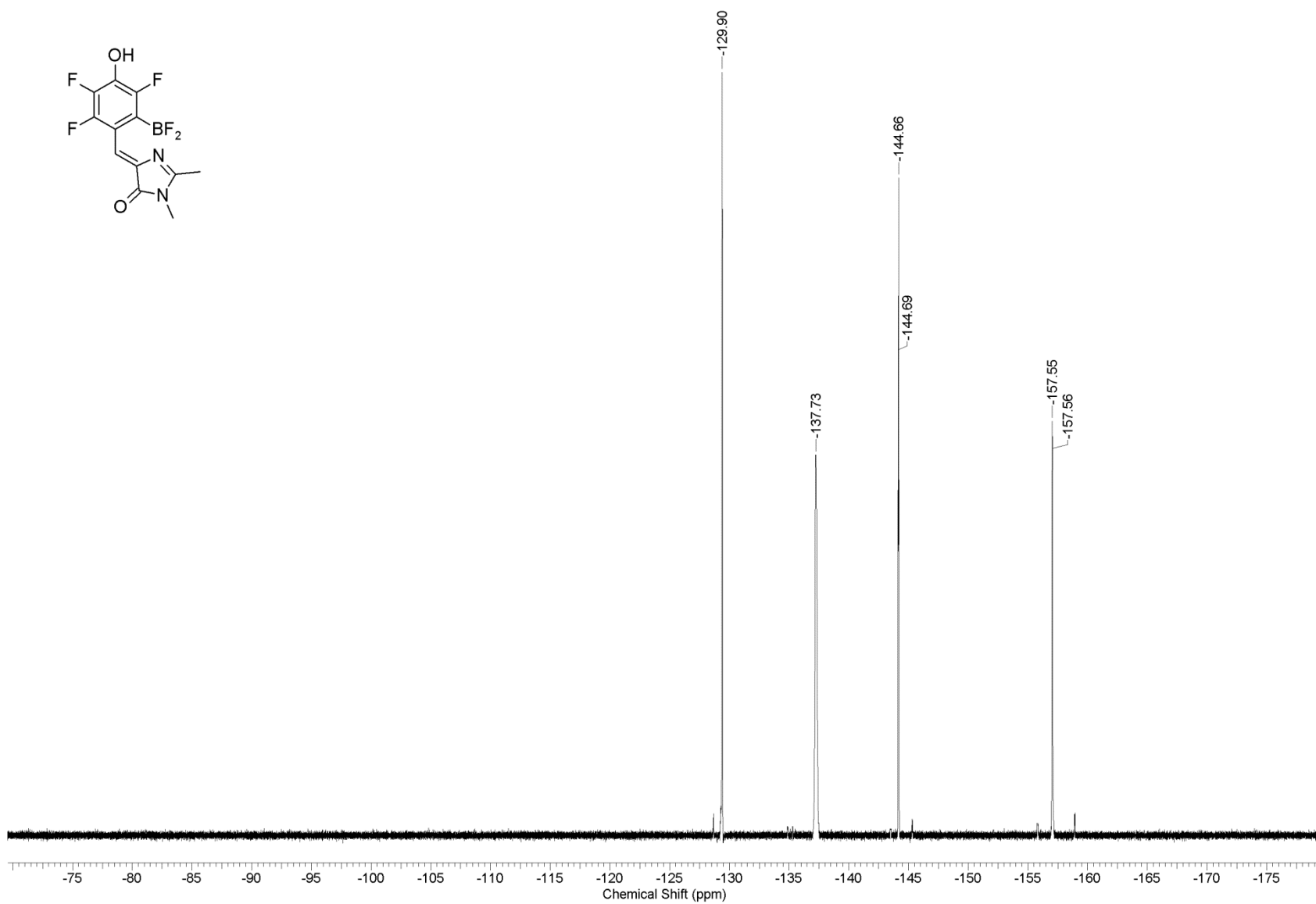


Figure S29.  $^{19}\text{F}$  NMR spectrum of M3F

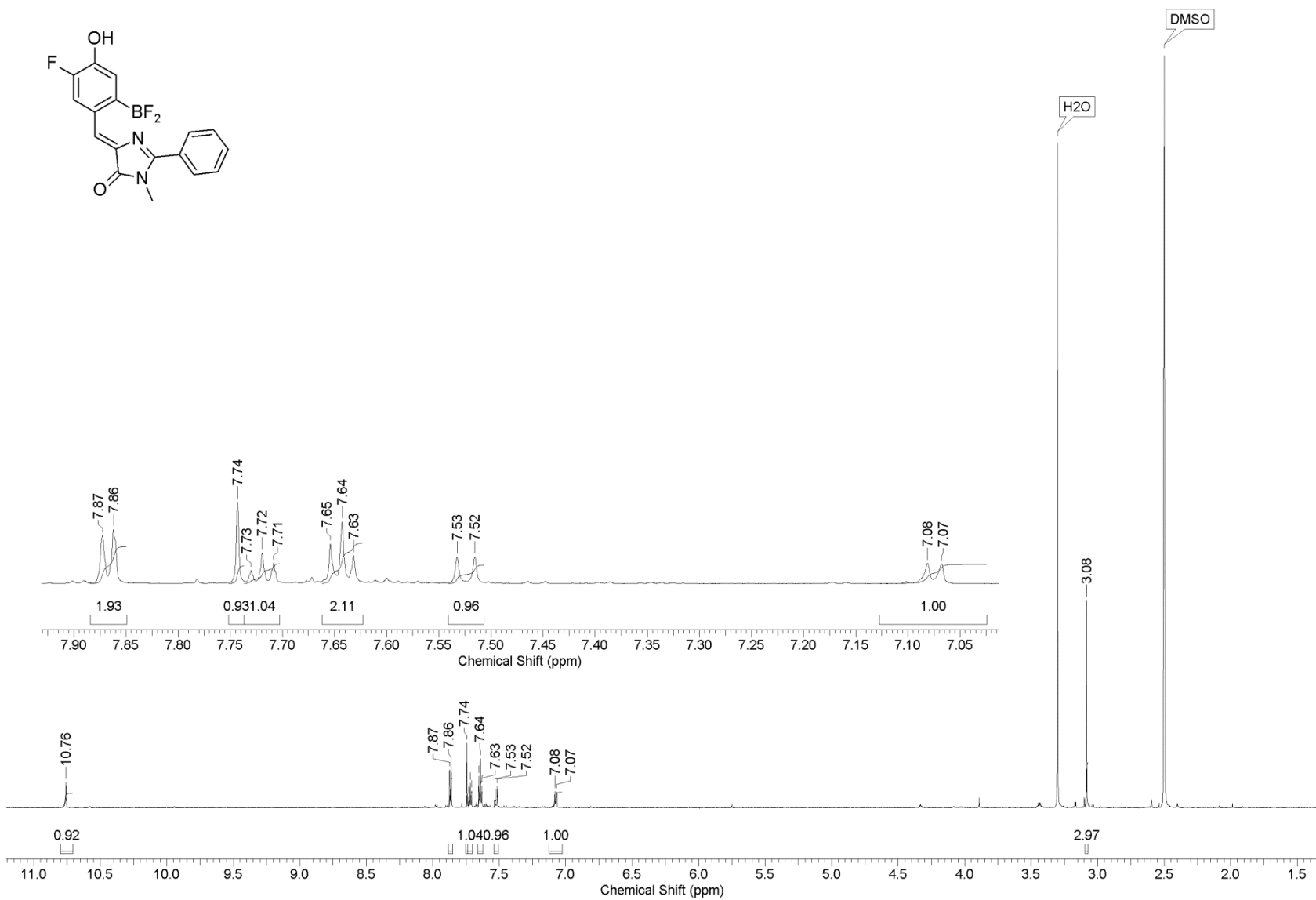


Figure S30. <sup>1</sup>H NMR spectrum of P1F

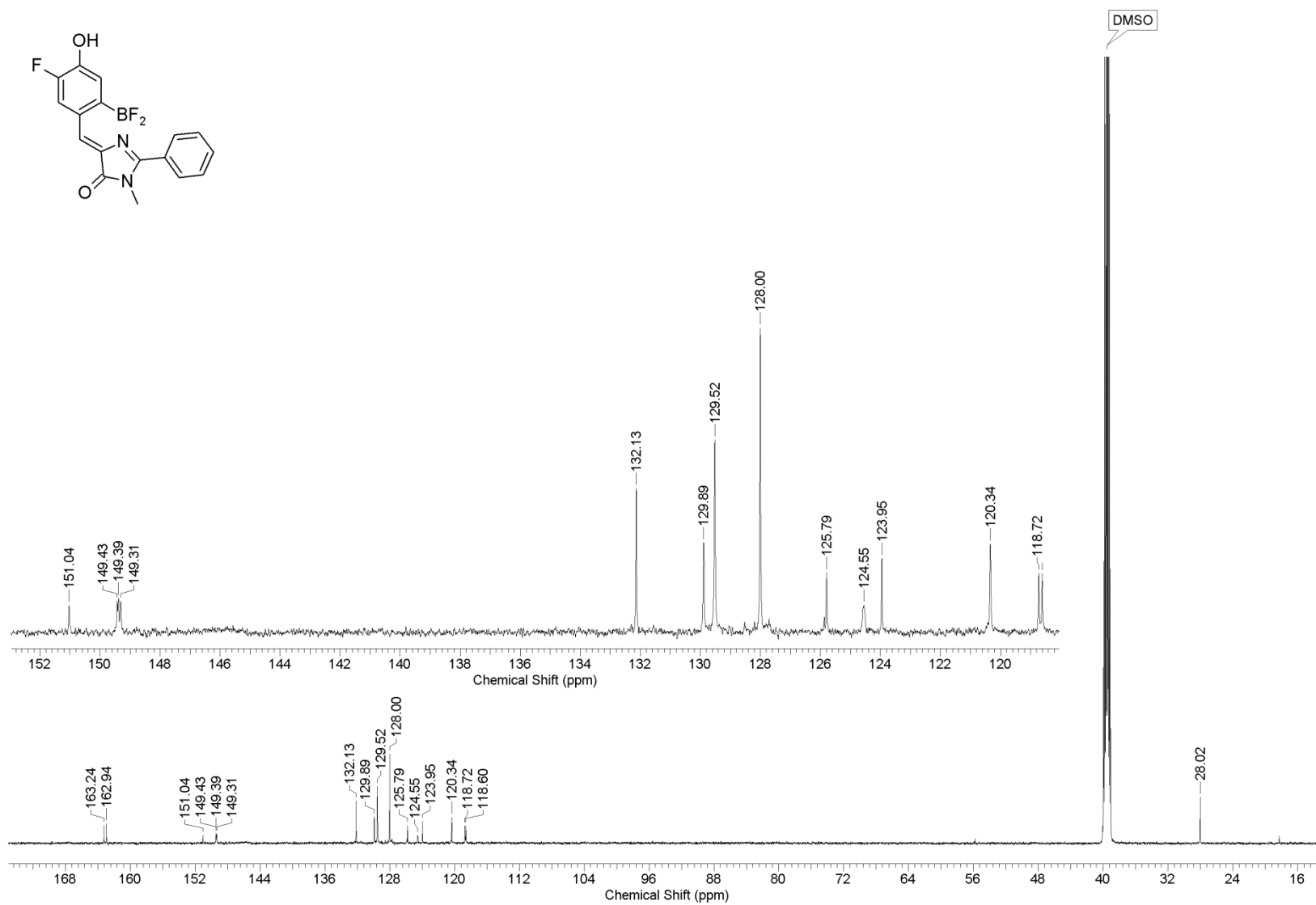
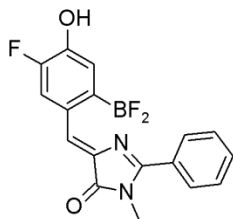


Figure S31.  $^{13}\text{C}$  NMR spectrum of P1F

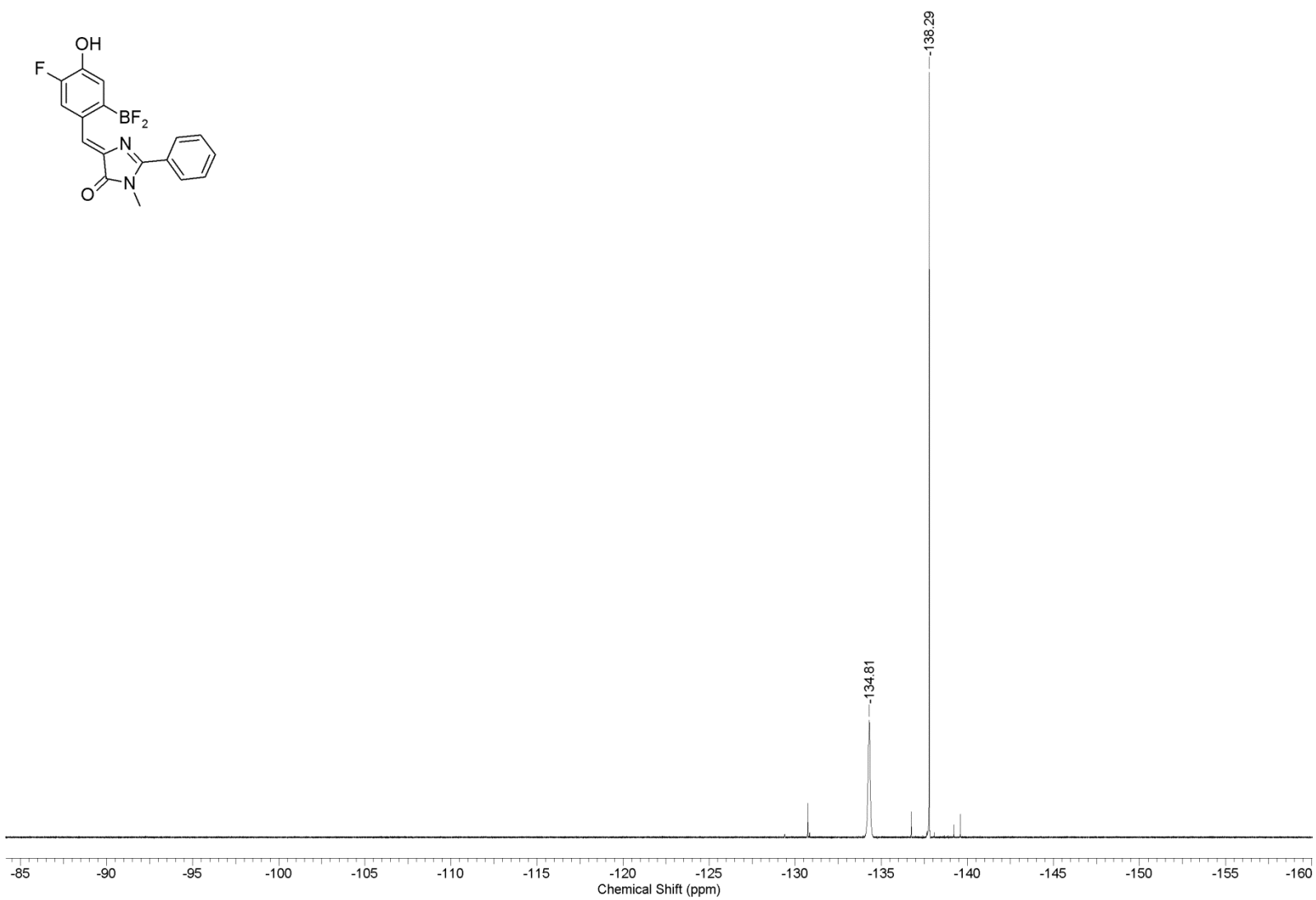


Figure S32.  $^{19}\text{F}$  NMR spectrum of P1F

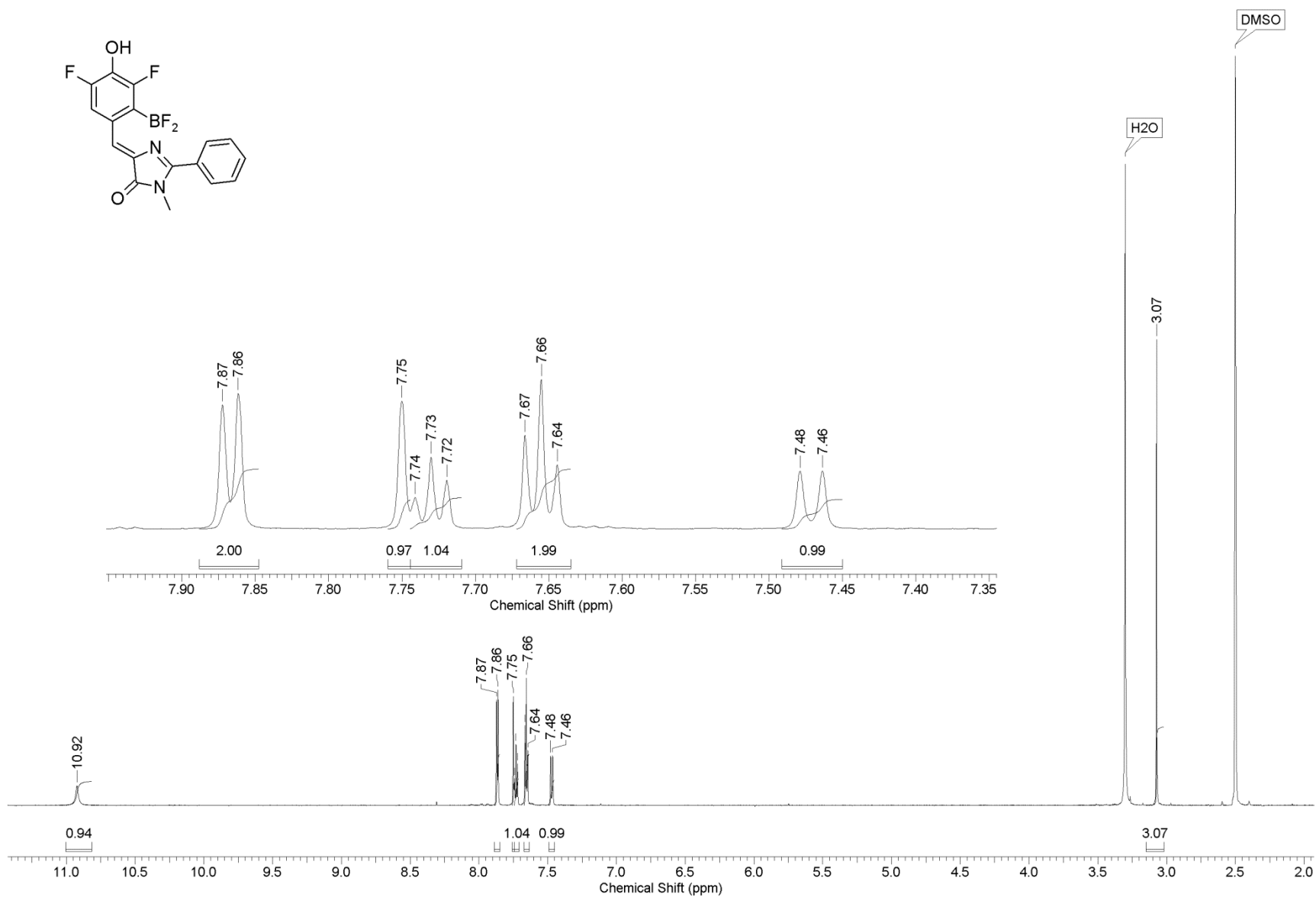
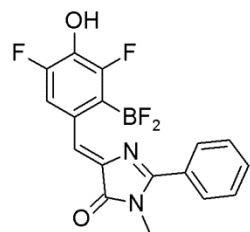


Figure S33.  $^1\text{H}$  NMR spectrum of P2F

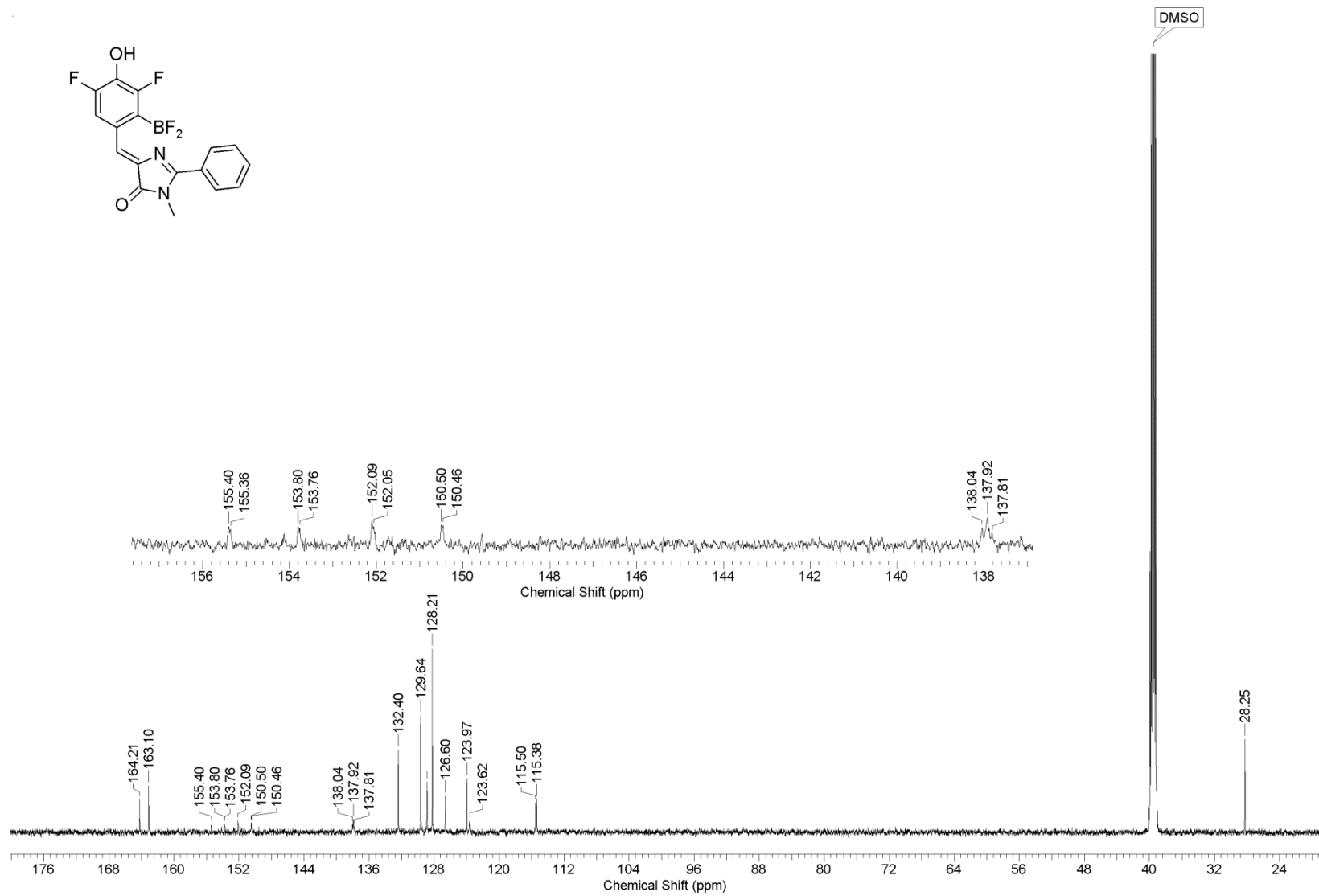
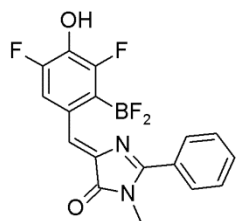


Figure S34. <sup>13</sup>C NMR spectrum of P2F

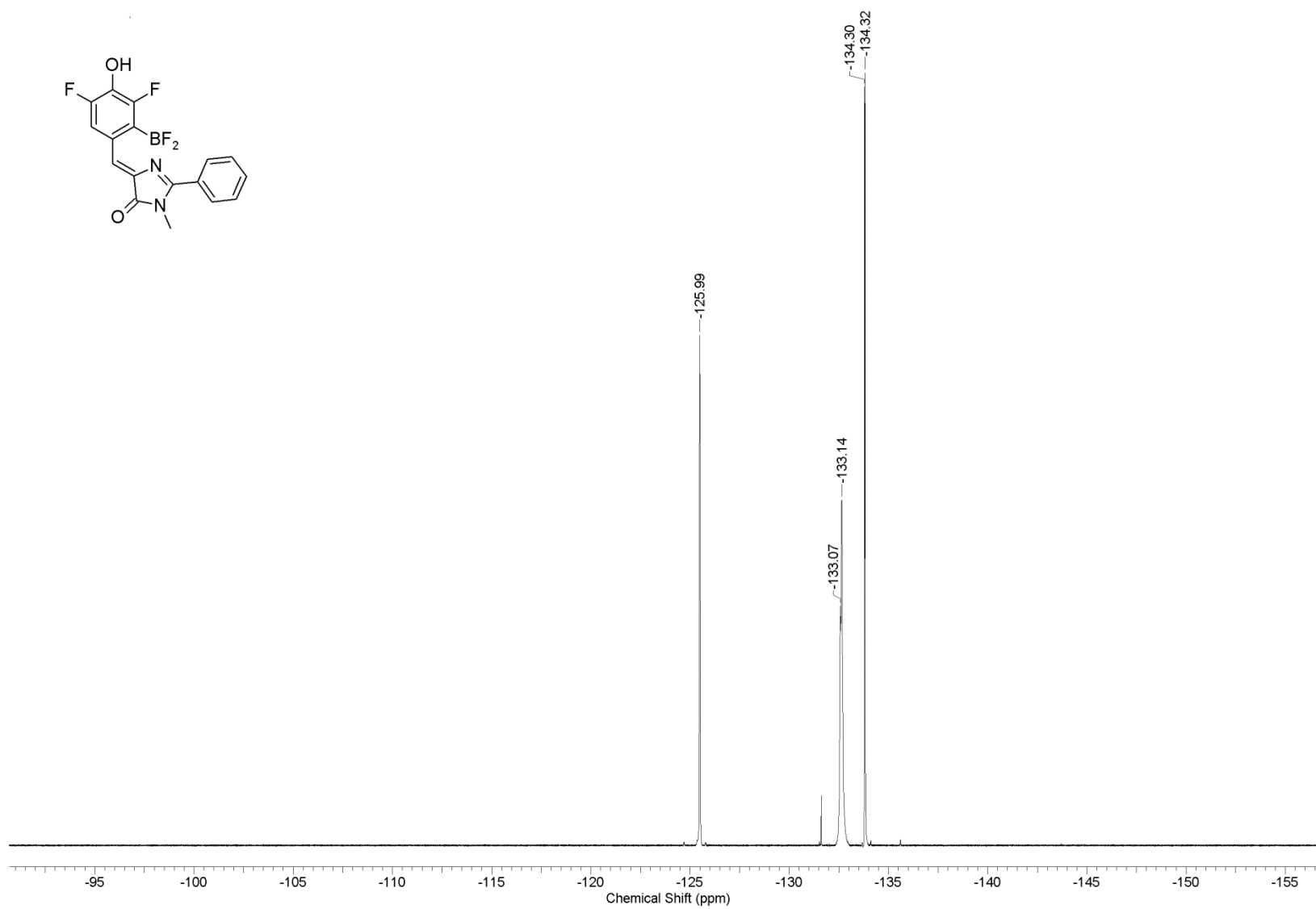
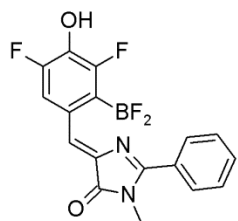


Figure S35.  $^{19}\text{F}$  NMR spectrum of P2F

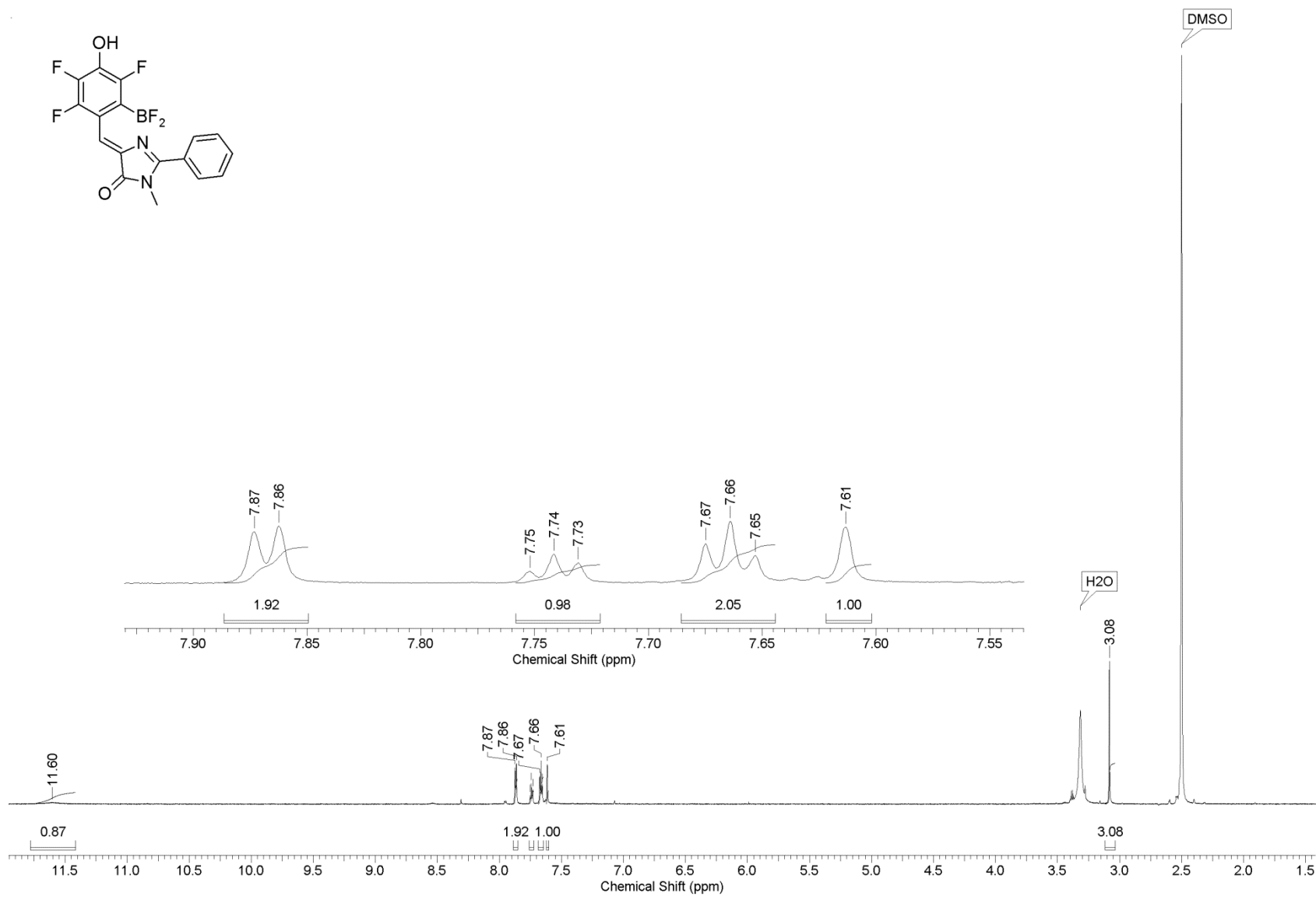
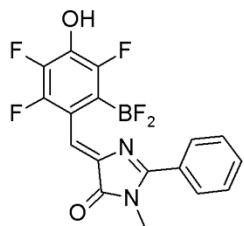


Figure S36.  $^1\text{H}$  NMR spectrum of P3F

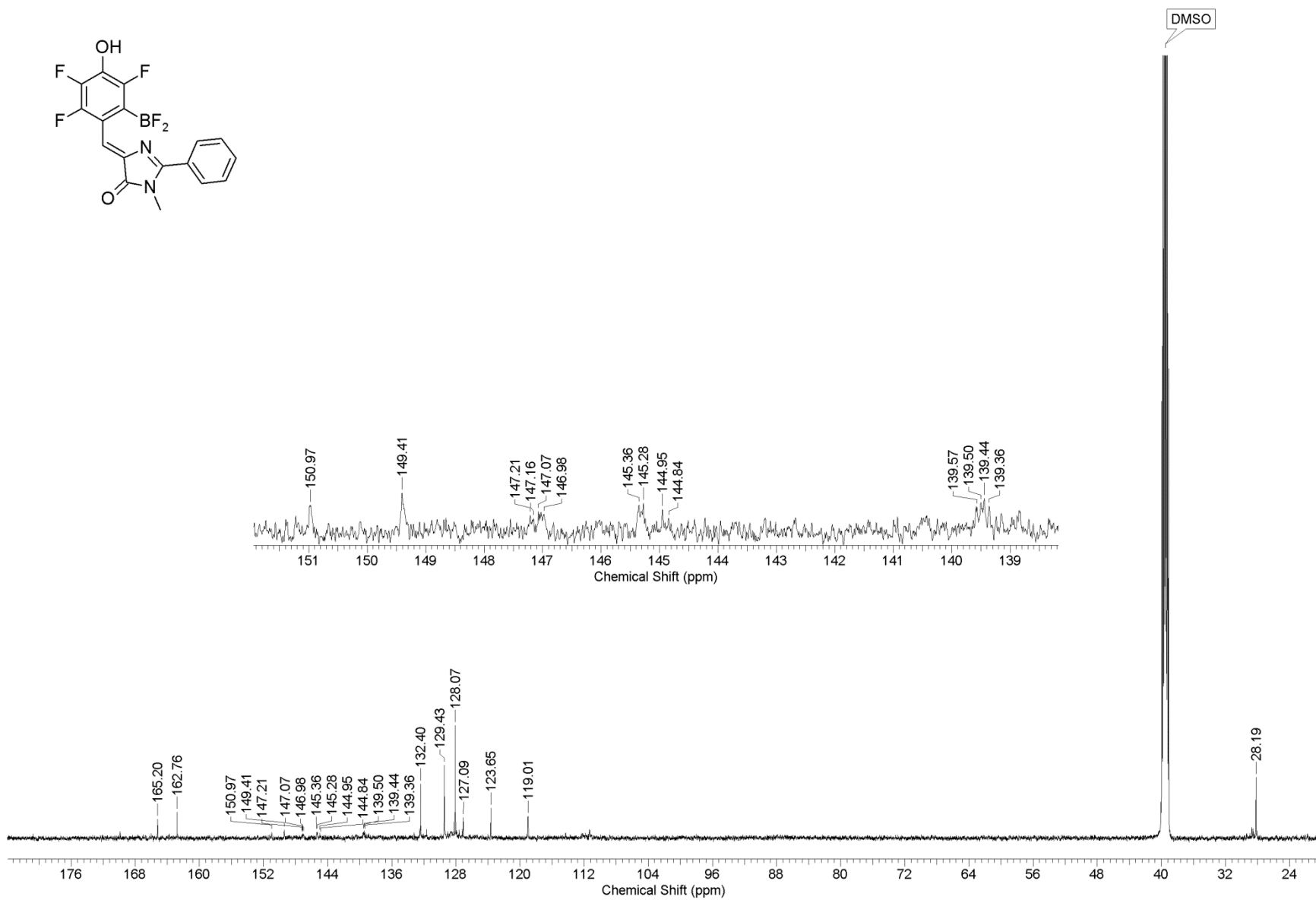
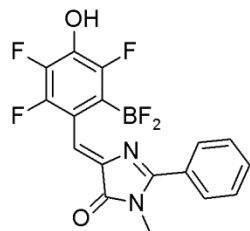


Figure S37.  $^{13}\text{C}$  NMR spectrum of P3F

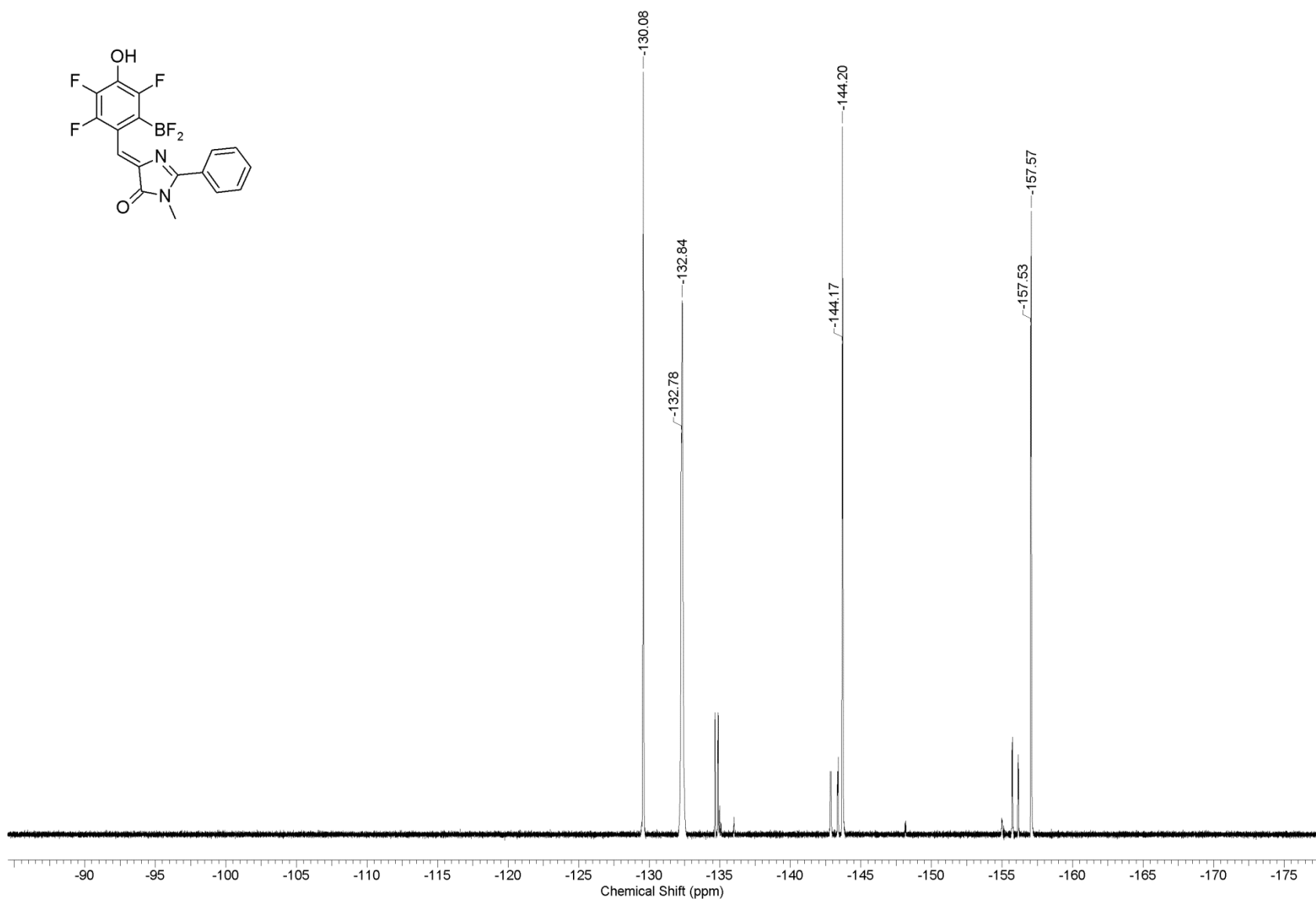


Figure S38.  $^{19}\text{F}$  NMR spectrum of P3F

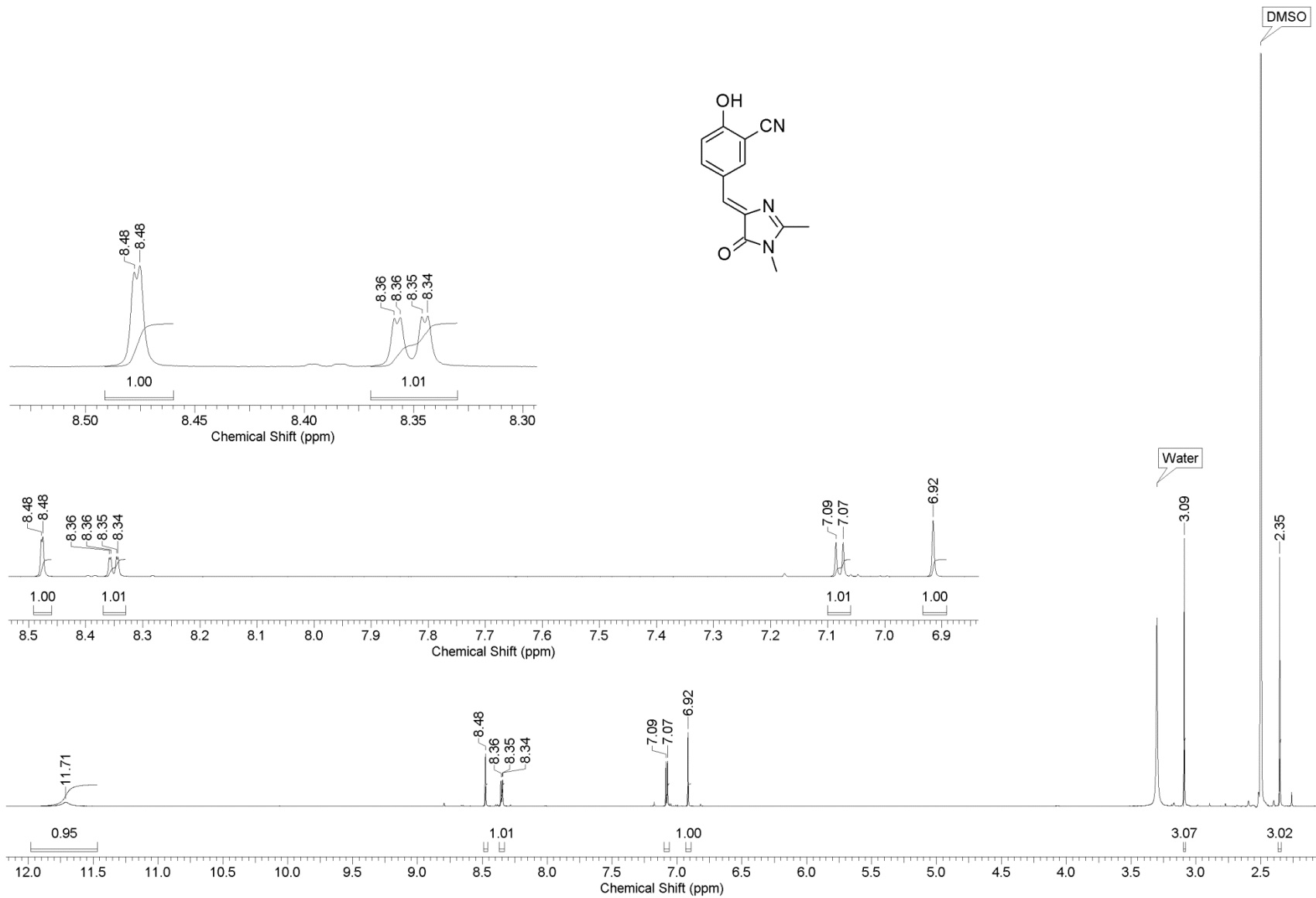
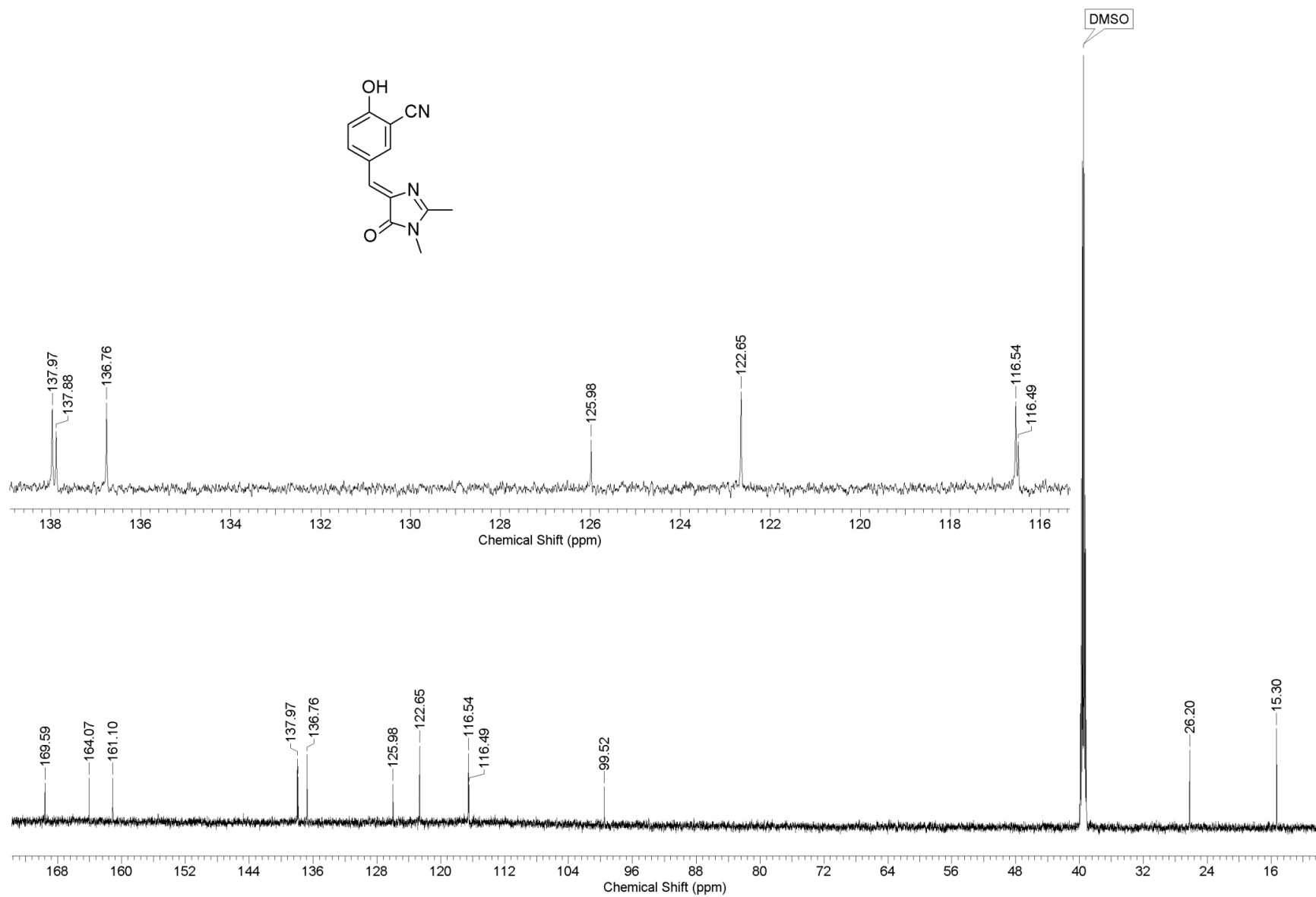
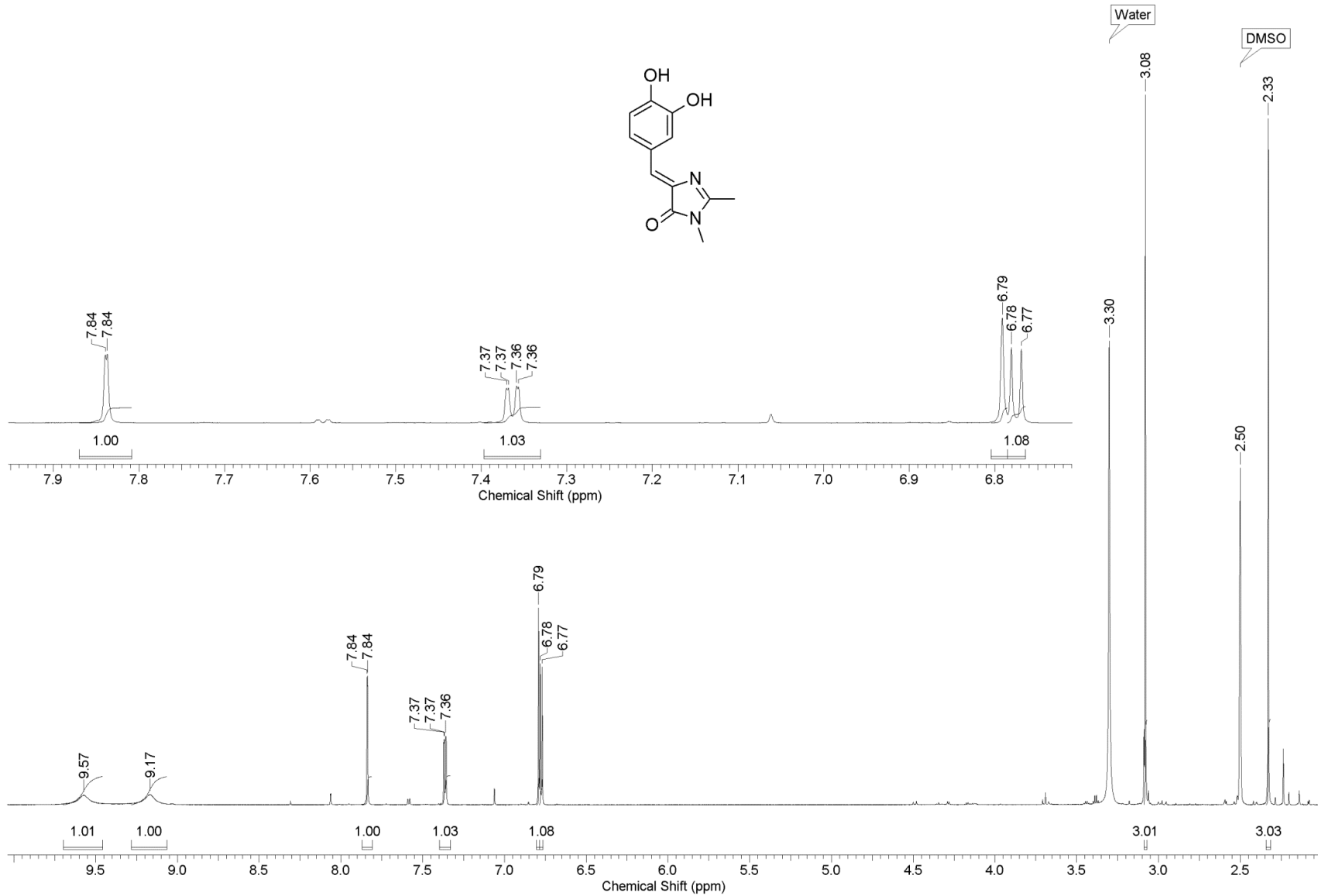


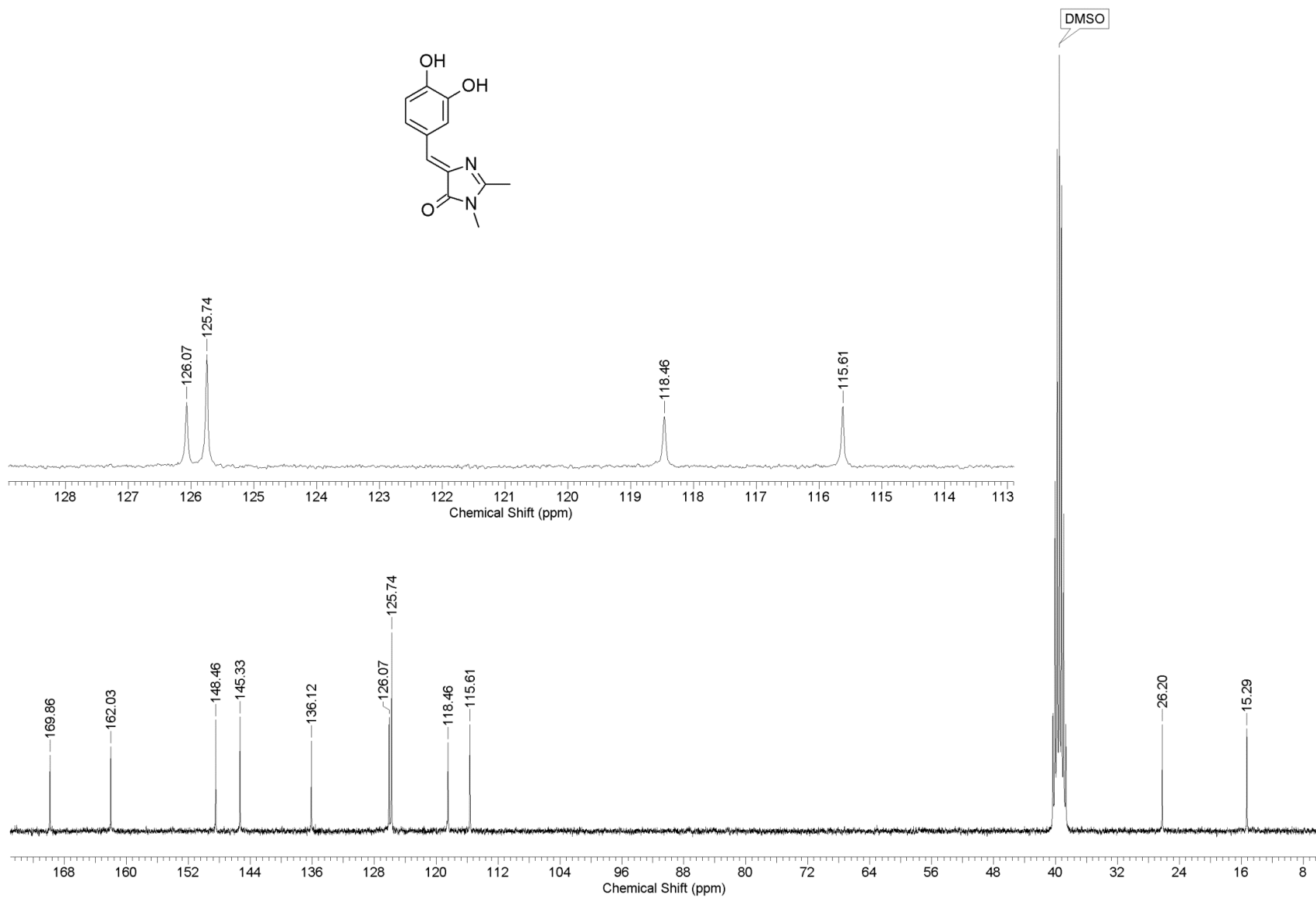
Figure S39. <sup>1</sup>H NMR spectrum of (Z)-4-(3-cyano-4-hydroxybenzylidene)-1,2-dimethyl-1H-imidazol-5(4H)-one (1a)



**Figure S40.** <sup>13</sup>C NMR spectrum of (Z)-4-(3-cyano-4-hydroxybenzylidene)-1,2-dimethyl-1H-imidazol-5(4H)-one



**Figure S41.**  $^1\text{H}$  NMR spectrum of (Z)-4-(3,4-dihydroxybenzylidene)-1,2-dimethyl-1H-imidazol-5(4H)-one (**1c**)



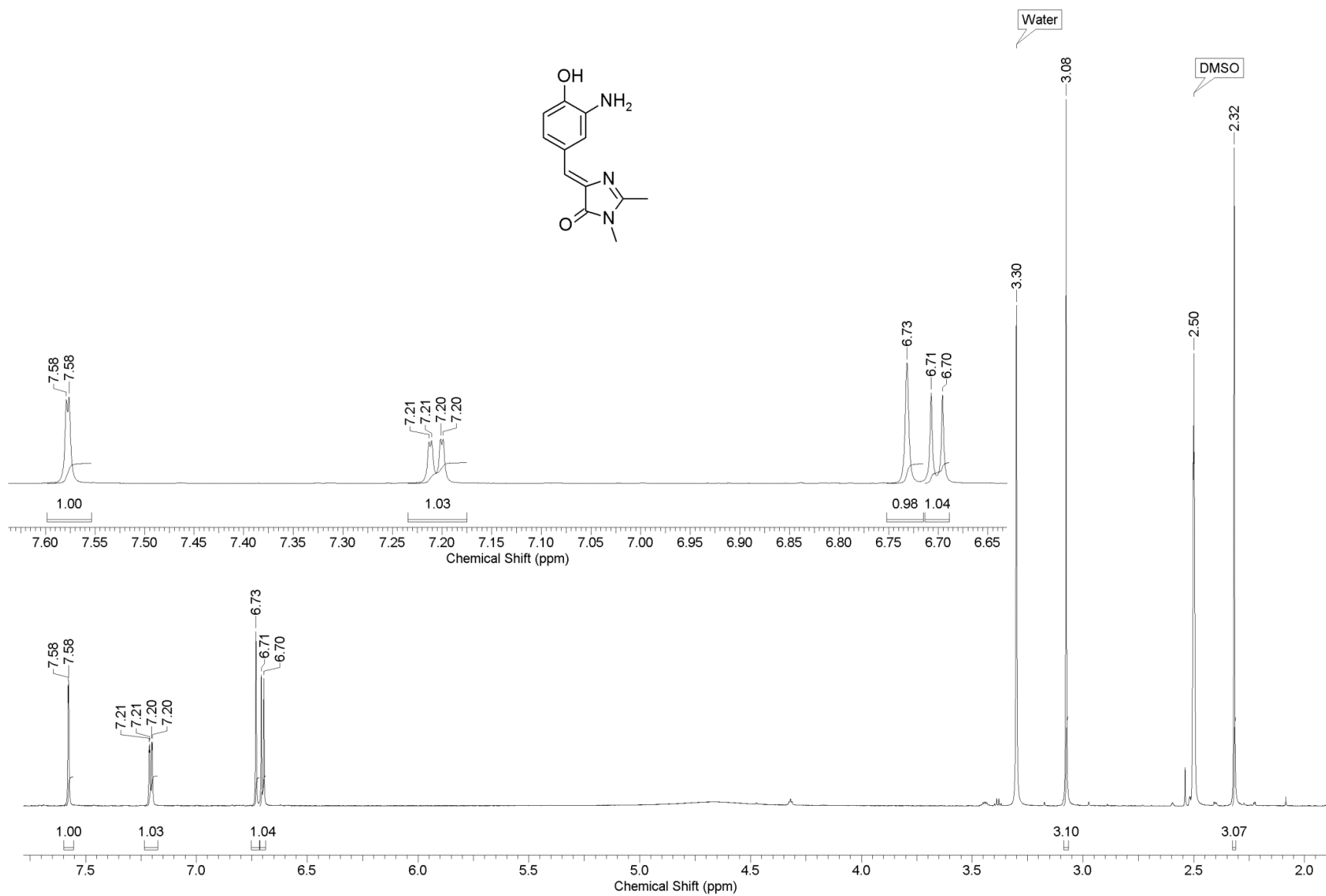


**Figure S43.**  $^1\text{H}$  NMR spectrum of *(Z)*-4-(3-amino-4-hydroxybenzylidene)-1,2-dimethyl-1*H*-imidazol-5(4*H*)-one (**1e**)

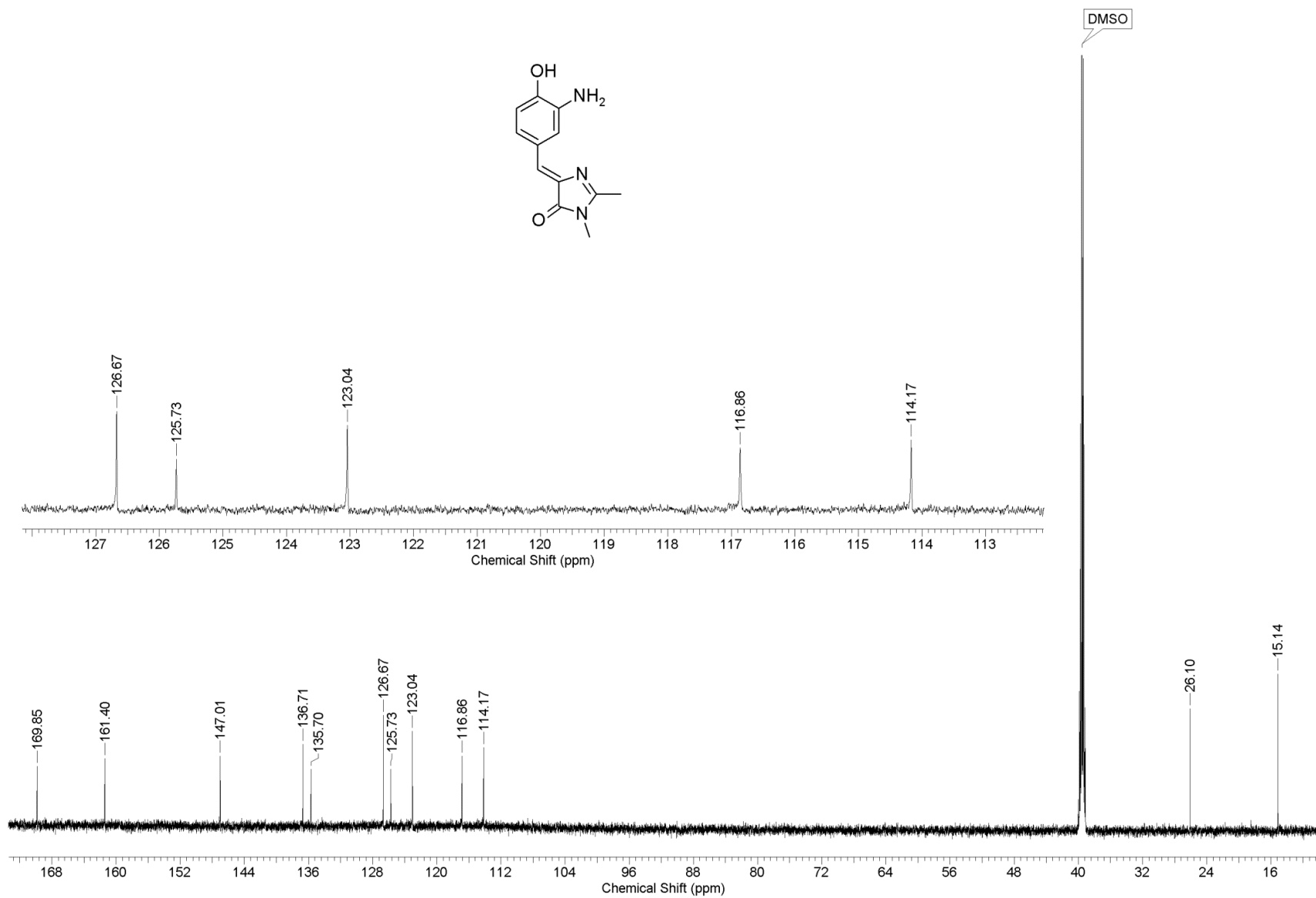


**Figure S44.**  $^{13}\text{C}$  NMR spectrum of (Z)-4-(3-amino-4-hydroxybenzylidene)-1,2-dimethyl-1H-imidazol-5(4H)-one

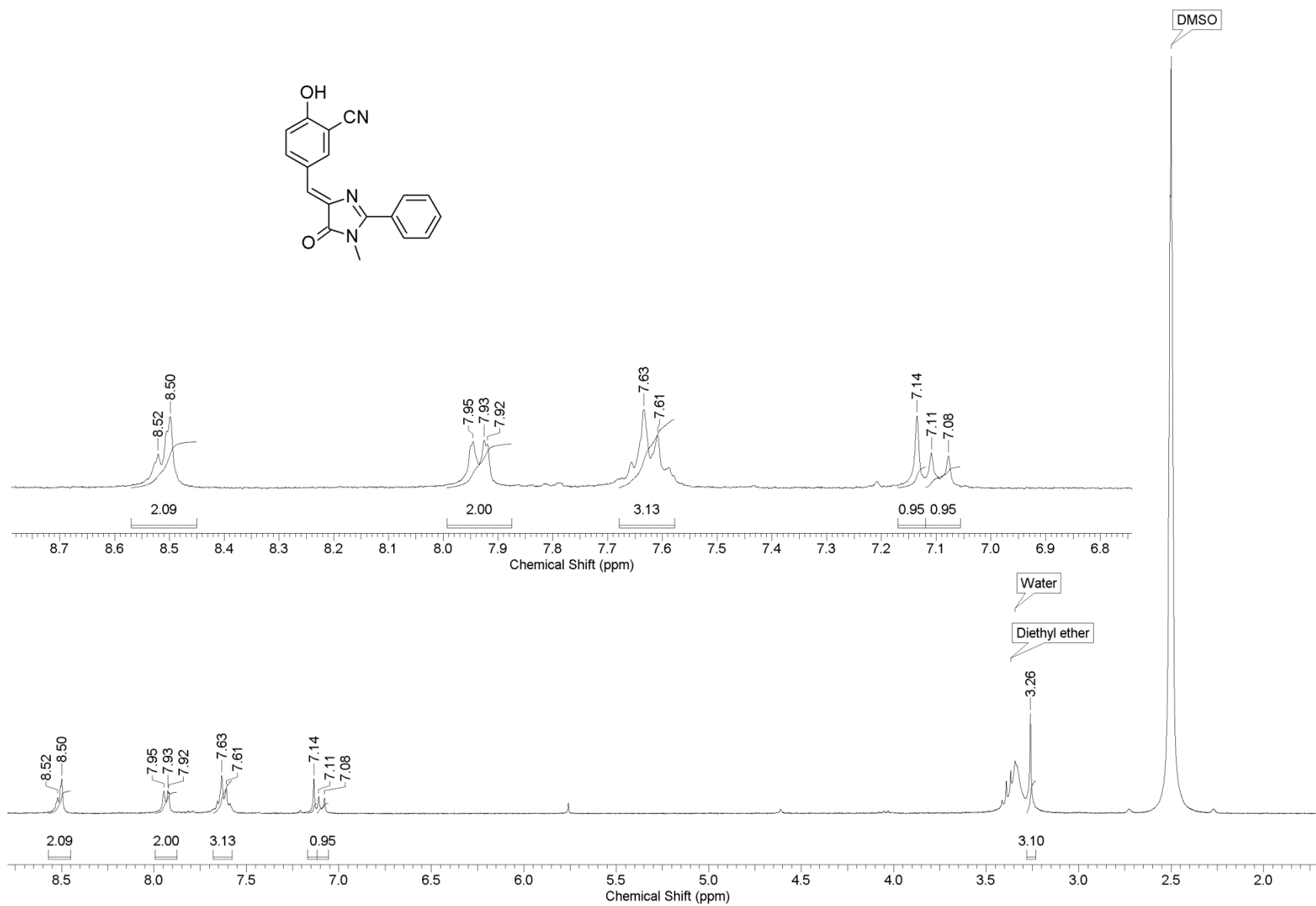
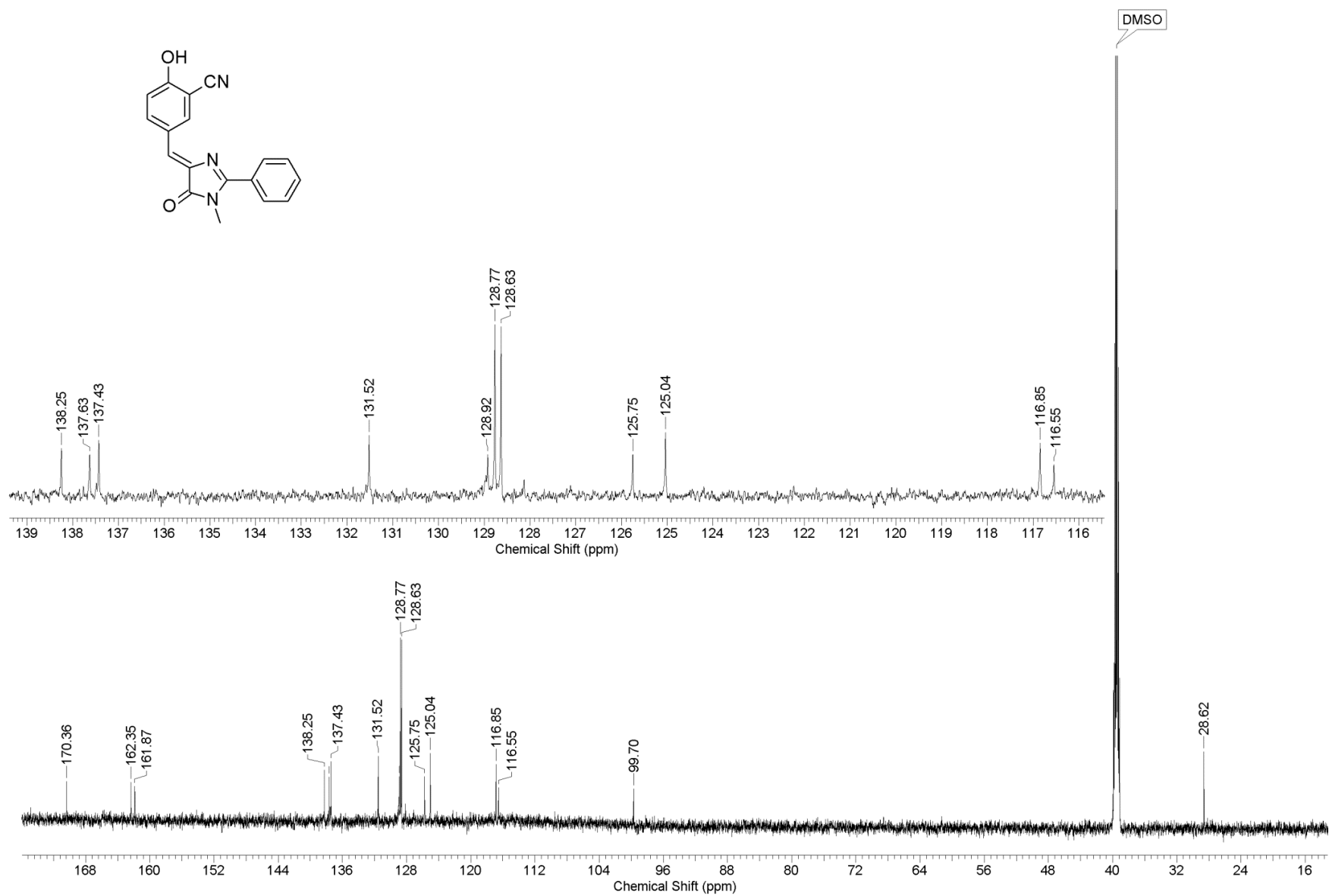
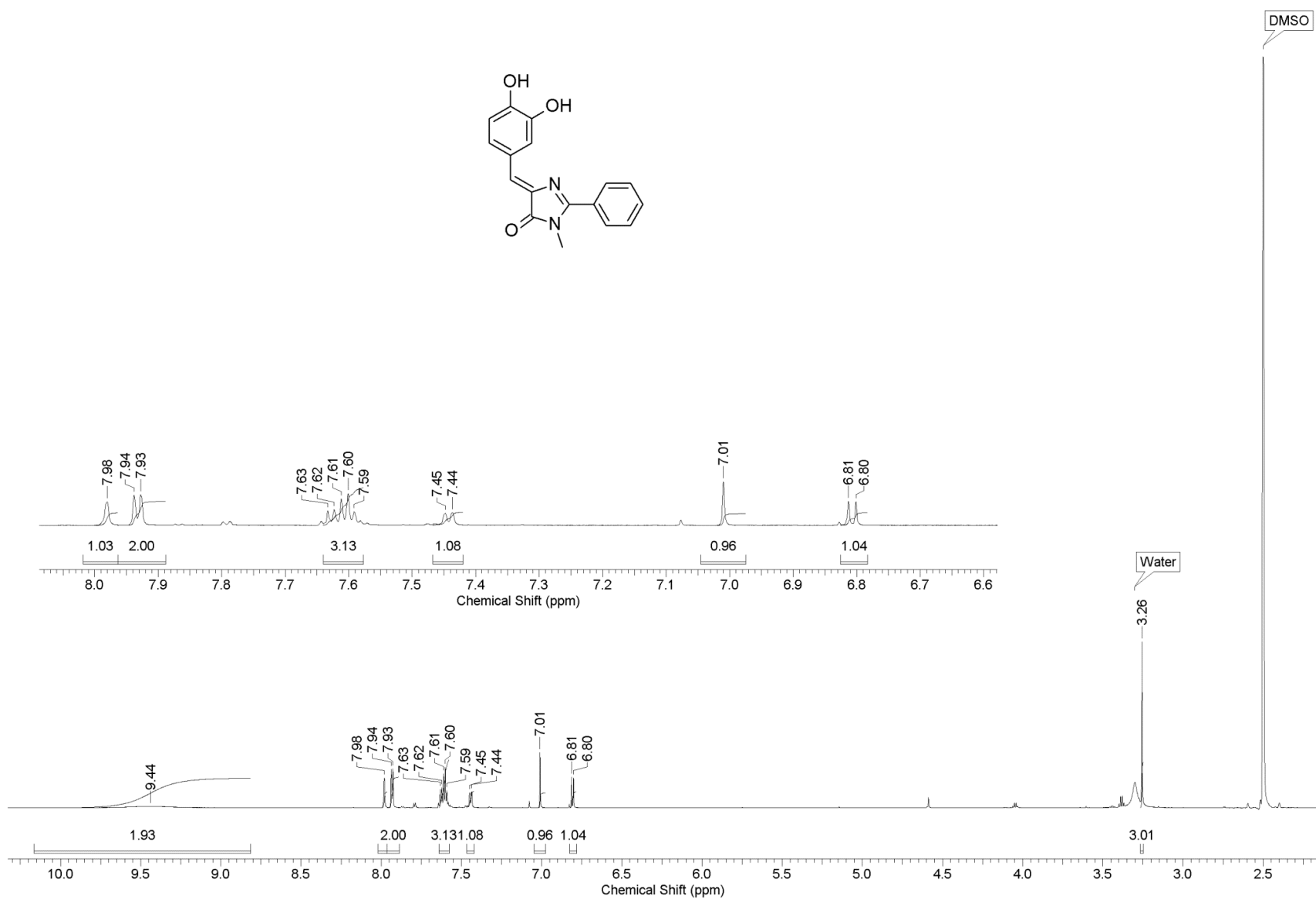
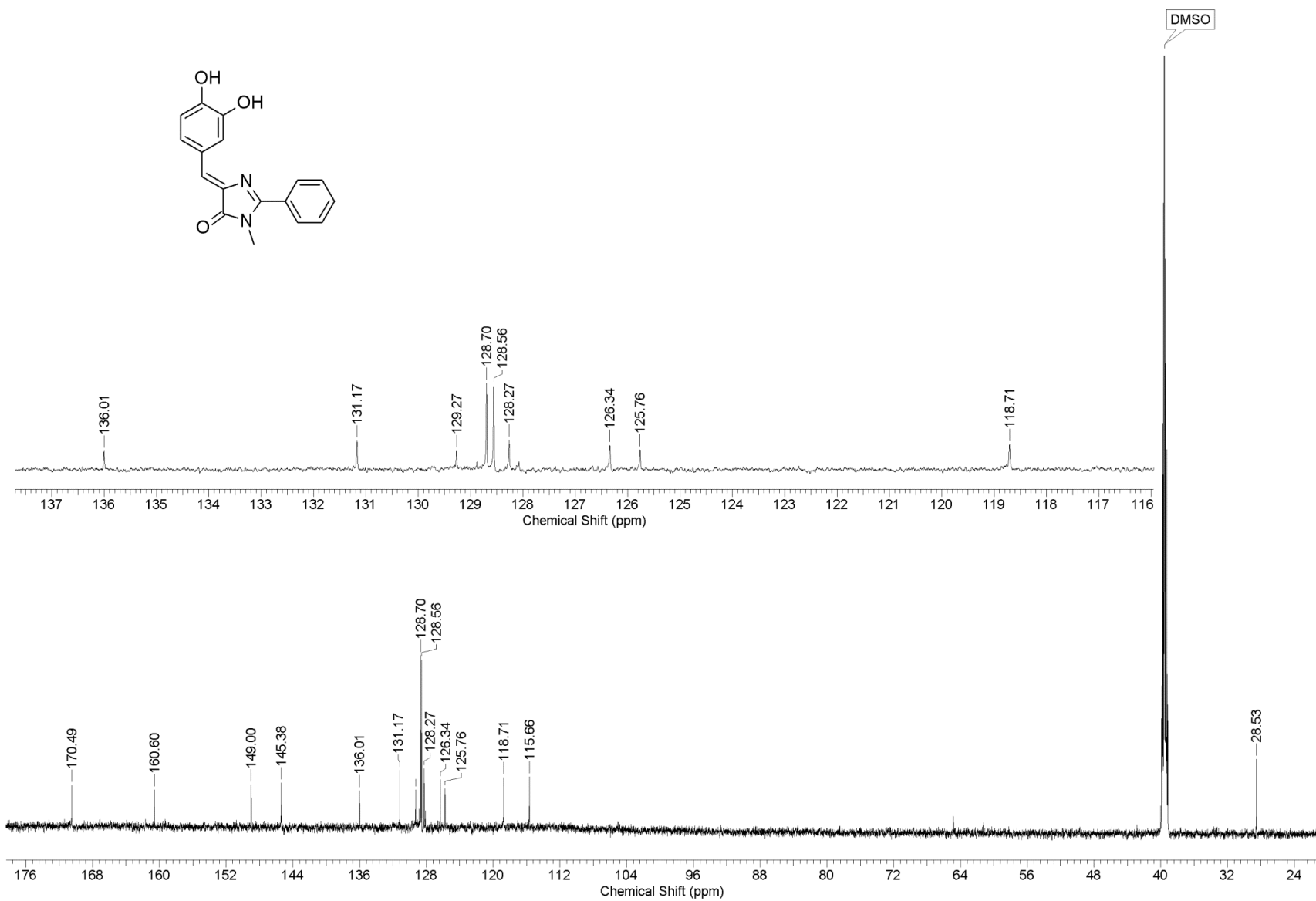


Figure S45. <sup>1</sup>H NMR spectrum of (Z)-4-(3-cyano-4-hydroxybenzylidene)-1-methyl-2-phenyl-1H-imidazol-5(4H)-one (2a)



**Figure S46.** <sup>13</sup>C NMR spectrum of (Z)-4-(3-cyano-4-hydroxybenzylidene)-1-methyl-2-phenyl-1H-imidazol-5(4H)-one





**Figure S48.** <sup>13</sup>C NMR spectrum of (Z)-4-(3,4-dihydroxybenzylidene)-1-methyl-2-phenyl-1H-imidazol-5(4H)-one

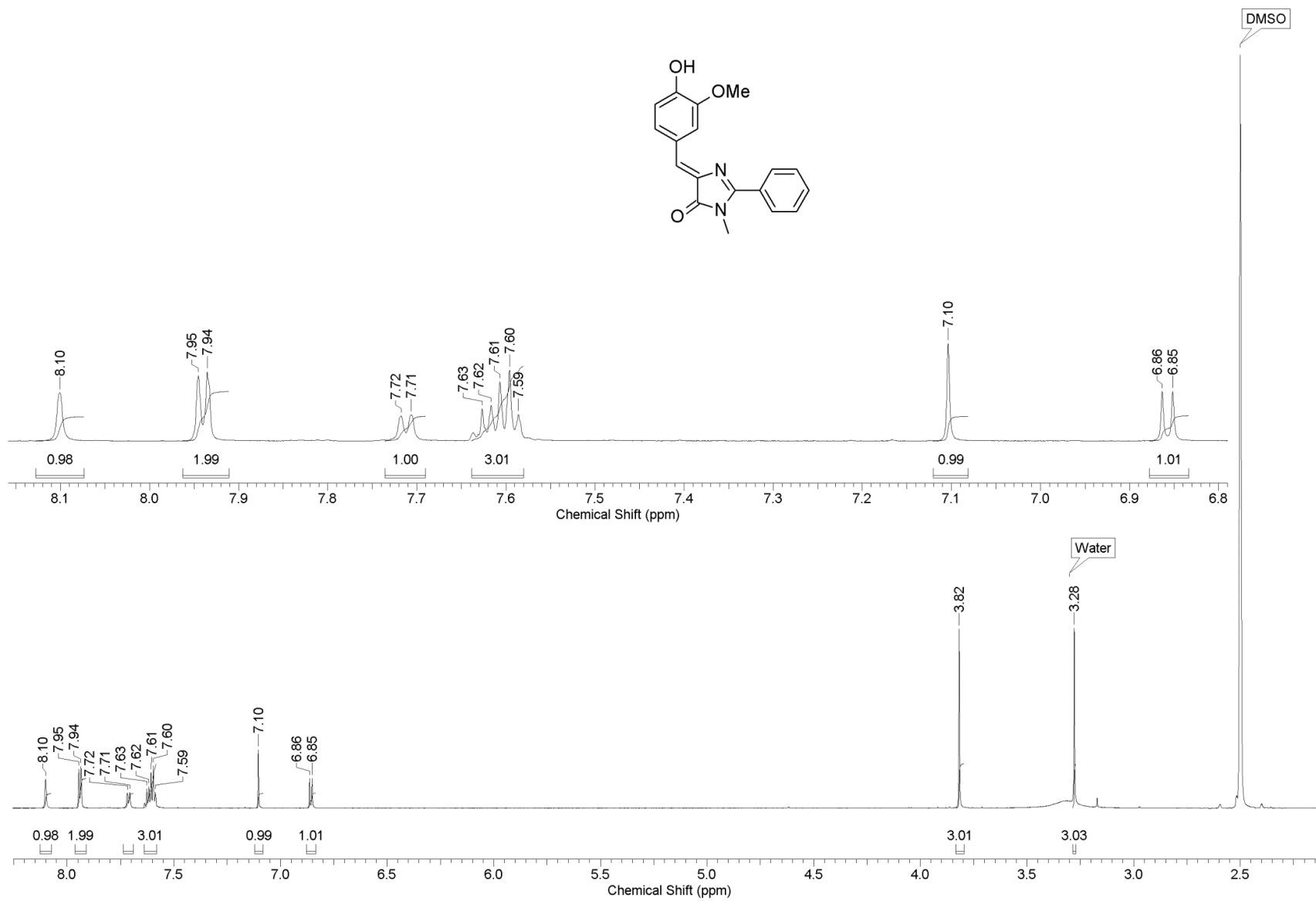


**Figure S49.** <sup>1</sup>H NMR spectrum of (Z)-4-(3-methoxy-4-hydroxybenzylidene)-1-methyl-2-phenyl-1H-imidazol-5(4H)-one (**2d**)

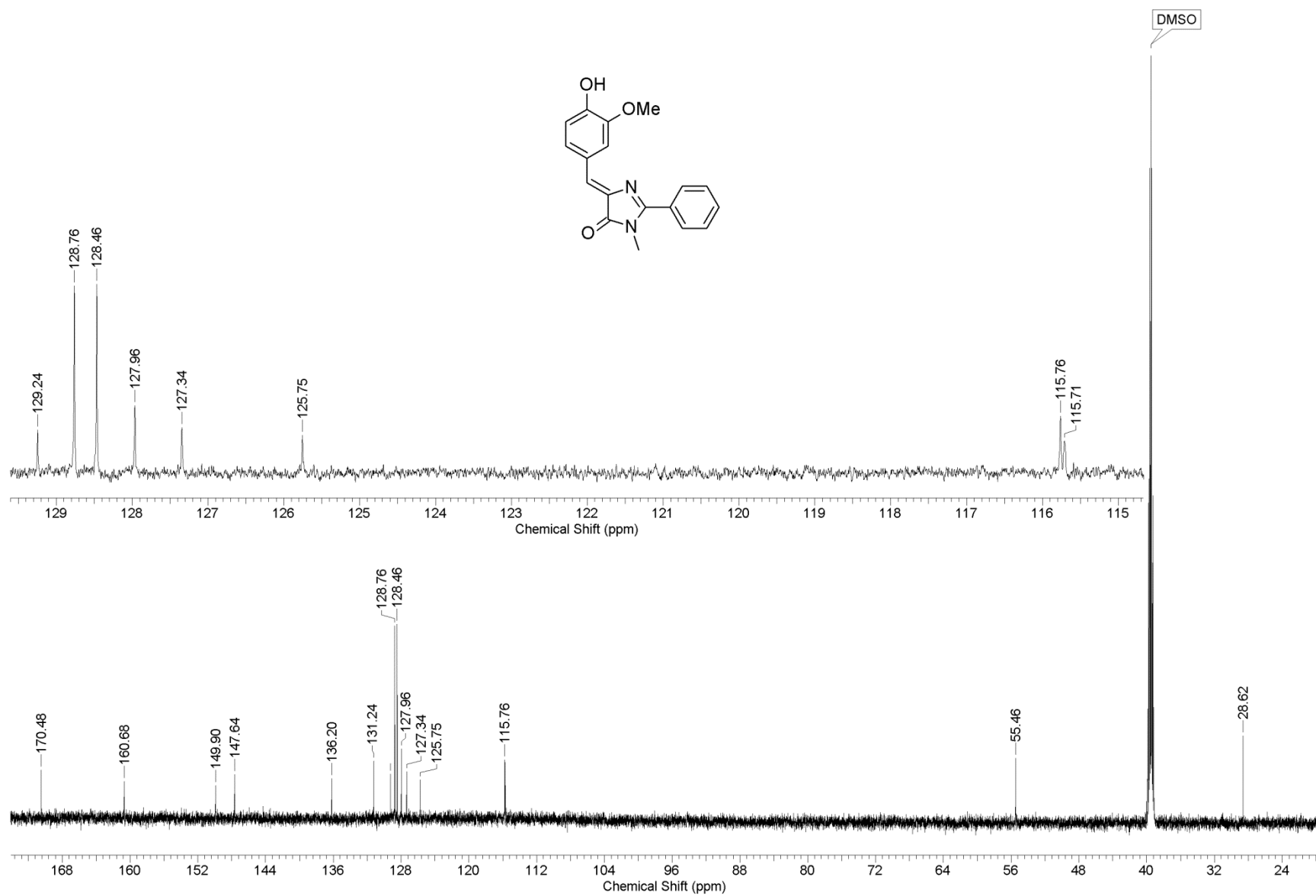


**Figure S50.** <sup>13</sup>C NMR spectrum of (Z)-4-(3-methoxy-4-hydroxybenzylidene)-1-methyl-2-phenyl-1H-imidazol-5(4H)-one

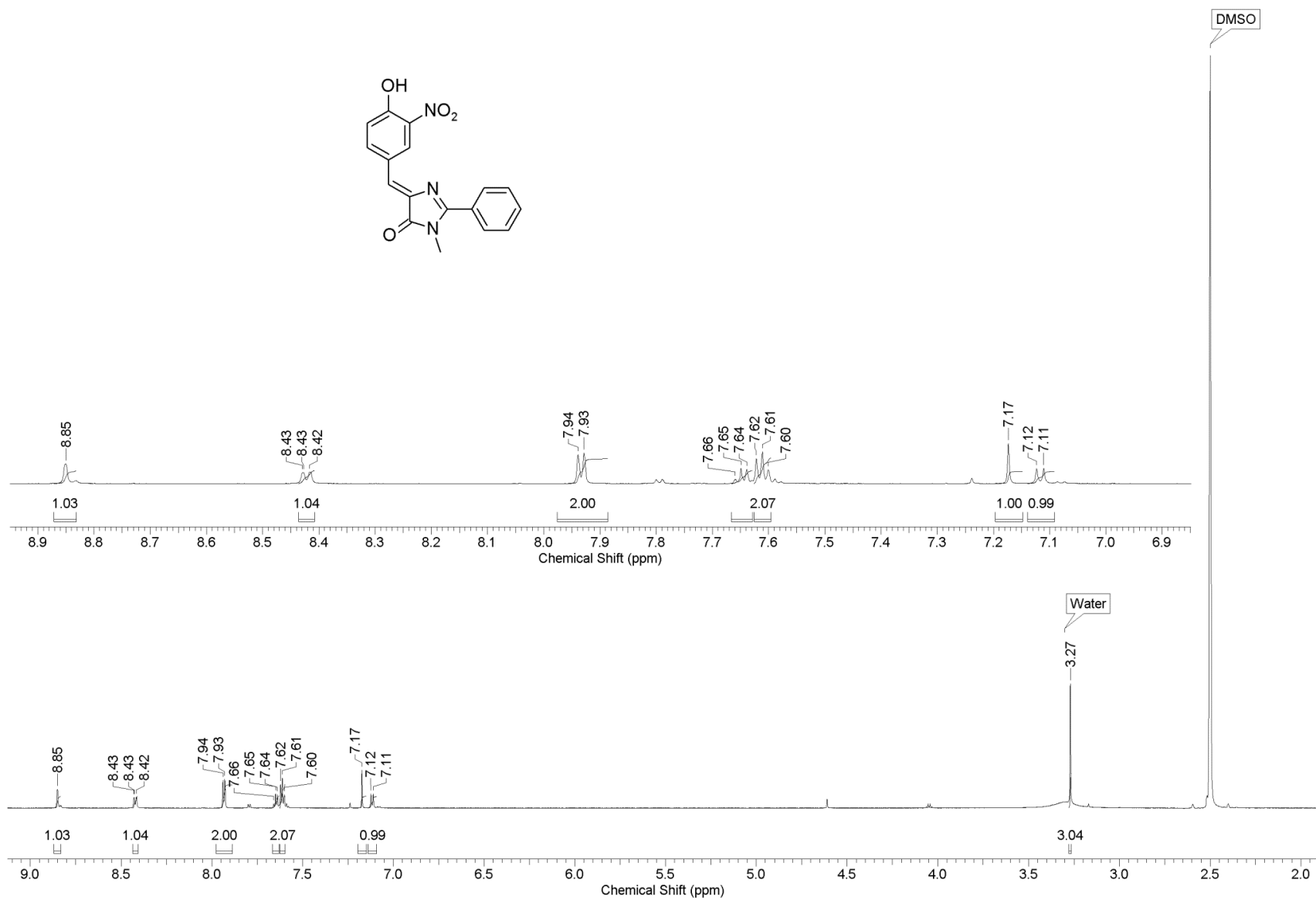


**Figure S51.** <sup>1</sup>H NMR spectrum of (Z)-4-(3-nitro-4-hydroxybenzylidene)-1-methyl-2-phenyl-1H-imidazol-5(4H)-one (**2f**)

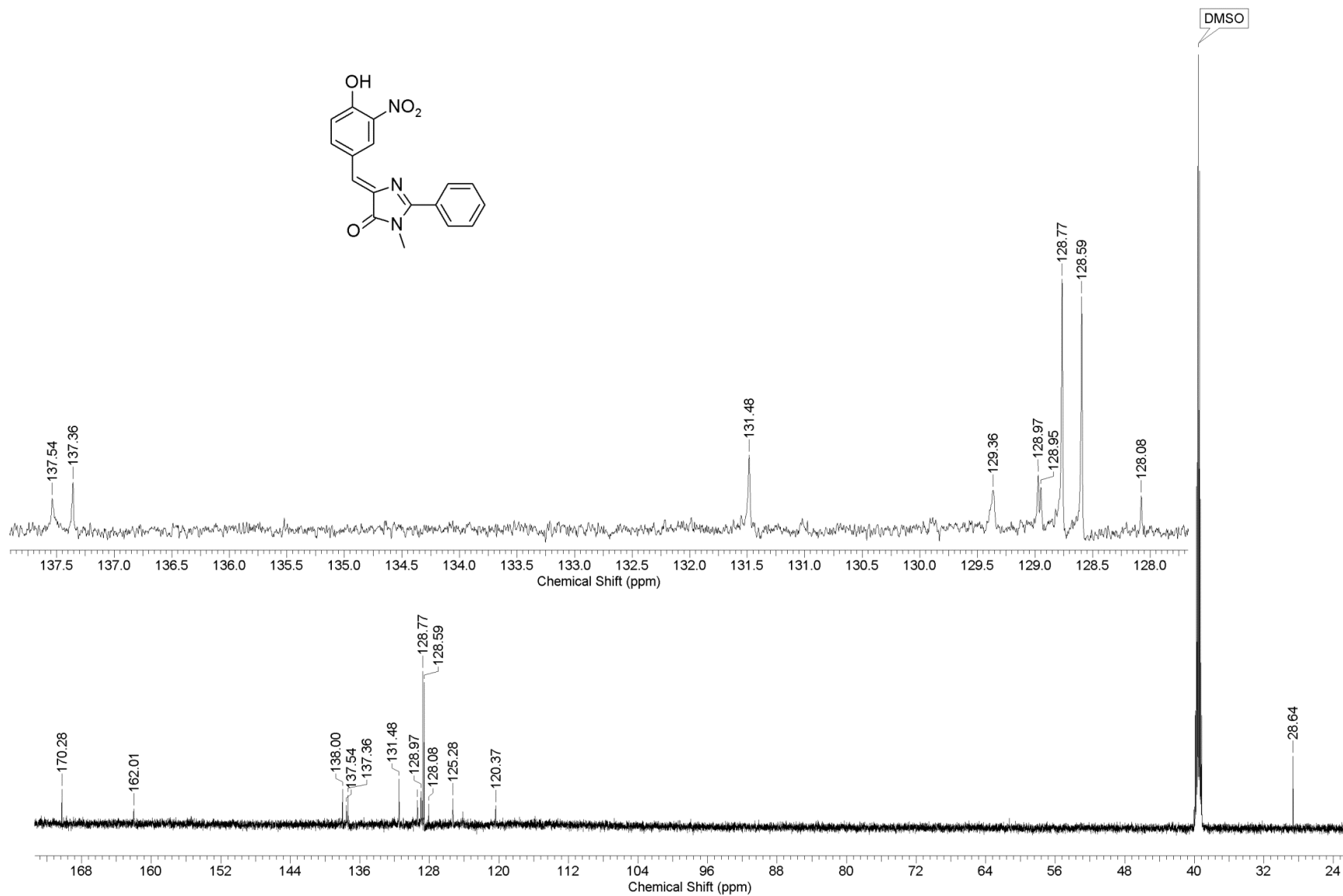


**Figure S52.** <sup>13</sup>C NMR spectrum of (Z)-4-(3-nitro-4-hydroxybenzylidene)-1-methyl-2-phenyl-1H-imidazol-5(4H)-one

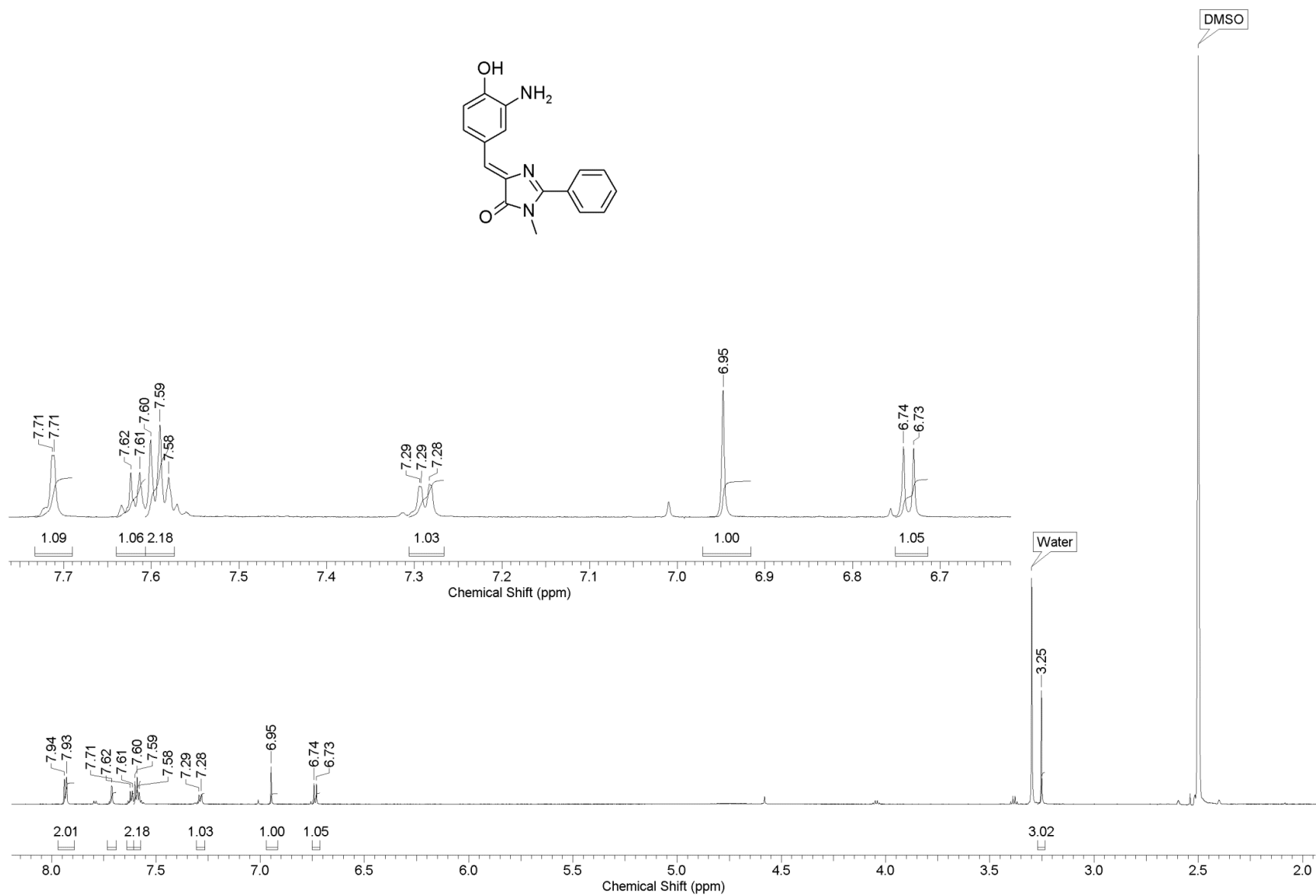


**Figure S53.** <sup>1</sup>H NMR spectrum of (Z)-4-(3-amino-4-hydroxybenzylidene)-1-methyl-2-phenyl-1H-imidazol-5(4H)-one (**2e**)

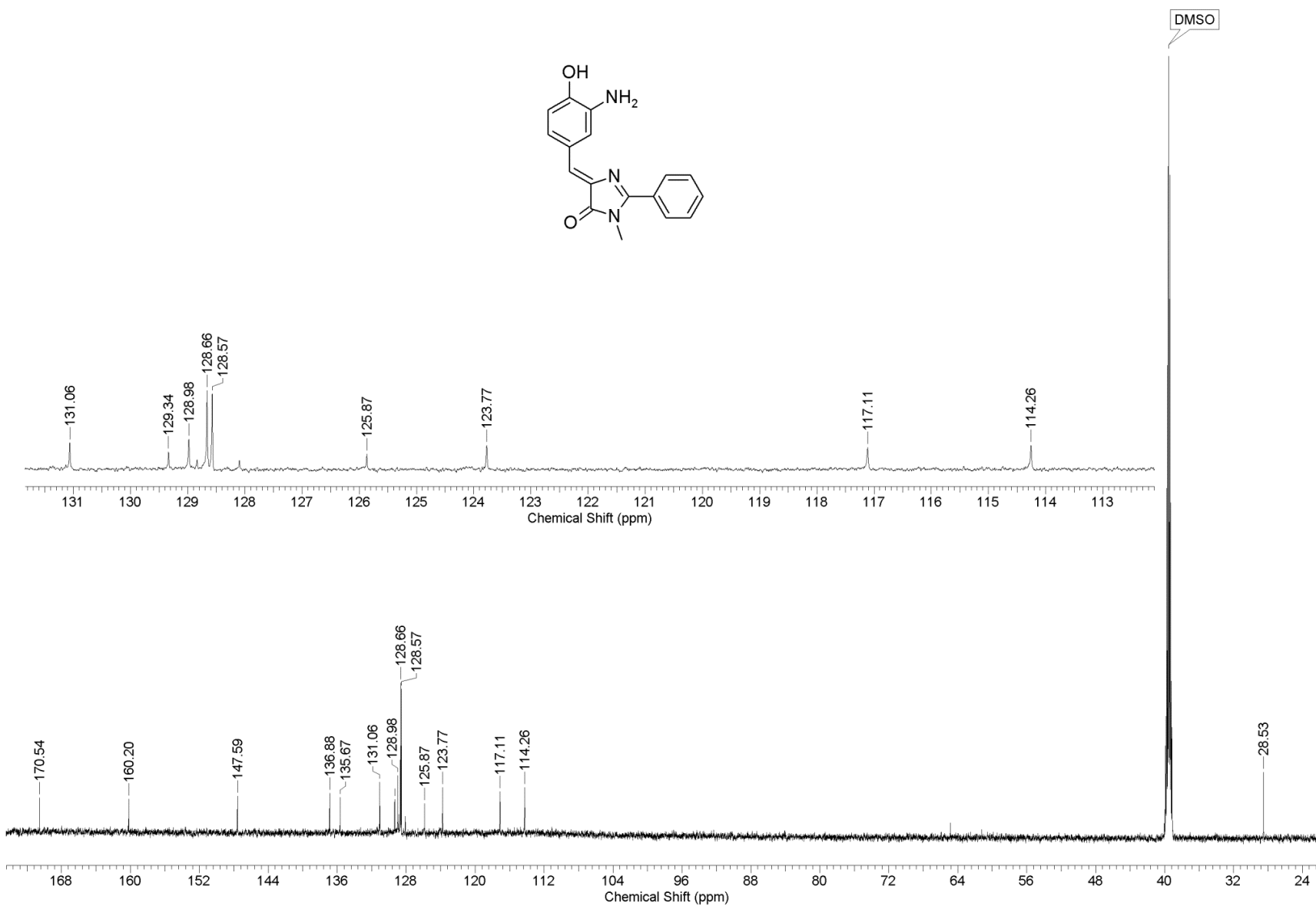


**Figure S54.**  $^{13}\text{C}$  NMR spectrum of (Z)-4-(3-amino-4-hydroxybenzylidene)-1-methyl-2-phenyl-1H-imidazol-5(4H)-one

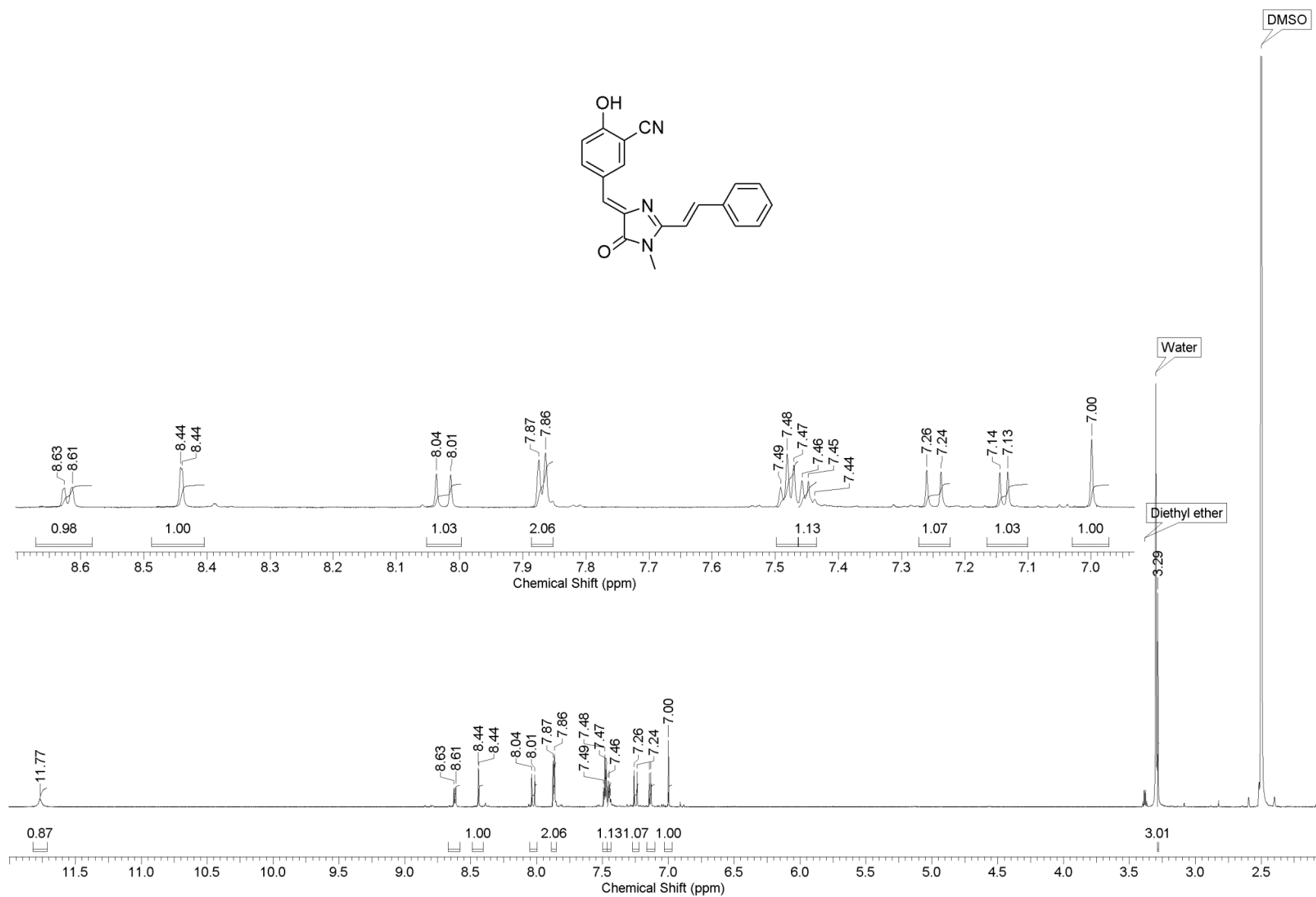


**Figure S55.** <sup>1</sup>H NMR spectrum of (Z)-4-(3-cyano-4-hydroxybenzylidene)-1-methyl-2-((E)-styryl)-1H-imidazol-5(4H)-one (3a)

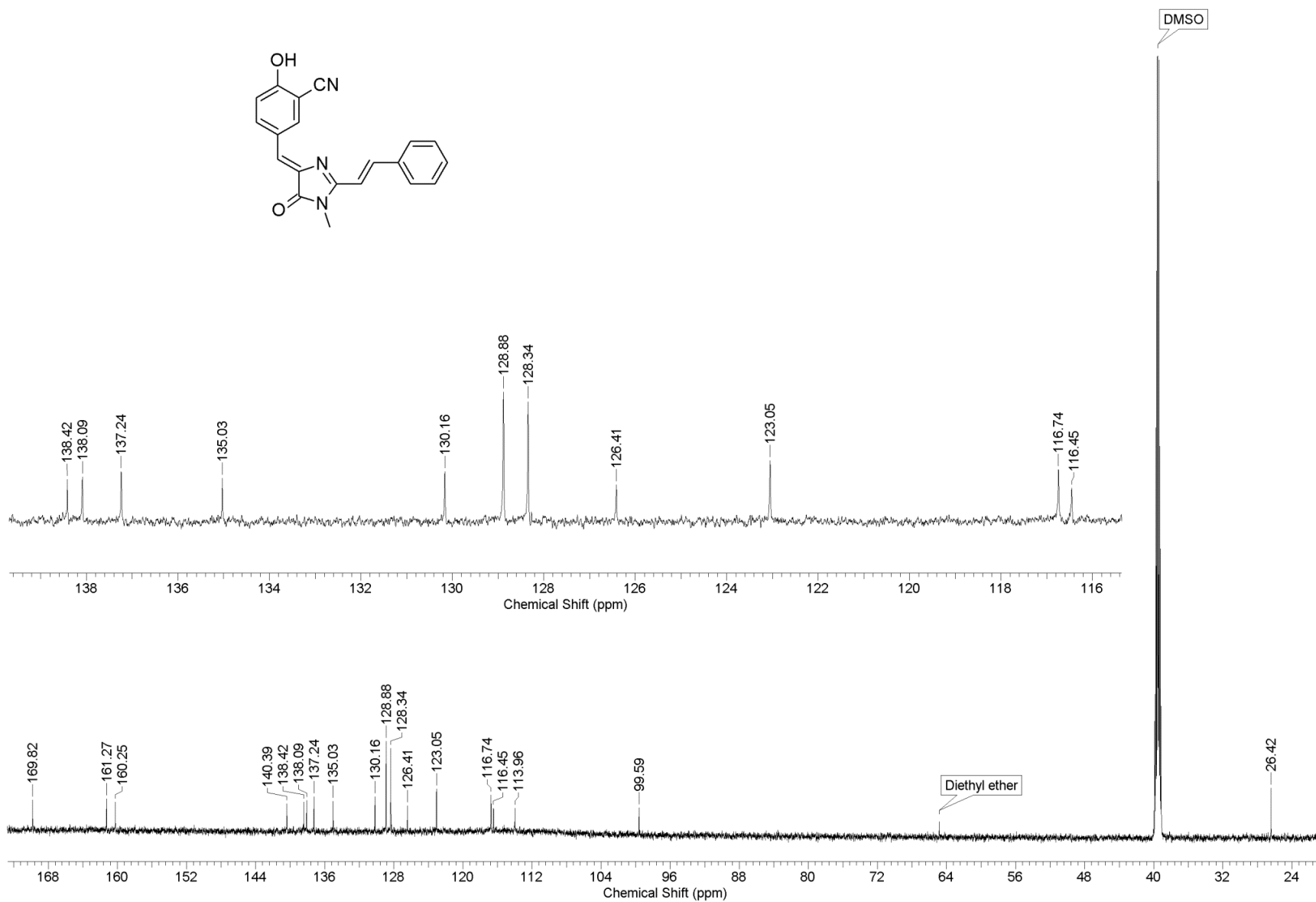


Figure S56. <sup>13</sup>C NMR spectrum of (Z)-4-(3-cyano-4-hydroxybenzylidene)-1-methyl-2-((E)-styryl)-1H-imidazol-5(4H)-one

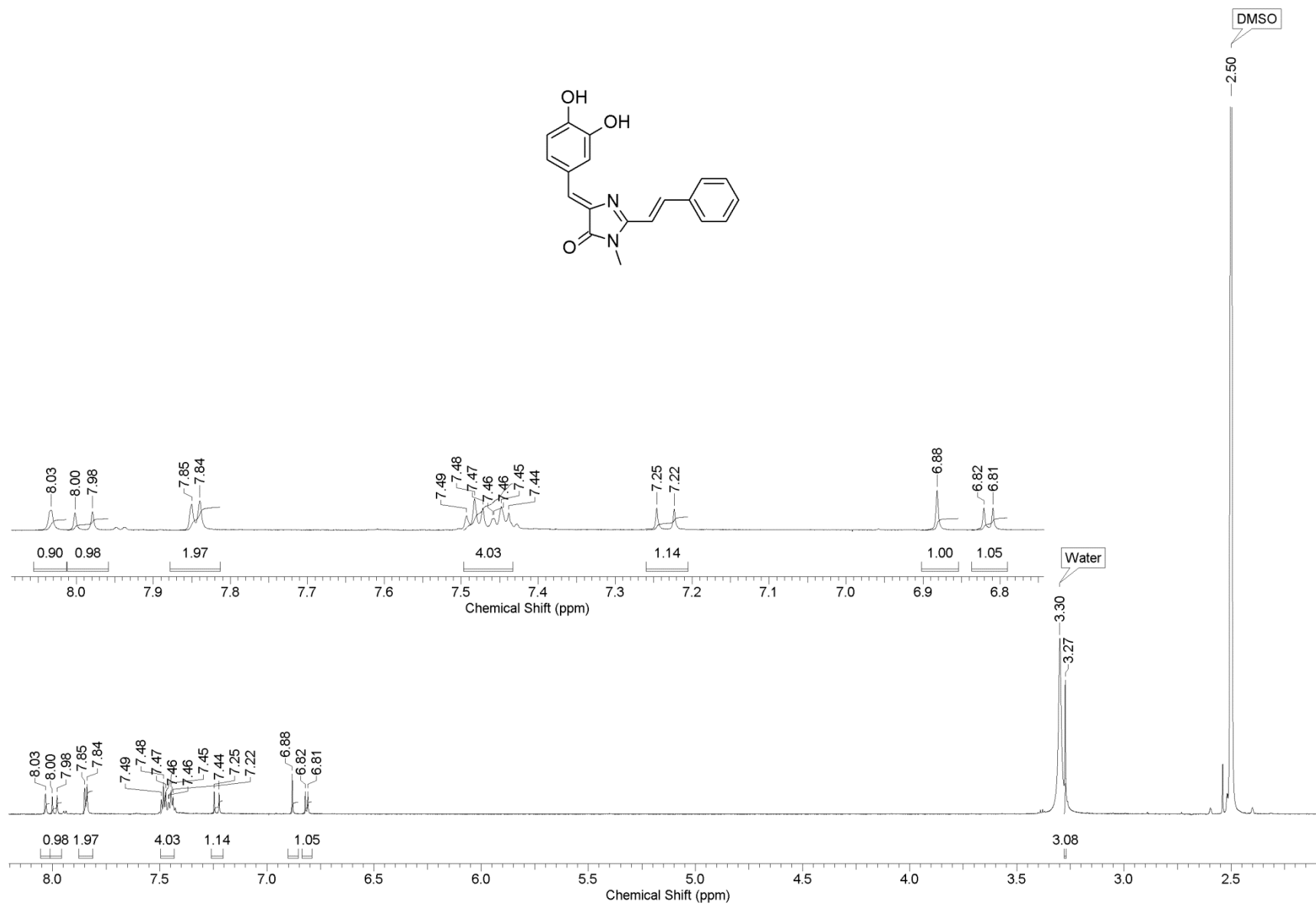
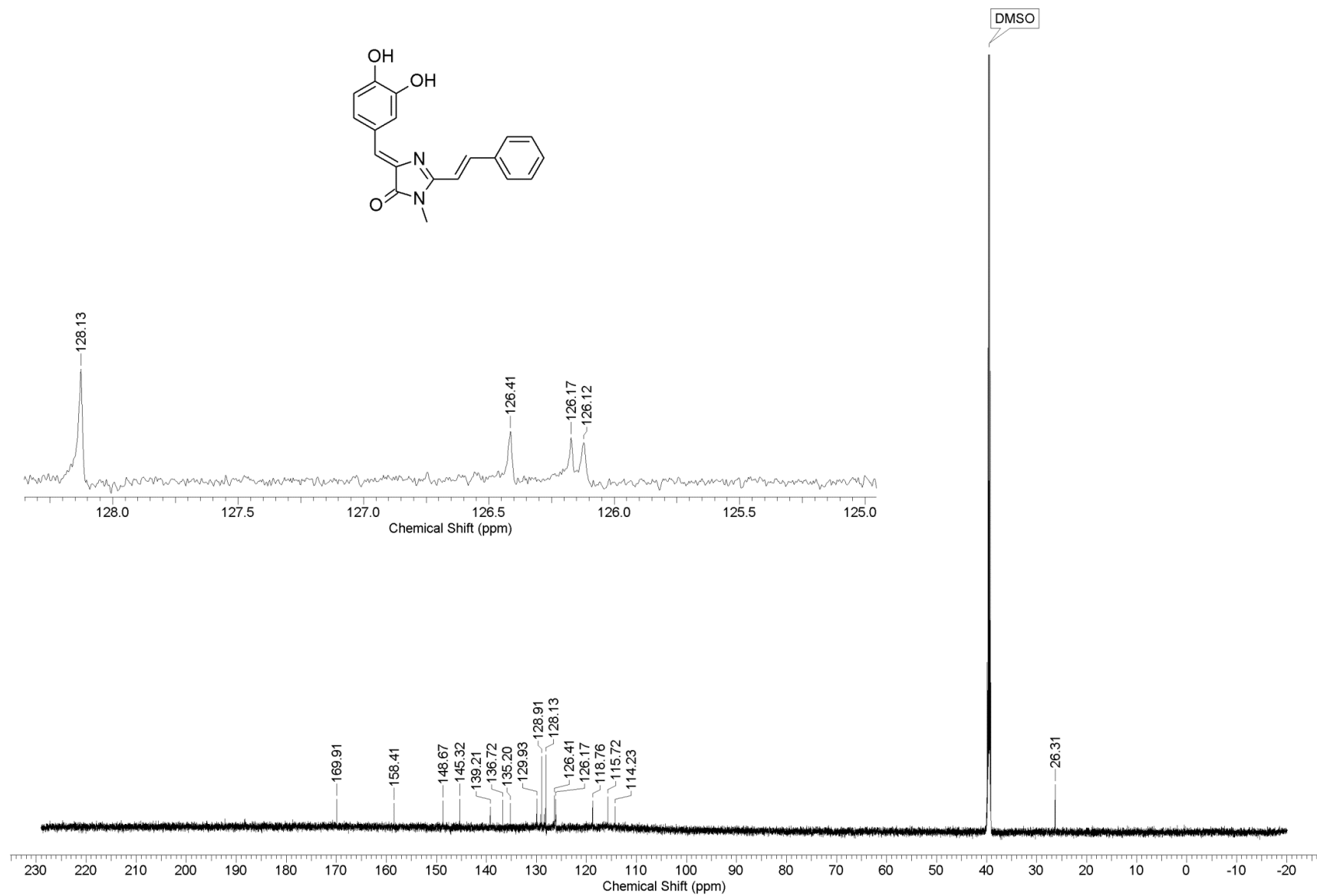
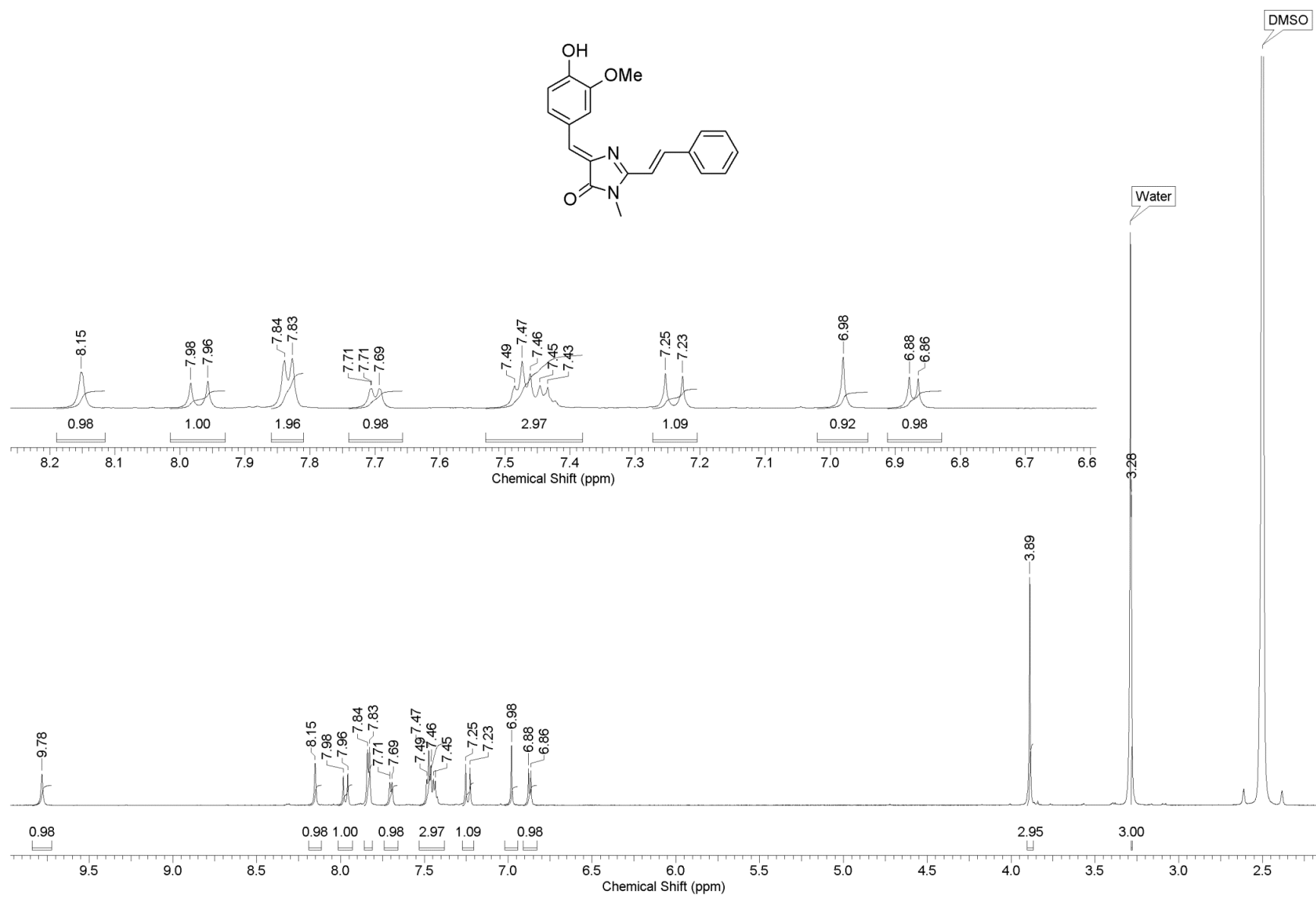


Figure S57. <sup>1</sup>H NMR spectrum of (Z)-4-(3,4-dihydroxybenzylidene)-1-methyl-2-((E)-styryl)-1H-imidazol-5(4H)-one (3c)



**Figure S58.** <sup>13</sup>C NMR spectrum of (Z)-4-(3,4-dihydroxybenzylidene)-1-methyl-2-((E)-styryl)-1H-imidazol-5(4H)-one



**Figure S59.** <sup>1</sup>H NMR spectrum of (Z)-4-(3-methoxy-4-hydroxybenzylidene)-1-methyl-2-((E)-styryl)-1H-imidazol-5(4H)-one (**3d**)

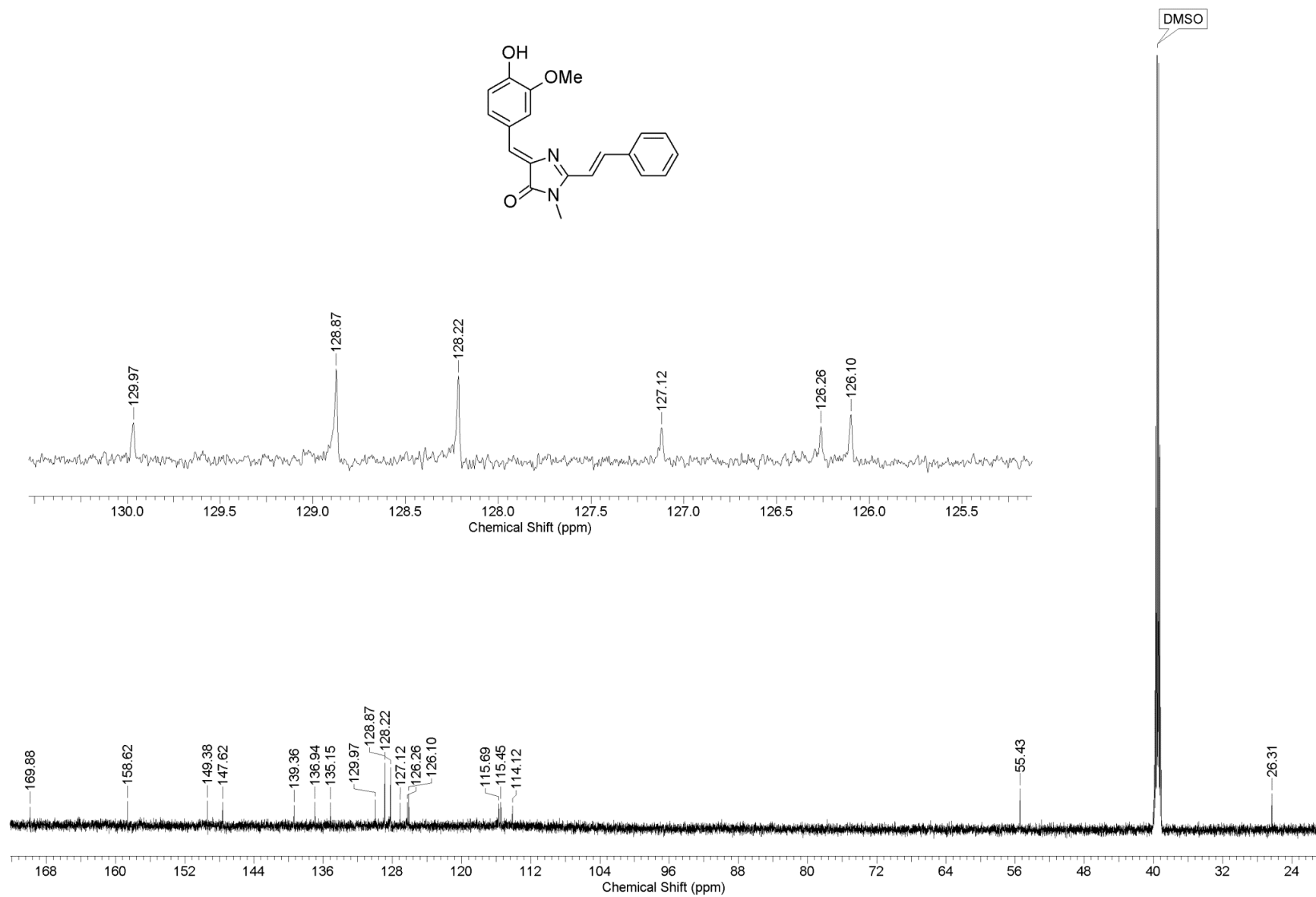


**Figure S60.** <sup>13</sup>C NMR spectrum of *(Z)*-4-(3-methoxy-4-hydroxybenzylidene)-1-methyl-2-((*E*)-styryl)-1*H*-imidazol-5(4*H*)-one

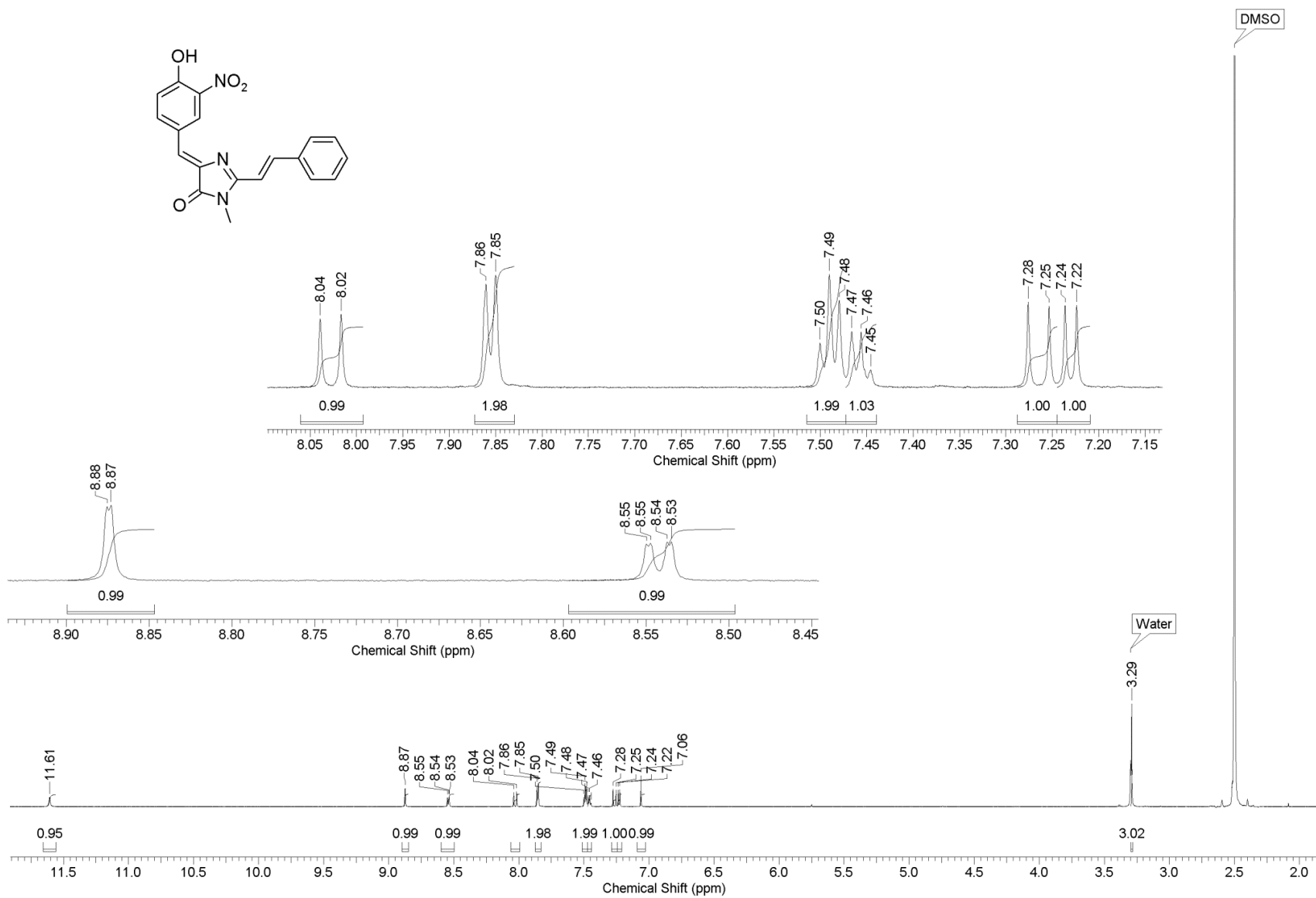


**Figure S61.** <sup>1</sup>H NMR spectrum of *(Z)*-4-(3-nitro-4-hydroxybenzylidene)-1-methyl-2-*((E)*-styryl)-1*H*-imidazol-5(4*H*)-one (**3f**)

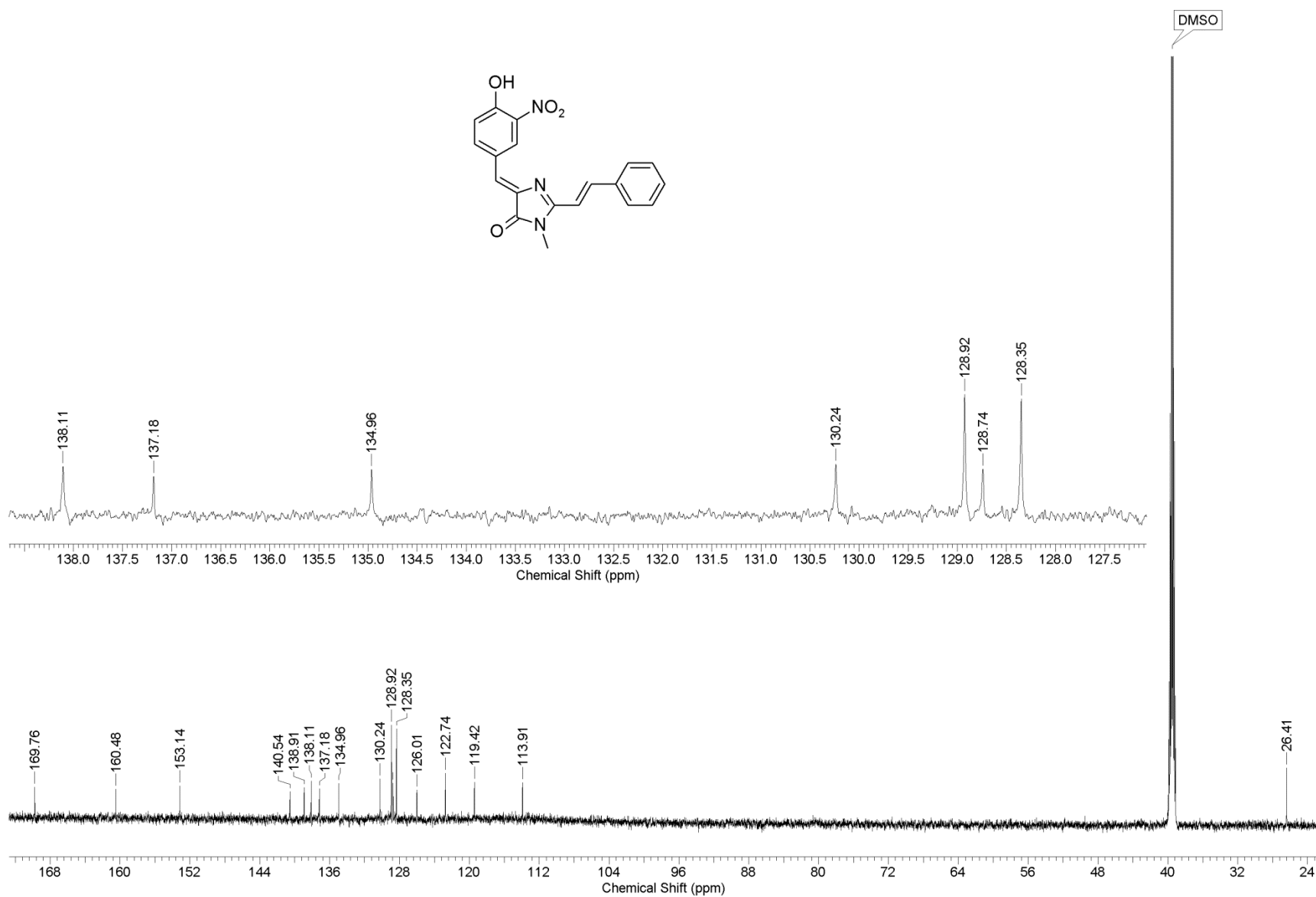
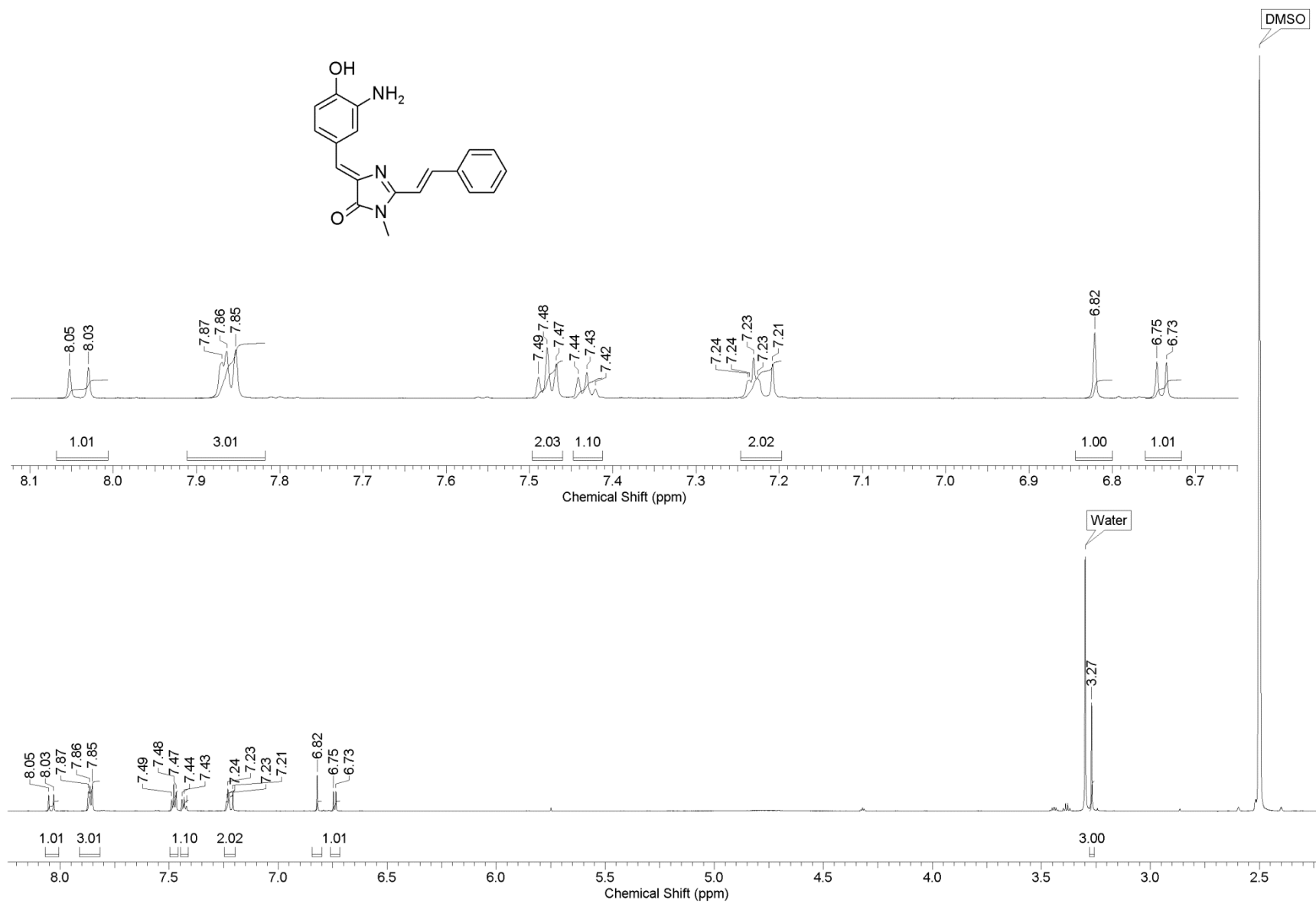
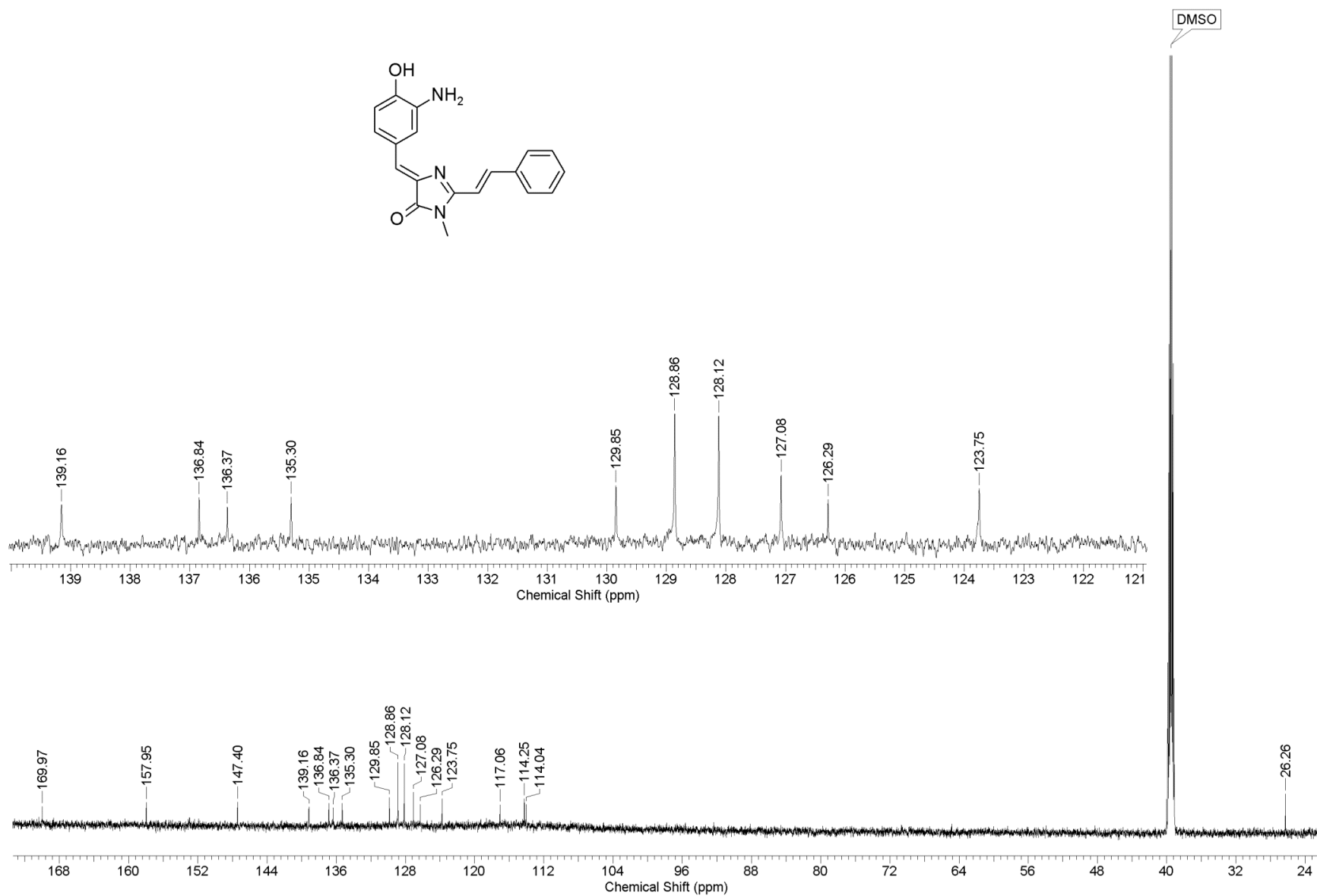


Figure S62. <sup>13</sup>C NMR spectrum of *(Z)*-4-(3-nitro-4-hydroxybenzylidene)-1-methyl-2-((*E*)-styryl)-1*H*-imidazol-5(4*H*)-one



**Figure S63.** <sup>1</sup>H NMR spectrum of *(Z)*-4-(3-amino-4-hydroxybenzylidene)-1-methyl-2-((*E*)-styryl)-1*H*-imidazol-5(4*H*)-one (**3e**)



**Figure S64.** <sup>13</sup>C NMR spectrum of *(Z)*-4-(3-amino-4-hydroxybenzylidene)-1-methyl-2-((*E*)-styryl)-1*H*-imidazol-5(4*H*)-one

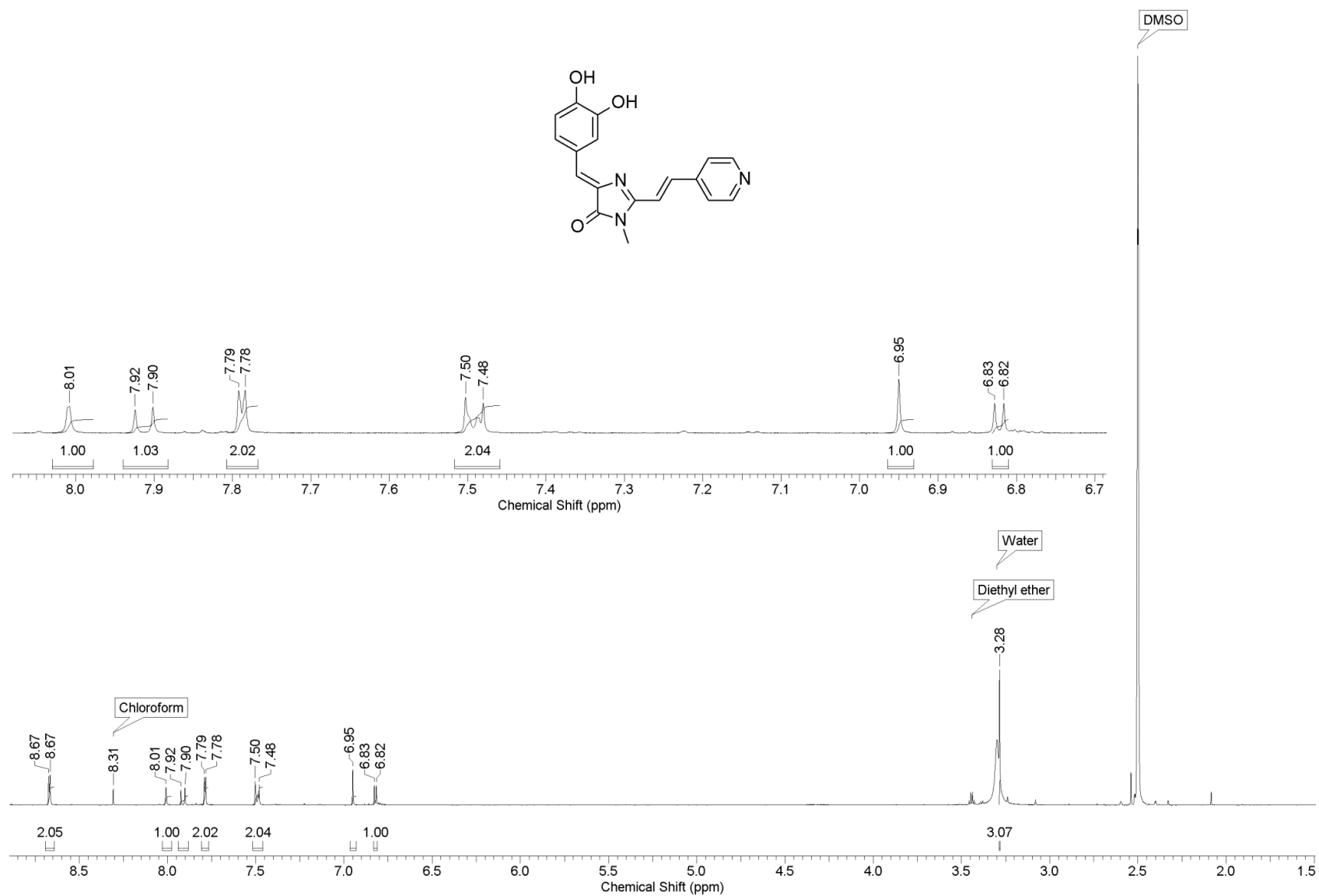


**Figure S65.** <sup>1</sup>H NMR spectrum of (*Z*)-4-(3,4-dihydroxybenzylidene)-1-methyl-2-((*E*)-2-(pyridin-4-yl)vinyl)-1*H*-imidazol-5(4*H*)-one (**4c**)

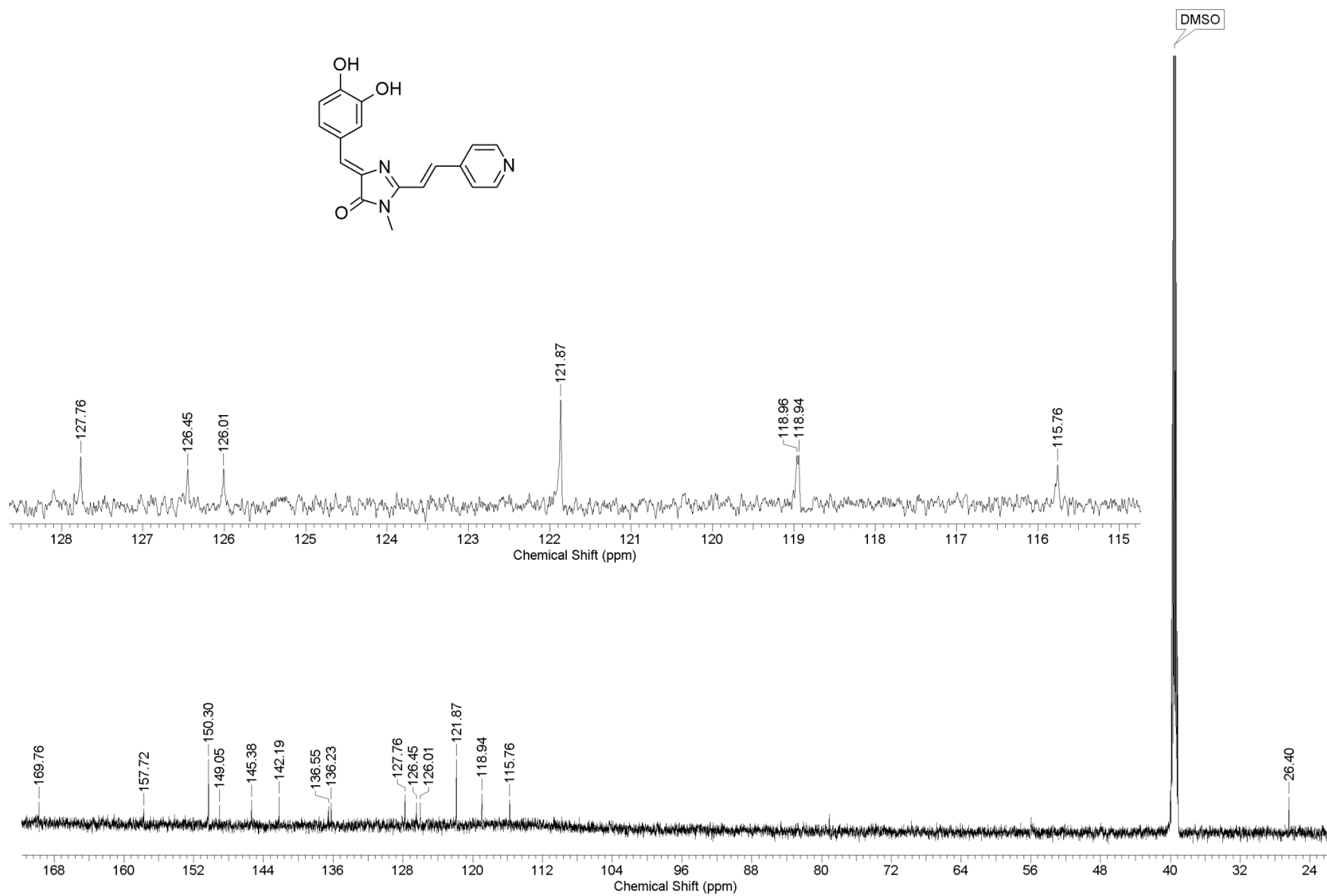


**Figure S66.** <sup>13</sup>C NMR spectrum of *(Z)*-4-(3,4-dihydroxybenzylidene)-1-methyl-2-((*E*)-2-(pyridin-4-yl)vinyl)-1*H*-imidazol-5(4*H*)-one

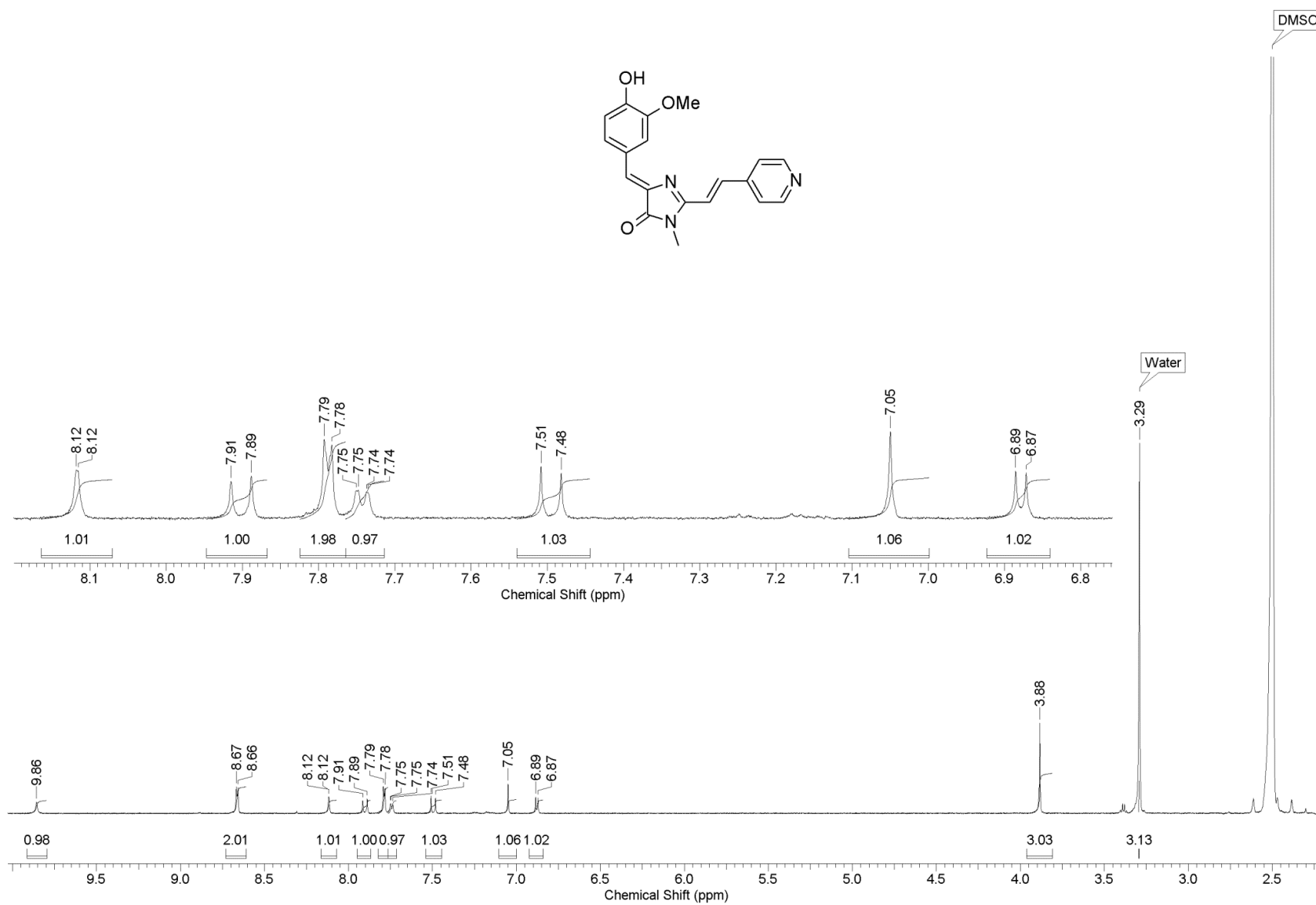


**Figure S67.**  $^1\text{H}$  NMR spectrum of *(Z)*-4-(3-methoxy-4-hydroxybenzylidene)-1-methyl-2-((*E*)-2-(pyridin-4-yl)vinyl)-1*H*-imidazol-5(4*H*)-one (**4d**)

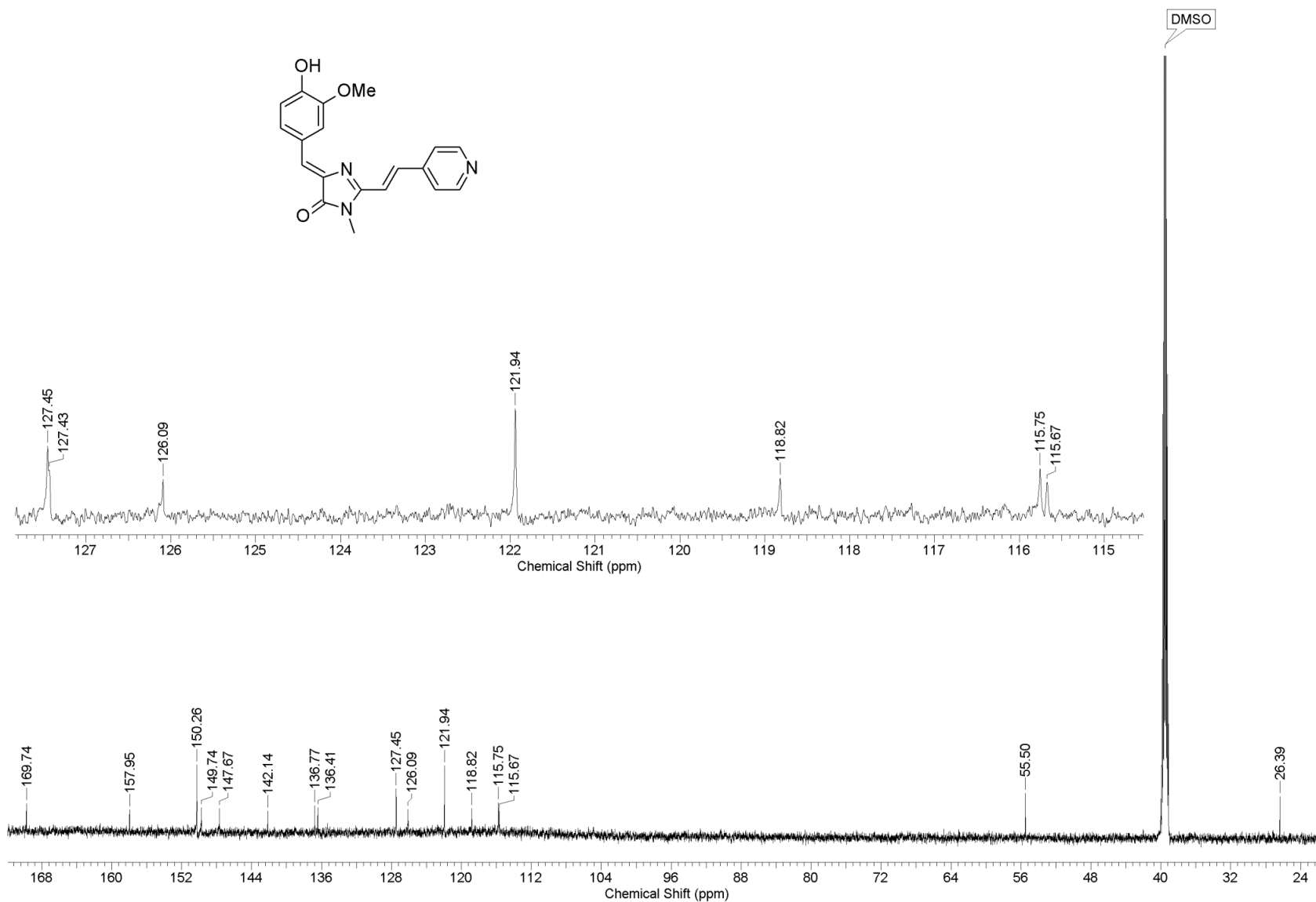


**Figure S68.** <sup>13</sup>C NMR spectrum of *(Z)*-4-(3-methoxy-4-hydroxybenzylidene)-1-methyl-2-((*E*)-2-(pyridin-4-yl)vinyl)-1*H*-imidazol-5(4*H*)-one

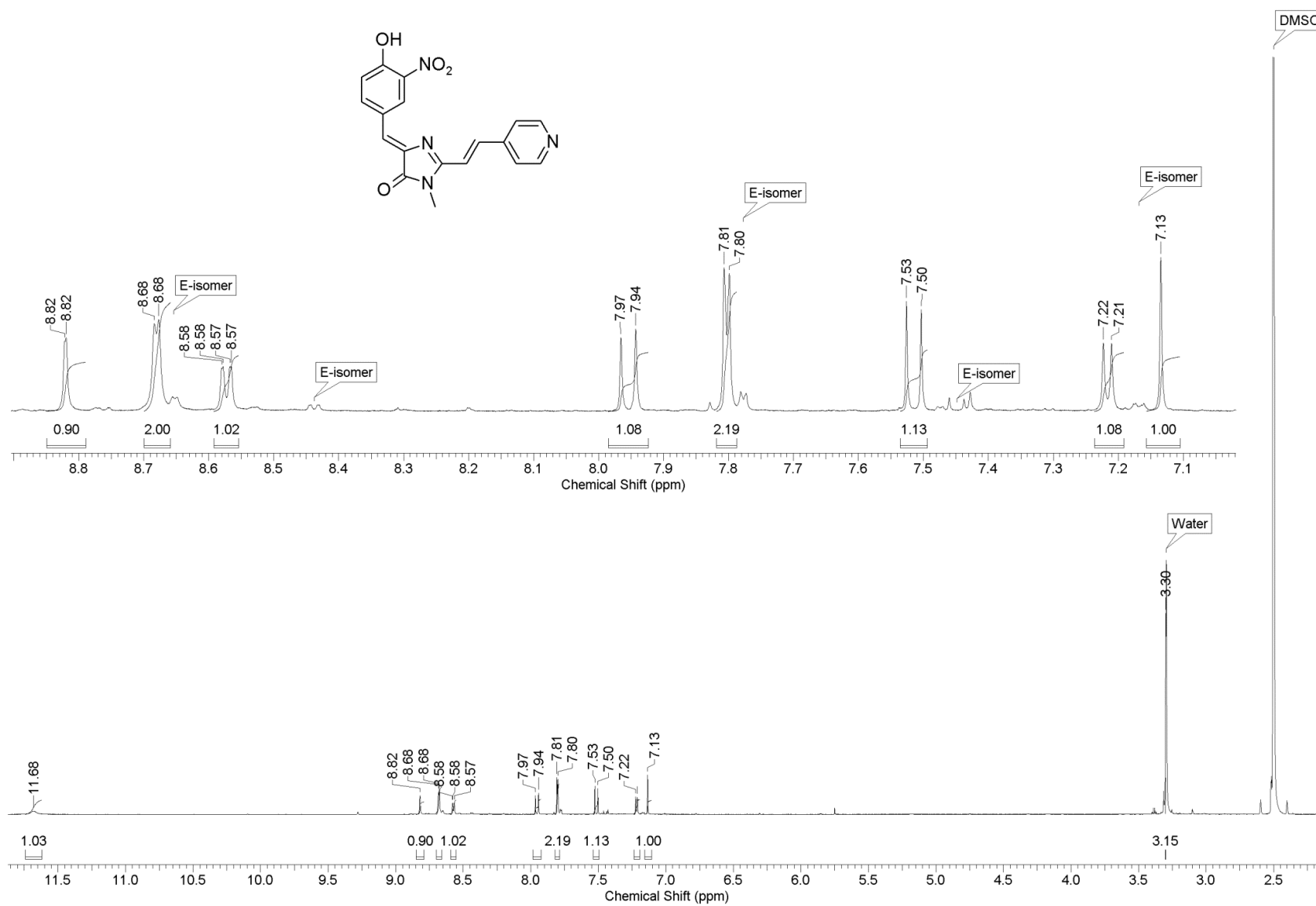


**Figure S69.** <sup>1</sup>H NMR spectrum of (Z)-4-(3-nitro-4-hydroxybenzylidene)-1-methyl-2-((E)-2-(pyridin-4-yl)vinyl)-1H-imidazol-5(4H)-one (**4f**)

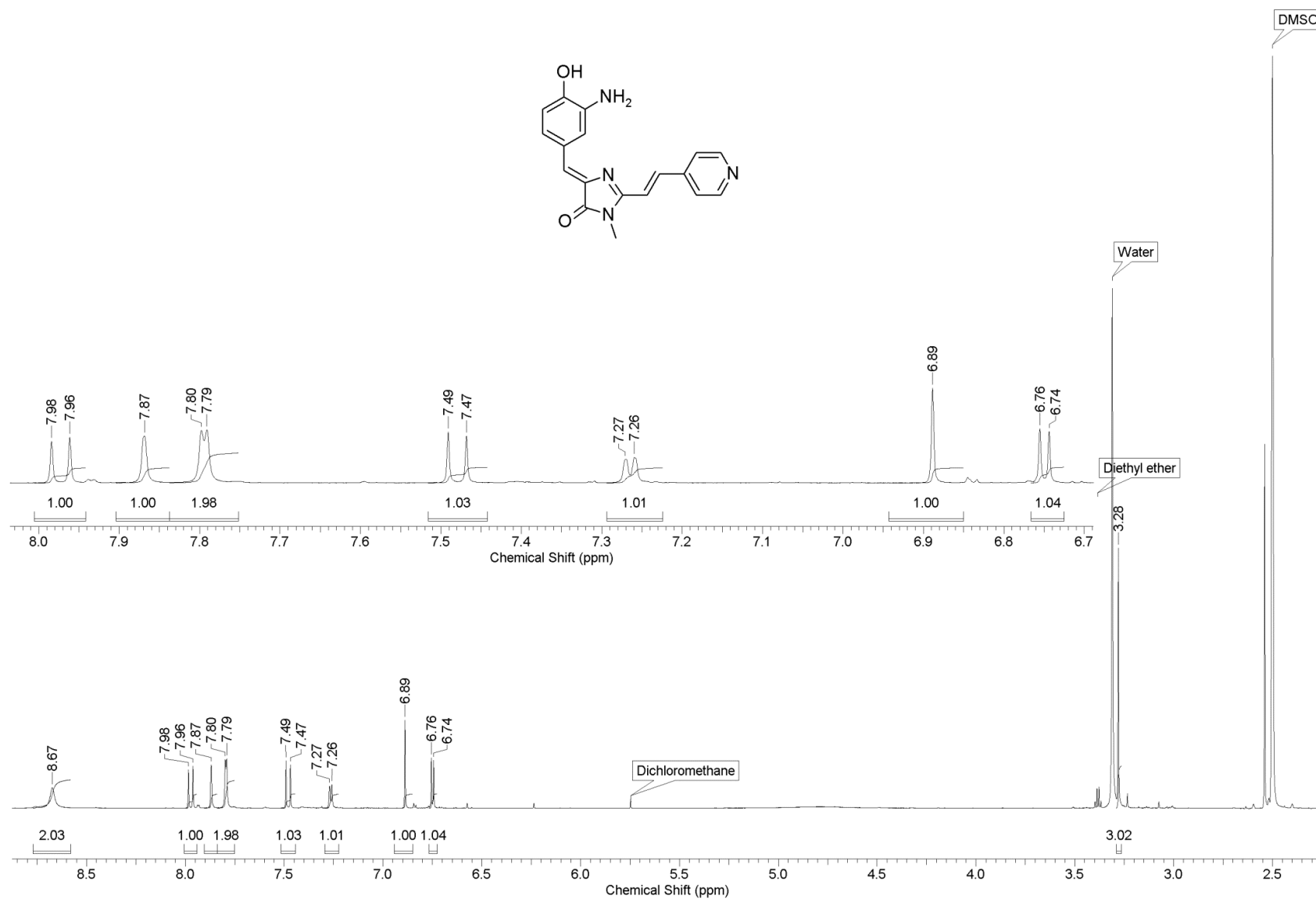


**Figure S70.**  $^1\text{H}$  NMR spectrum of *(Z)*-4-(3-amino-4-hydroxybenzylidene)-1-methyl-2-((*E*)-2-(pyridin-4-yl)vinyl)-1*H*-imidazol-5(4*H*)-one (**4e**)

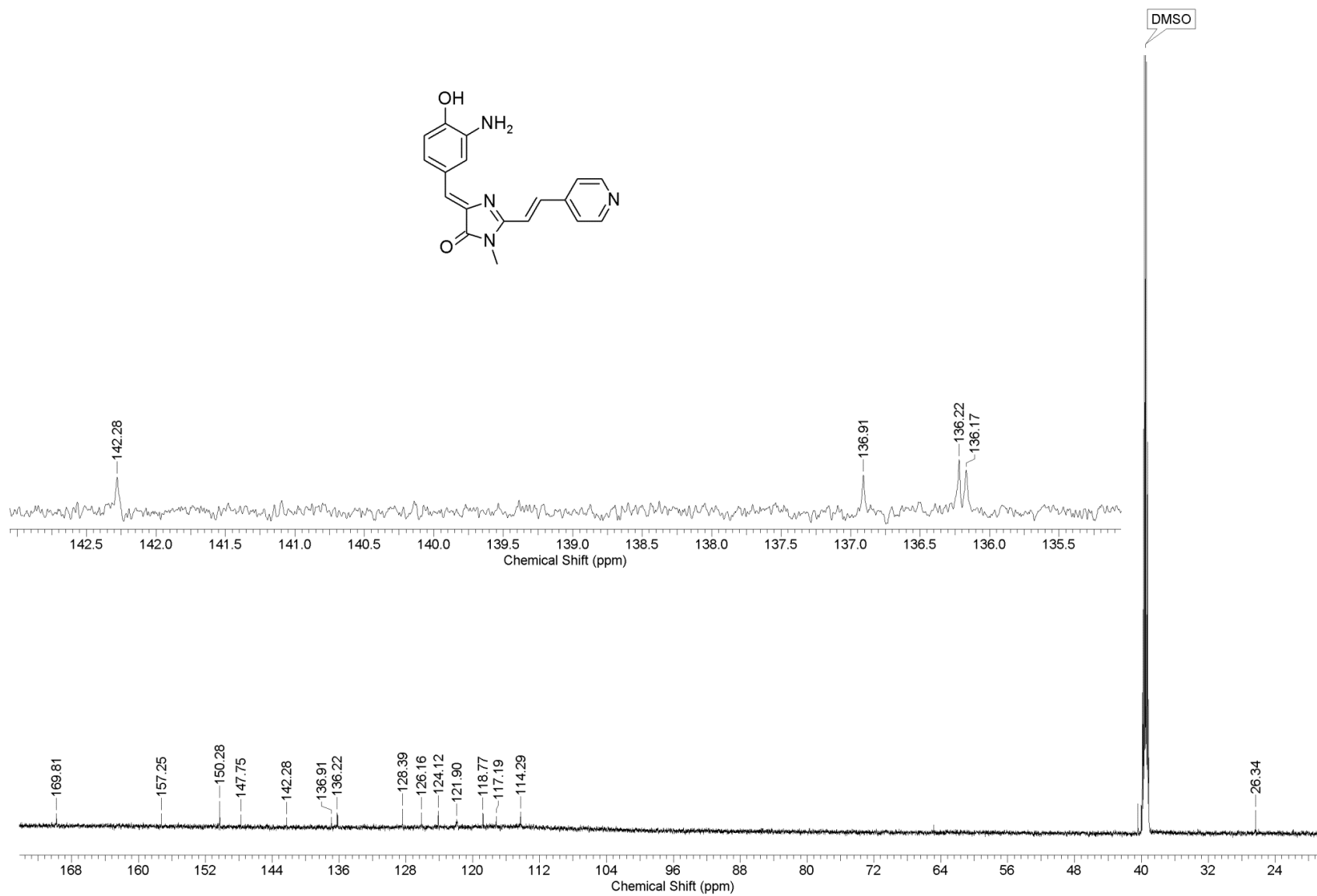


**Figure S71.** <sup>13</sup>C NMR spectrum of *(Z)*-4-(3-amino-4-hydroxybenzylidene)-1-methyl-2-((*E*)-2-(pyridin-4-yl)vinyl)-1*H*-imidazol-5(4*H*)-one